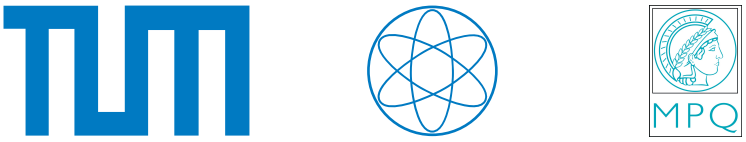

Open quantum spin systems in semiconductor quantum dots and atoms in optical lattices

Heike Schwager

Dissertation

Technische Universität München
Max-Planck-Institut für Quantenoptik

Technische Universität München
Max-Planck-Institut für Quantenoptik

Open quantum spin systems in semiconductor quantum dots and atoms in optical lattices

Heike Schwager

Vollständiger Abdruck der von der Fakultät für Physik
der Technischen Universität München
zur Erlangung des akademischen Grades eines

Doktors der Naturwissenschaften (Dr. rer. nat.)

genehmigten Dissertation.

Vorsitzender:	Univ.-Prof. Dr. R. Gross
Prüfer der Dissertation:	1. Hon.-Prof. J. I. Cirac, Ph.D.
	2. Univ.-Prof. J. J. Finley, Ph.D.

Die Dissertation wurde am 12.06.2012
bei der Technischen Universität München eingereicht
und durch die Fakultät für Physik am 04.07.2012 angenommen.

Abstract

In this Thesis, we study open quantum spin systems from different perspectives. The first part is motivated by technological challenges of quantum computation. An important building block for quantum computation and quantum communication networks is an interface between material qubits for storage and data processing and travelling photonic qubits for communication. We propose the realisation of a quantum interface between a travelling-wave light field and the nuclear spins in a quantum dot strongly coupled to a cavity. Our scheme is robust against cavity decay as it uses the decay of the cavity to achieve the coupling between nuclear spins and the travelling-wave light fields. A prerequiste for such a quantum interface is a highly polarized ensemble of nuclear spins. High polarization of the nuclear spin ensemble is moreover highly desirable as it protects the potential electron spin qubit from decoherence. Here we present the theoretical description of an experiment in which highly asymmetric dynamic nuclear spin pumping is observed in a single self-assembled InGaAs quantum dot.

The second part of this Thesis is devoted to fundamental studies of dissipative spin systems. We study general one-dimensional spin chains under dissipation and propose a scheme to realize a quantum spin system using ultracold atoms in an optical lattice in which both coherent interaction and dissipation can be engineered and controlled. This system enables the study of non-equilibrium and steady state physics of open and driven spin systems. We find, that the steady state expectation values of different spin models exhibit discontinuous behaviour at degeneracy points of the Hamiltonian in the limit of weak dissipation. This effect can be used to dissipatively probe the spectrum of the Hamiltonian. We moreover study spin models under the aspect of state preparation and show that dissipation drives certain spin models into highly entangled state. Finally,

we study a spin chain with subwavelength interatomic distances that exhibits long rage interactions.

What lies at the heart of all these approaches is the endeavour to include the coupling to the environment into the description of the physical system with the aim of harnessing dissipative processes. While decoherence masks or destroys quantum effects and is considered as the main adversary of any quantum information application, we turn the existence of the dissipative coupling of spin systems to the environment into a fruitful resource.

Zusammenfassung

Die vorliegende Arbeit behandelt dissipative Quanten Spin-Systeme unter verschiedenen Aspekten. Während der erste Teil der Arbeit durch technologische Herausforderungen der Quanteninformationsverarbeitung motiviert ist, werden im zweiten Teil Fragestellungen zu dissipativen Spin-Modellen behandelt. Diese können unter anderem mithilfe von kalten Atomen in optischen Gittern realisiert werden.

Eine Quantenschnittstelle zwischen Licht und Materie ist ein grundlegender Baustein für Quantennetzwerke und Quantencomputer. In dieser Doktorarbeit wird ein theoretisches Konzept vorgestellt, welches die Realisierung einer Schnittstelle zwischen Licht und den Kernspins eines selbstorganisierten Halbleiter-Quantenpunktes ermöglicht. Der Quantenpunkt ist stark an einen optischen Resonator gekoppelt. Das hier vorgeschlagene Konzept ist robust gegenüber dem Zerfall der Resonatormode durch Kopplung an die Umgebung. Es eröffnet die Möglichkeit, hochdimensionale photonische Quantenzustände in die Kernspins eines Quantenpunktes zu schreiben und auszulesen, ohne sie vorher in den Resonator einkoppeln zu müssen. Eine Voraussetzung für dieses Konzept ist eine hohe Polarisation der Kernspins. Polarisierte Kernspins haben außergewöhnlich lange Lebensdauern und stellen daher ein hervorragendes Speichermedium für Quanteninformation dar. Des Weiteren verlängert ein hoch polarisiertes Kernspinensemble die Kohärenzzeiten der in den Elektronenspin kodierten Quanten-Bits eines potenziellen Quantencomputers. In selbstorganisierten Quantenpunkten können Kernspins durch optisches Pumpen von Exzitonen polarisiert werden. Wir stellen hier die theoretische Beschreibung eines parallel zu dieser Arbeit an der TU München durchgeführten Experiments zur Kernspinpolarisation in einem Quantenpunkt vor, und erklären die physikalischen Mechanismen, die den experimentellen Beobachtungen zugrunde liegen.

Der zweite Teil der Arbeit behandelt eindimensionale Spinmodelle und die gezielte Manipulation der Wechselwirkung der Spins mit der Umgebung. Wir zeigen, wie eindimensionale Spinsysteme mit ultrakalten Atomen in optischen Gittern mithilfe von verschiedenen Bewegungszuständen des Fallenpotentials realisiert werden können. Durch optische Anregung von internen atomaren Zuständen und deren Zerfall kann die Dissipation des Systems gezielt designt werden. Derartige Systeme eröffnen die Möglichkeit, Nicht-Gleichgewichtsphysik und stationäre Zustände von dissipativen, getriebenen Spin-Systemen zu untersuchen. Durch numerische Modellierung derartiger dissipativer Spin-Systeme haben wir einen unerwarteten Effekt entdeckt. Im Grenzfall schwacher Dissipation treten Unstetigkeiten in den Erwartungswerten der stationären Zustände auf, die im Zusammenhang mit den Entartungspunkten des System-Hamiltonians stehen. Wir untersuchen diesen Effekt für verschiedene Spin Modelle und leiten Bedingungen für das Auftreten derartiger Unstetigkeiten her. Des Weiteren zeigen wir, dass sich bestimmte Spin Modelle zur dissipativen Präparation von vollständig verschränkten Zuständen eignen. Außerdem leiten wir eine theoretische Beschreibung von atomaren Ketten her, deren interatomare Abständen die Wellenlänge eines treibenden Feldes deutlich unterschreiten. In diesen Systemen spielen langreichweitige Wechselwirkungen eine Bedeutung, die es ermöglichen, stark-korrelierte und kollektive Effekte zu studieren.

Publications

1. **A quantum interface between light and nuclear spins in quantum dots**
   Heike Schwager, J. Ignacio Cirac, and Geza Giedke.
   Phys. Rev. B **81**, 045309 (2010), See Chapter 2

2. **Interfacing nuclear spins in quantum dots to cavity or traveling-wave fields**
   Heike Schwager, J. Ignacio Cirac, and Geza Giedke.
   New J. Phys. **12**, 043026 (2010), See Chapter 2

3. **A comprehensive experimental and theoretical study of asymmetric optical nuclear spin pumping in single neutral InGaAs quantum dots**
   F. Klotz, V. Jovanov, J. Kierig, E.C. Clark, M. Bichler, G. Abstreiter, M.S. Brandt, J.J. Finley, H. Schwager, and G. Giedke.
   In preparation, See Chapter 3

4. **Asymmetric optical nuclear spin pumping in a single uncharged quantum dot**
   F. Klotz, V. Jovanov, J. Kierig, E.C. Clark, M. Bichler, G. Abstreiter, M.S. Brandt, J.J. Finley, H. Schwager, and G. Giedke.
   Phys. Rev. B **82**, 121307(R) (2010), See Chapter 3

5. **Dissipative spin chains: Implementation with cold atoms and steady state properties**
   Heike Schwager, J. Ignacio Cirac, and Geza Giedke
   arXiv:1207.5768, See Chapter 4 & 5

Contents

Chapter 1

Introduction

1.1 Motivation

At the beginning of the twentieth century, the development of quantum mechanics radically changed physical concepts describing our world and puzzled a whole generation of physicists. While doubts remained over the following decades, and questions like "Can Quantum Mechanical description of physical reality be considered complete?" [1] posed in a seminal work 1935 by Einstein, Podolsky and Rosen (EPR) remained controversial, the society was revolutionized by new technologies. Applying quantum theory to the development of semiconductors lead to the invention of the transistor in 1948 [2], that paved the way to the information age. Another ground-breaking technology based on quantum mechanics was the invention of the laser in the 1950's. In 1964, John Bell revisited the question posed by EPR thirty years back [3]. He showed that the concept of local realism favoured by EPR contradicts quantum mechanics. Bell derived inequalities that opened the path for experimental tests of fundamental concepts of quantum mechanics. These experiments corroborated the understanding of entanglement, which Einstein called "a spooky action at a distance", and showed that it cannot be understood as classical correlations between particles.

Today, integrated circuits have reached sizes of less than 50 nm with 10^9 transistors per chip. The progress of computer technology is facing difficulties of size as it is moving closer and closer towards the frontier of the atomic scale, on which quantum effects

become dominant. A solution to this problem might be provided by the field of quantum information science [4] based on quantum mechanical concepts such as the superposition principle and entanglement. It started out in the 1980's, when conceptual ideas were developed that showed that quantum mechanics allows for new algorithms that are for certain problems much faster than their classical counterparts [4, 5]. Quantum information research promises much more than computers. To name a few examples, similar technologies allow for unconditionally secure cryptography protocols [6], for long-distance quantum communication [7] and highly sensitive measurements in the field of quantum metrology [8].

Today, quantum information science has emerged into a vibrant field with many research groups worldwide working on different physical systems towards the highly ambitious goal of building a quantum computer and similar technologies. There are a number of physical systems considered to be candidates for quantum information technologies, for a review see [9]. One of the pioneering systems are ions in electromagnetical traps. Laser-induced interactions allow for the implementation of single-qubit and multi-qubit quantum gates by coupling the internal states of ions to their motion [10, 11] and recently, states with 14 entangled quantum bits have been realized [12]. Another promising system are cold atoms in optical lattices where atoms can be manipulated with laser forces depending on their internal qubit levels which allows for the realization of entangling quantum gate operations [13]. A drawback of using single atoms for quantum computing purposes is the need to cool and trap them. Large arrays of qubits might be easier to implement with solid state systems. Aiming towards scalability and miniaturization, it would be convenient to use materials that are used for current computers and electronics: silicon, GaAs and similar semiconductor materials. This motivated the research towards semiconductor quantum dots, NV-centers and phosphorus donors in silicon [9]. A detailed introduction into the field of semiconductor quantum dots and cold atoms in optical lattices, that are the two physical systems that are mainly studied in this Thesis, will be given in the following.

The answer to the question which physical system is the most promising one for achieving a scalable quantum computer is still open. While reliable quantum com-

munication setups exist and quantum cryptography is already operating, the field of quantum computation is still struggling with problems of decoherence and scalability. Quantum computation works on the level of single quantum systems that have to be well isolated from the environment. The interaction with the "outside world" destroys quantum effects and leads to decoherence of the qubits. Thus, dissipation is the strongest adversary of quantum information science. Which physical system might be best suited for quantum computation is difficult to answer, as complete architectures of a quantum computer have to be compared rather than comparing only the coherence time of the qubit to the timescales that are required to control, initialize and measure the qubit. The latter comparison is not sufficient, as the performance of the quantum gates depends critically on the quantum error correction scheme applied.

Harnessing dissipation: While all proposals and experiments in the field of quantum information struggle with dissipation and different ways to avoid decoherence are being pursued, a new trend of *harnessing* dissipation has emerged in recent years. The idea is to engineer the dissipative coupling between the system and the environment such, that the environment drives the system into the desired state. It has been shown that the coupling to an environment can be harnessed to generate useful quantum states [14, 15, 16, 17]. The coupling to the environment can even be used to perform quantum information tasks. The idea of dissipative quantum computation is proposed in [17, 18]. Here, dissipation drives the system into a steady state in which the outcome of the computation is encoded. Recently, purely dissipative entanglement generation between two atomic ensembles has been reported [19], following the theoretical proposal of Muschik et al. [20]. Another recent proposal [18] shows, that entanglement distillation can also be realized dissipatively. In this setup, the performance is improved by adding noise to the system.

1.1.1 Harnessing dissipation - in the context of this Thesis

The endeavour to *include* the coupling to the environment into the description of the physical system and to turn its existence into a fruitful discussion lies at the heart of this Thesis. Here, we study open quantum spin systems from different perspectives. In

Chapter 2 we propose a quantum interface between light and nuclear spins of a quantum dot. Such an interface is an important building block for quantum computation and quantum communication networks, coupling the "stationary" qubits for storage and data processing to mobile "flying" qubits for communication (typically photons). The system we study is a quantum dot strongly coupled to a cavity. We include the coupling to the environment, which leads to decay of the cavity, into our description, and propose a protocol for an interface between light and the nuclear spins of the quantum dot that is robust against cavity decay. In **Chapter 3** we study a physical mechanism that leads to Dynamical Nuclear Spin Polarisation (DNP) of the nuclear spins. Here, we include the tunnelling of electron spins from the quantum dot to the leads into the description, and find, that this dissipative setup enables the polarization of the nuclear spins. The second part of the Thesis is devoted to fundamental studies of dissipative spin systems. In **Chapter 4** we propose a scheme to realize a quantum spin system using ultracold atoms in an optical lattice in which both coherent interaction and dissipation can be engineered and controlled. This system is an interesting toy model to simulate one dimensional spin models like the Ising and the XXZ model, and enables the study of non-equilibrium and steady state physics of open and driven spin systems. In **Chapter 5** we investigate under which conditions dissipation drives these spin models into interesting steady states. We find, that the steady state expectation values of different spin models, including the XXZ and Ising model, exhibit discontinuous behavior at degeneracy points of the Hamiltonian in the limit of weak dissipation. This is a peculiar effect that is highly interesting as it can be used to dissipatively probe the spectrum of the Hamiltonian. Moreover, we study different spin models under the aspect of state preparation and show, that certain spin models can be dissipatively driven into highly entangled states. Here, we use collective dissipation of spins all coupled to one single mode, and show, that such a setup can be realized with a Bose-Einstein Condensate in an optical cavity. Finally, we derive the master equation of a driven spin chain in the subwavelength regime where long-range interactions play a role. This system allows to study strongly-correlated and collective effects and might be realized in plasmonic structures or with atoms encapsulated in carbon nanotubes.

More details on the before-mentioned four projects presented in this Thesis will be given in the context of the physical systems discussed in the next section.

1.2 Physical systems

Here, we introduce briefly the physical systems which are considered in this thesis. We discuss semiconductor quantum dots and cold atoms in the context of the results presented in the following Chapters and motivate why they are interesting candidates for the implementation of the ideas put forward in the following Chapters.

1.2.1 Semiconductor quantum dots

A quantum dot is a small semiconductor structure in which an electron or hole is confined in all three spatial directions. The localized wave function of the confined electron or hole leads to a discrete, "atom-like" energy spectrum. The most prominent examples are self-assembled quantum dots [21] and electrically defined quantum dots that are both grown by molecular beam epitaxy. With this method, semiconductor structures are grown layer by layer, allowing to stack materials with different band gaps. When a layer of a lower bandgap semiconductor (for example InGaAs) is embedded in a layer of a larger bandgap semiconductor (for example GaAs), the electrons, that originate from optical excitation, current injection or doping, become confined in the material with the lower bandgap and form a two dimensional electron gas (2DEG). Further confinement in the remaining two dimensions leads to a quantum dot. In electrostatically defined quantum dots, this is achieved by electrostatic potentials. These potentials are created by applying voltages to lithographically defined metal-contacts (Schottky contacts) on top of the quantum well, depleting small regions of the 2DEG. Self-assembled quantum dots are created by a random semiconductor growth process. Due to their lattice mismatch, droplets of e.g., InGaAs self-assemble on a GaAs substrate in order to minimize surface strain. Subsequently, these droplets are covered by GaAs [22].

The main difference between these two types of quantum dots is the depth of their confining potential. While very low temperatures (< 1K) are required for experiments with electrostatically defined quantum dots, the deep trapping potentials of

self-assembled quantum dots allows to perform experiments at 4 K. Moreover, self-assembled quantum dots allow to trap not only electrons but also holes. While in electrostatically defined quantum dots, loading and measuring of electrons is accomplished by changing the gate voltages and detecting currents, self-assembled quantum dots allow for coherent optical manipulation of charges.

Quantum computation with quantum dots: The ability to trap single charges in quantum dots led to the famous Loss-DiVincenzo proposal to use single electron spins confined to electrostatically defined quantum dots as qubits [23]. The proposal envisions a scalable implementation of a quantum computer with arrays of quantum dots each containing a single electron. These qubits allow for local gating operations and controllable interaction through exchange coupling between neighboring spins, that can be moved closer and further from each other by changing the gate voltages. Today, many elements that are necessary for quantum computation with electrostatically defined quantum dots have been realized, such as initialization of the qubit, single-shot read-out of spin states [24], a two-qubit gate, i.e., coherent exchange of two electron spins in a double dot system [25], and driven coherent spin rotations of a single electron spin [26]. However, interactions between electrostatically defined quantum dots are very short-range, enabling quantum-computer architectures with nearest-neighbor interaction only. Considering the constraints due to the requirements of fault-tolerant Quantum Error Correction (QEC) with nearest-neighbor communication on the one hand, and the space that the electrical leads, that define the qubit, require in this setup on the other hand, a scalable architecture requires long-distance transport of quantum information [9].

This requirement could be fulfilled with self-assembled quantum dots, that have successfully been coupled to optical microcavities [27, 28, 29]. Shortly after the famous Loss-DiVincenzo proposal, Imamoglu et. al. [30] proposed to use optical means to couple, manipulate, and read out qubits implemented in optically active quantum dots, where the coupling to a mode of a microcavity mediates the interaction between different qubits. Coherent control and measurement of electrons in self-assembled quantum dots has progressed a lot in recent years. Electrons (and holes [31]) can be initialized

very fast [32, 33] and a complete set of all optical single qubit rotations has been demonstrated using ultrafast pulses [33]. A first step towards logic between quantum dots in microcavities has been achieved with a single quantum dot coupled to a photonic crystal nanocavity [34]. Recently, mutual coupling of two semiconductor quantum dots via a photonic crystal nanocavity has been achieved by Laucht et al. [35]. However, a two-qubit gate with self-assembled quantum dots has not been demonstrated yet, and many challenges still remain on the way towards quantum computing. One problem is that self-assembly implicates a certain randomness in view of the spatial position and the spectral properties of the dots. Moreover, both self-assembled and electrostatically defined quantum dots suffer from an even more severe problem, the nuclear-spin induced decoherence of the electron spin qubit. The hyperfine interaction of the electron spin and the surrounding 10^4-10^6 nuclear spins of the atoms in the quantum dot is the strongest source of decoherence for the electron spin qubit in quantum dots. This decoherence could be in principle suppressed by polarizing the nuclei with magnetic fields, but due to their small magnetic moment, the thermal state of the nuclear spins is unpolarized even at the strongest magnetic fields and lowest temperatures available in laboratories.

For self-assembled quantum dots, a solution in this respect is provided by the concept of "Dynamical Nuclear Spin Polarization" (DNP) which uses optical methods to polarize the nuclear spins (for a review see [36]). The electron is initialised via optical pumping and can interact with the surrounding nuclear spins via the hyperfine interaction, which enables transfer of spin angular momentum from the electron to the nuclear spin. Thereby, the nuclear spins become polarized and act back on the electron spin. The resulting changes in electron spin orientation and transitions energies can be measured and give insight into the nuclear spin polarization. Different groups achieved high nuclear spin polarization in charged and neutral self-assembled quantum dots, see [36]. Moreover, it has been shown that in uncharged quantum dots, the nuclear spin system can be stable for up to several hours [37, 38]. This makes this system highly interesting for information storage [39, 40] and even for quantum information processing [41].

1.2.2 Semiconductor quantum dots - in the context of this Thesis

While a quantum memory for electron spin qubits in the nuclear spins of a quantum dot has been proposed in recent years [39, 40], direct coherent coupling between the optical field and the nuclear spins in a QD, enabling the storage of photonic states while avoiding electron spin decoherence, had not been studied before. In **Chapter 2** we show how to realize a quantum dot-based quantum interface between the nuclear spins in a quantum dot and a traveling-wave light field. We show how to couple an optical field directly to the nuclear spin ensemble, thus interfacing light to an exceptionally long-lived mesoscopic system that enables the storage and retrieval of higher-dimensional states. We study a singly charged self-assembled quantum dot strongly coupled to a cavity. The scheme we propose is robust against cavity decay as it *uses* the decay of the cavity to achieve the coupling between nuclear spins and the traveling-wave light fields. The write-in of information, encoded in the state of the light field, proceeds by deterministic creation of entanglement between the nuclear spins and the cavity output-mode. This entangled state between the output field of the cavity and the nuclear spins is a resource state for teleportation [42] and overcomes the in-coupling problem as the traveling-wave light field can be teleported onto the nuclear spins. The read-out maps the nuclear state to the output mode of the cavity. We discuss the performance of the scheme and provide a convenient description of the dipolar dynamics of the nuclei for highly polarized spins, demonstrating that this process does not affect the performance of our protocol. A prerequisite for such a quantum interface is a highly polarized ensemble of nuclear spins.

As discussed before, high nuclear spin polarization can be achieved by the concept of DNP. In **Chapter 3** we present an experimental and theoretical investigation of asymmetric unidirectional nuclear spin pumping in an uncharged self-assembled InGaAs quantum dot [43, 37]. The experiment was carried out by Florian Klotz under the supervision of Prof. Finley at the Walter-Schottky Institute of the TU Munich. In the experiment, highly asymmetric dynamic nuclear spin pumping is observed in a quantum dot subject to resonant optical pumping of the neutral exciton transition leading to a large maximum polarization of 54%. The theoretical model gives new insights into

the mechanism leading to the observed DNP effect. It can be understood in terms of electron-nuclear spin flip-flop processes exchanging the orientation of an electron and nuclear spin and transferring the exciton from a optically active bright into an optically inactive dark state which then decays non-radiatively. The model allows to perform numerical calculations that simulate the actual measurement procedure and quantitatively reproduce the experimentally observed characteristic features of the achievable steady state nuclear polarization.

1.2.3 Ultracold atoms

Ultracold atoms are very interesting candidates for studying many-body quantum physics and can serve as quantum simulators for condensed matter phenomena. These systems are very clean and moreover well-controllable, making them a nice toy model for real solid state crystals. Standing wave laser fields can be arranged to form structures that have the form of an artificial crystal, i.e., they form a periodic potential which can trap atoms, with the distance between single lattice sites being on the order of an optical wavelength. The dimensionality, depth, form and position of this potential can be controlled very precisely via the intensity, geometry and other properties of the external laser fields. When an optical lattice is loaded with a Bose condensate, the atoms become trapped in the lattice potential. Depending on the depth of the lattice potential, there is a competition between tunnelling between neighboring lattice sites and on-site interaction between the atoms. There are two extreme cases, the superfluid phase in which each atom is spread out over the entire lattice and the Mott insulator phase in which the atoms are "frozen" to an integer number of atoms in each lattice site. Starting in the superfluid phase and increasing the depth of the lattice potential, the system undergoes a quantum phase transition. The experimental observation of the superfluid-Mott insulator transition by Greiner et al. [44] based on a proposal by Jaksch et al. [45] stood at the beginning of experiments studying strongly correlated systems with ultracold atoms. A huge variety of experimental studies of the dynamical evolution of strongly correlated quantum many-body systems and the investigation of the static quantum phases with cold atoms followed. Prominent examples are the experimental

realization of the fermionized Tonks-Girardeau gas for bosonic particles [46, 47], the BCS-BEC crossover [48, 49, 50] and the fermionized Mott Insulator [51, 52]. In all these systems, strong interactions between the particles compete with their kinetic energy, which leads to the generation of correlated quantum states. Considerable progress has been made in the imaging of the correlated many body systems with single-site resolution [53]. The demonstration of strong coupling of a Bose-Einstein Condensate to the quantized field of an optical cavity [54], where all atoms couple identically to one single mode of the cavity, opened up the route to study many-body physics of cold gases with cavity-mediated long-range interactions. A first groundbreaking experiment in this direction was the demonstration of the Dicke quantum phase transition [55] that was predicted more than thirty years before [56, 57, 58]. Moreover, cold atoms allow for practically perfect realizations of quantum spin models. Quantum spins on a lattice that are coupled through magnetic interactions give rise to magnetically ordered ground states, such as paramagnets, ferromagnets and antiferromagnets. Spin systems have been realized using two internal states of the atoms to represent the magnetic spins. The interactions between the spins allow the system to be switched between antiferromagnetic and ferromagnetic spin interactions [59]. While the interactions in this system are quite weak, recently, a one-dimensional chain of Ising spins with stronger interactions has been realized using a Mott insulator of spinless bosons in a tilted optical lattice [60].

1.2.4 Ultracold atoms - in the context of this Thesis

We propose to simulate different quantum spin models using the *motional* degrees of freedom of cold bosonic atoms in the Mott insulator regime in an optical lattice potential (see **Chapter 4**). Changing the strength of the trapping lasers, different spin models like the XXZ or the Ising model can be realized. Moreover, we show, how engineerable dissipation can be added to this system. We give a detailed derivation of how optical driving (and decay) of internal atomic levels can be used to realize tunable dissipation. We moreover show how optical driving can be used to simulate an effective transversal magnetic field. This system comprises an interesting toy model for one-dimensional

spin chains under dissipation. In **Chapter 5** we study the steady state properties of local one dimensional spin Hamiltonians under different types of dissipation. We find that in the limit of weak dissipation, these peaks indicate discontinuities in the steady state. We show that the steady state expectation values exhibit discontinuous behavior at the degeneracy points of the Hamiltonian. This effect can be used to dissipatively probe the degeneracy of the Hamiltonian's spectrum. Then we study dissipative spin systems under the aspect of state preparation. We show that there exist certain spin models, that are dissipatively driven into highly entangled states. We study different types of dissipation and show, that apart from the setup discussed before in **Chapter 4**, a Bose-Einstein Condensate strongly coupled to an optical cavity [54] that we discussed in the previous Section has interesting properties for our purposes. We show that adiabatic elimination of the cavity leads to collective dissipation, which makes this system attractive from the point of view of state preparation and studying phase transitions.

1.3 Outline of this Thesis

The various chapters of this thesis are written in a self-contained style that allows the interested reader to study different chapters individually. In the introduction, the general context of the following chapters has been established. Each chapter contains an individual introduction into the specific topic and is supplemented by some concluding remarks and outlooks. Here we give an overview over the following chapters:

In **Chapter 2** we propose a quantum interface between a traveling-wave light field and the polarized nuclear spins in a singly charged quantum dot strongly coupled to a high-finesse optical cavity. We show that by adiabatically eliminating the trion and the electron spin different effective couplings between light and nuclear spins can be achieved. Direct mapping of the state of the cavity field requires very long cavity lifetimes. To circumvent this problem, we include the dissipative coupling of the cavity to the environment in our description and propose a scheme, which is robust against cavity decay. Our system *uses* the cavity decay to achieve the coupling between nuclear spins and the traveling-wave light fields. The write-in of states of the light field proceeds

by deterministic creation of entanglement between the nuclear spins and the cavity output-mode and subsequent teleportation. The read-out maps the nuclear state to the output mode of the cavity. We discuss the performance of the scheme and provide a convenient description of the dipolar dynamics of the nuclei for highly polarized spins, demonstrating that this process does not affect the performance of our protocol.

In **Chapter 3** we present an experimental and theoretical investigation of asymmetric unidirectional nuclear spin pumping in an uncharged self-assembled InGaAs quantum dot. The experiment was carried out by Florian Klotz under the supervision of Prof. Finley at the Walter-Schottky Institute of the TU Munich. In the experiment, highly asymmetric dynamic nuclear spin pumping is observed, leading to a large maximum polarization of 54%. We discuss the physical effects that account for the observed behavior. We explain that the observed asymmetric DNP effects can be understood in terms of electron-nuclear spin flip-flop processes exchanging the orientation of an electron and nuclear spin. Thereby, the exciton is transferred from an optically active bright into an optically inactive dark state which then decays non-radiatively. Moreover, we present a detailed theoretical model of the driven neutral QD that allows to perform numerical calculations simulating the actual experimental procedure used in the measurements. We find that the results of the numerical calculations account for the observed behavior.

In **Chapter 4** we propose a quantum optical implementation of a class of dissipative spin systems with ultracold atoms in optical lattices using detuned Raman transitions in the Lamb-Dicke regime. We show that using the *motional* degrees of freedom of cold bosonic atoms described by the two-band Mott insulator model, different spin models like the XXZ or the Ising model can be realized. We show in detail, how engineerable dissipation can be realized in this system with optical driving (and decay) of internal atomic levels. We moreover show how an effective transversal magnetic field can be simulated with optical couplings. This system comprises an interesting toy model for one-dimensional spin chains under dissipation studied in the following Chapter.

In **Chapter 5** we study the steady state properties of local one dimensional spin Hamiltonians under different types of dissipation. First, we study small spin chains and

find, that for weak dissipation, steady state expectation values show pronounced peaks at certain critical system parameters. We find that in the limit of weak dissipation, these peaks indicate discontinuities in the steady state expectation values. We show how to use this effect to dissipatively probe the Hamiltonian's spectrum and derive a condition that elucidates the occurrence of discontinuities in the steady state expectation values. We moreover study state preparation with dissipative spin systems and show, that for certain spin Hamiltonians under dissipation, fully entangled unique steady states of spin chains of N atoms can be prepared. Then, we show how collective dissipation can be experimentally realized with cold atoms in an optical cavity. Moreover, we derive a master equation for a driven atomic spin systems with interatomic spacing in the subwavelength regime in which long-range interactions play a significant role. Such a system might be realized with atoms trapped in carbon nanotubes or plasmonic structures.

Chapter 2

A quantum interface between light and nuclear spins

The coherent coupling of flying photonic qubits to stationary matter-based qubits is an essential building block for quantum communication networks. We show how such a quantum interface can be realized between a traveling-wave optical field and the polarized nuclear spins in a singly charged quantum dot strongly coupled to a high-finesse optical cavity. By adiabatically eliminating the electron a direct effective coupling is achieved. Depending on the laser field applied, interactions that enable either write-in or read-out are obtained. We discuss the performance of the scheme and provide a convenient description of the dipolar dynamics of the nuclei for highly polarized spins, demonstrating that this process does not affect the performance of our protocol.

2.1 Introduction

An important milestone on the path to quantum computation and quantum communication networks is the coupling of "stationary" qubits for storage and data processing (usually assumed to be realized by material systems such as atoms or electrons) and mobile "flying" qubits for communication (typically photons) [61, 62]. Detection and

subsequent storage of information is inapplicable in quantum information as an unknown quantum state cannot be determined faithfully by a measurement. Hence the development of "light-matter interfaces" that allow the coherent write-in and read-out of quantum information has been the subject of intense theoretical research [63, 64, 65]. Two paths have been identified to make light efficiently couple to a single atomic quantum system: the use of a high-finesse cavity coupled to a single atom or the use of an optically thick ensemble of atoms, in whose *collective* state the quantum information is to be stored. Both have resulted in the experimental demonstration of such interfaces [66, 67, 68, 69, 70]. Even without strong coupling a quantum interface can be realized by combining the probabilistic creation of entanglement between atom and light with teleportation. This approach has been demonstrated with trapped ions [71].

For qubits realized by electron spins in quantum dots [23, 30] such interfaces have yet to be realized, though in particular for self-assembled quantum dots [72], which have many atom-like properties, several proposals exist to map photonic states to an electron in a quantum dot [30, 73] in analogy to the atomic schemes. Strong coherent coupling between a single quantum system and a single mode of high-Q micro- and nano-cavities has been demonstrated experimentally [74, 75, 76, 77], raising the prospect of coupling light to the quantum dot's electronic state by adapting protocols such as [63]. Despite their good isolation from many environmental degrees of freedom, the electron-spin coherence time in today's quantum dots is limited mainly due to strong hyperfine coupling to lattice nuclear spins. Moreover, the capacity of such an interface is one qubit only, making the interfacing difficult for many-photon states of the light field as used in continuous variable quantum information processing. In contrast, the ensemble of lattice nuclear spins could provide a high-dimensional and long-lived quantum memory [40].

Here we will show how to realize a QD-based quantum interface between the *nuclear spins* in a QD and the optical field. We show how to couple an optical field directly to the nuclear spin ensemble, thus interfacing light to an exceptionally long-lived mesoscopic system that enables the storage and retrieval of higher-dimensional states and is amenable to coherent manipulation via the electron spin [41]. The system we consider

is a charged quantum dot strongly coupled to a high-finesse optical cavity by a detuned Raman process. We show that by adiabatically eliminating the trion and the electron spin different effective couplings between light and nuclear spins are achieved. As demonstrated in our publication [78] and my diploma thesis [79], the state of the cavity field can be directly mapped to the nuclear spins using the methods of STIRAP and Landau-Zener transitions. However, the drawback of this approach is that it requires very long cavity lifetimes.

To address this problem we propose in Section 2.3 a scheme, which is robust against cavity decay as it *uses* the decaying field of the cavity to achieve the coupling between nuclear spins and the traveling-wave fields: the read-out maps the nuclear state to the output mode of the cavity, while the write-in proceeds by deterministic creation of entanglement between the nuclear spins and the cavity output-mode and subsequent teleportation [42]. Our scheme has several attractive features: the very long nuclear spin lifetimes make the nuclei attractive for storing quantum information [40] and the use of collective states makes it possible to map not just qubits but also multi-photon states. In addition, typical electron spin decoherence processes will be suppressed: the major such process – hyperfine interaction with the lattice nuclear spins [80] – is harnessed to achieve the desired coupling and the influence of other processes is weakened since the electronic states can be adiabatically eliminated from the dynamics. The price for this is a reduction in the speed of the mapping process and the necessity to initialize the nuclear spin ensemble in a highly polarized state. In view of the progress in Dynamical Nuclear Polarization (DNP) experiments (for a review see [36]) with nuclear polarization up to $> 80\%$ [81], the proposed protocol enables the high-fidelity mapping between a (traveling) optical field and the nuclear spin ensemble in a realistic setup.

2.1.1 Reader's guide

The Chapter is organized as follows: In Section 2.2, we introduce the setup: a singly charged quantum dot with highly polarized nuclear spins coupled to an optical cavity. In Section 2.2.1 we sketch the adiabatic elimination that yields the Hamiltonians that describes the effective coupling between light and nuclear spins (a detailed derivation

can be found in Appendix 2.C). In Section 2.3 we discuss the interface between light and nuclear spins of the quantum dot. We investigate the time evolution of the system, the fidelity of both write-in and read-out processes, and the intermediate entanglement properties of the involved systems. Moreover, we show in Section 2.4 that apart from mapping light states to the nuclear spins, the interaction we describe can be used to generate an arbitrary Gaussian state. In Section 2.5 we discuss different aspects concerning the experimental realization and the approximations used in our scheme. We investigate the internal nuclear dynamics, dominated by dipolar interactions, and model the dipolar interaction of a singly charged quantum dot with highly polarized spins numerically. Finally, we discuss corrections to the first order bosonic description. In Appendix 2.A, we introduce a simplified toy model of our system, that also allows for the quantum interface protocol as discussed in Section 2.3. The toy model provides an easier description of our system and might be of interest for the reader who is more interested in the quantum interface protocol than in the specific physical realization. In Appendix 2.B we discuss a physical implementation of the toy model with self-assembled quantum dots that involves mixing of the trion states by a microwave field. This system is experimentally more difficult to realize than the system discussed in Section 2.2. In Appendix 2.D we give a detailed derivation of the adiabatic elimination used and in Appendix 2.E we briefly summarize the main properties of Gaussian states and operations with particular regard to their entanglement.

2.2 The system

We consider a self-assembled III-V quantum dot (QD) with a single conduction-band electron strongly coupled to a high-Q nano-cavity [see Fig. 2.1a)]. At zero magnetic field, the two electronic ground states $|\pm 1/2\rangle$ (s-type conduction band states) are degenerate and the only dipole allowed transitions are to the trion states $|\pm 3/2\rangle$ with spin $+3/2$ and spin $-3/2$ (heavy-hole valence band state) with $\sigma^{\pm}$ polarized light. An external magnetic field B_z in z-direction, perpendicular to the growth (y-) direction (Voigt geometry), Zeeman splits the two electronic states and the trion states and leads to eigenstates $|\pm\rangle = \frac{1}{\sqrt{2}}(|1/2\rangle \pm i\,|-1/2\rangle)$ and $|T_{\pm}\rangle = \frac{1}{\sqrt{2}}(|3/2\rangle \pm i\,|-3/2\rangle)$. The states

$|+\rangle \Leftrightarrow |T_+\rangle$ and $|-\rangle \Leftrightarrow |T_-\rangle$ can be coupled [see Fig. 2.1b)] by horizontally polarized light, and $|+\rangle \Leftrightarrow |T_-\rangle$ and $|-\rangle \Leftrightarrow |T_+\rangle$ by vertically polarized light:

$$\begin{aligned} H_{\text{opt}} = \; & \tfrac{\Omega_c}{2}\left(a^\dagger |-\rangle\langle T_+| + a^\dagger |+\rangle\langle T_-| + \text{h.c.}\right) + \tfrac{\Omega_l}{2}\left(e^{+i\omega_l t}(|+\rangle\langle T_+| + |-\rangle\langle T_-|) + \text{h.c.}\right) \\ & + \omega_c\, a^\dagger a + \omega_{T_+}\, |T_+\rangle\langle T_+| + \omega_{T_-}\, |T_-\rangle\langle T_-| + \omega_e S^z. \end{aligned} \tag{2.1}$$

Here, S^z is the electron spin operator and $a^\dagger$, a are creation and annihilation operators of the single mode cavity field. ω_c, ω_l denote the cavity and the laser frequency (which are vertically/horizontally polarized, respectively) and Ω_c, Ω_l the Rabi frequencies of the cavity and the laser field, respectively. The energies of the trion states $|T_+\rangle$, $|T_-\rangle$ are $\omega_{T_+} = \omega_T + \omega_h/2$ and $\omega_{T_-} = \omega_T - \omega_h/2$ where ω_T is the energy of the trion (without magnetic field), ω_h the energy of the hole Zeeman splitting and $\omega_e = g_e\,\mu_b B_y$ denotes the Zeeman splitting of the electronic states. The first term of the Hamiltonian given by Eqn. (2.1) describes the coupling to the cavity field and the second term the coupling to a classical laser field in the rotating wave approximation. We assume both cavity decay and spontaneous emission rate of the QD to be much smaller than Ω_c and omit both processes in Eqn. (2.1). Besides the coupling to optical fields, the electron spin in a QD also has a strong hyperfine interaction with the lattice nuclear spins, which is for s-type electrons dominated by the Fermi contact term

$$H_{\text{hf}} = \frac{A}{2}(A^+ S^- + S^+ A^-) + A S^z A^z, \tag{2.2}$$

where $S^{\pm,z}$ are the electron spin operators and $A^{\pm,z} = \sum_j \alpha_j I_j^{\pm,z}$ are the collective nuclear spin operators (in a typical GaAs quantum dot, the number of Ga and As nuclei lies between $N \sim 10^4$-10^6). The individual coupling constants α_j are proportional to the electron wave function at site j (and the magnetic dipole moment of the jth nucleus) [80] and are normalized to $\sum_j \alpha_j = 1$. The requirement for using nuclear spins as a quantum memory is to initialize them in a well-defined, highly polarized state. By this we mean that $\langle A^z \rangle$ is close to its minimum value $\langle A^z \rangle_{\text{min}}$ ($\approx -1/2$ for spin-1/2 nuclei) and define the polarization as $P = \langle A^z \rangle \,/\, \langle A^z \rangle_{\text{min}}$. Due to their small magnetic moments, nuclear spins are almost fully mixed even at dilution-fridge temperatures and fields of several Tesla. Over the past years, large progress in Dynamical Nuclear

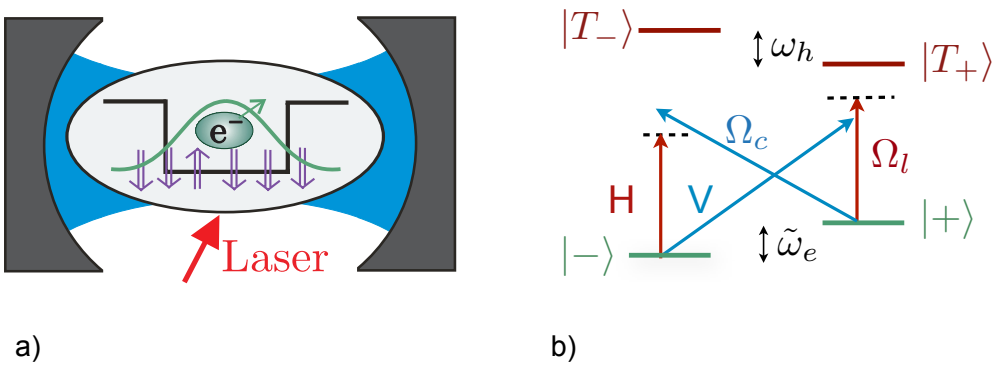

Figure 2.1: a) A singly charged QD coupled to a high-Q optical cavity. b) Level scheme of the QD (Voigt geometry)

Polarization (DNP) experiments (for a review see [36]) has been reported with nuclear polarization up to $> 80\%$ [81].

A convenient and intuitive description of the highly polarized nuclei with homogeneous coupling to the electron is provided by the Holstein Primakoff transformation [82], by which collective nuclear spin operators $A^{\pm,z}$ can be mapped to the bosonic operators b,$b^\dagger$, associating $A^- \rightarrow \frac{1}{\sqrt{N}}\sqrt{1-\frac{b^\dagger b}{N}}\,b$ and $A^z \rightarrow \frac{1}{N}\left(b^\dagger b - \frac{N}{2}\right)$. Assuming high polarization, the electron spin couples to a bosonic "spin wave" described by $A^- = \frac{1}{\sqrt{N}}b$ and $A^z = \frac{1}{N}(b^\dagger b - N/2)$ by a Jaynes-Cummings-like interaction

$$H_{\mathrm{hf}} = \frac{g_n}{2}(b^\dagger S^- + S^+ b) + \frac{g_n}{\sqrt{N}} S^z \left(b^\dagger b - \frac{N}{2}\right), \tag{2.3}$$

with $g_n = A/\sqrt{N}$. The initial state of the nuclear spins is represented by a collection of bosonic modes, with b in the vacuum state. One can generalize this description to the case of inhomogeneous coupling to the electron ($g_n = A\sqrt{\sum_i \alpha_i^2}$) and obtains an identical description in 0th order in $\left\langle \frac{b^\dagger b}{N} \right\rangle = (1-P)/2$ [83]. Corrections to this description arising from inhomogeneous coupling and not fully polarized nuclear spins will be discussed briefly in Section 2.5.2 and a detailed discussion can be found in [84]. It should be noted that the scheme we present does not *require* the bosonic description and could also be discussed directly in terms of the collective spin operators. The Fock basis would be replaced by $(A^+)^n |\downarrow \ldots \downarrow\rangle$ and errors due to the inhomogeneity would have to be treated along the lines of [40] and [78]. The bosonic picture, however, allows

a much more transparent treatment of the corrections to the ideal case, emphasizes the relation to quantum optical schemes, and gives access to the Gaussian toolbox of entanglement criteria and transformations.

2.2.1 Effective coupling between nuclei and cavity

Our aim is to obtain from $H = H_{\rm opt} + H_{\rm hf}$ a direct coupling between nuclear spins and light. The Hamiltonian H describes a complicated coupled dynamics of cavity, nuclei and quantum dot. Instead of making use of the full Hamiltonian (and deriving the desired mapping, e.g., in the framework of optimal control theory) we aim for a simpler, more transparent approach. We adiabatically eliminate [85] (see also Appendix 2.C for a detailed derivation of the adiabatic elimination) the trion and the electronic spin degree of freedom, which leads to a Hamiltonian $H_{\rm el}$ that describes a direct coupling between nuclear spins and light. As explained later, this can be achieved if the couplings (the Rabi frequency of the laser/cavity, the hyperfine coupling, respectively) are much weaker than the detunings to the corresponding transition:

$$\Delta'_{T_\pm} \gg \Omega_l, \Omega_c\sqrt{n}, \tag{2.4}$$

$$\sqrt{\Delta'_{T_\pm}\,\tilde{\omega}_e} \gg \Omega_l, \Omega_c\sqrt{n}, \tag{2.5}$$

$$\tilde{\omega}_e \gg g_n\sqrt{m}. \tag{2.6}$$

Here, $\tilde{\omega}_e = \omega_e - \frac{A}{2}$, $\Delta'_{T_\pm} = \omega_T - \omega_l \pm \omega_h/2 + \tilde{\omega}_e/2 = \Delta' \pm \omega_h/2 + \tilde{\omega}_e/2$ with $\Delta' = \omega_T - \omega_l$, n is the number of cavity photons and m the number of nuclear excitations. Note that typically $\tilde{\omega}_e < \Delta'_{T_\pm}$ such that condition (2.4) becomes redundant. In addition to (2.4)-(2.6), we choose the adjustable parameters such that all first order and second order processes described by H are off-resonant, but the (third order) process in which a photon is scattered from the laser into the cavity while a nuclear spin is flipped down (and its converse) is resonant. This leads to the desired effective interaction.

The idea of adiabatic elimination is to perturbatively approximate a given Hamiltonian by removing a subspace from the description that is populated only with a very low probability due to chosen initial conditions and detunings or fast decay processes. If initially unpopulated states (in our case the trion states and the electronic spin-up

state $|\uparrow\rangle$) are only weakly coupled to the initially occupied states, they remain essentially unpopulated during the time evolution of the system and can be eliminated from the description. The higher order transitions via the eliminated levels appear as additional energy shifts and couplings in the effective Hamiltonian on the lower-dimensional subspace.

The starting point is the Hamiltonian $H = H_{\rm opt} + H_{\rm hf}$ given by Eqns. (2.1) and (2.2). In order to get a time-independent Hamiltonian, we go to a frame rotating with $U^\dagger = \exp\left[-i\omega_l t(a^\dagger a + |T_+\rangle\langle T_+| + |T_-\rangle\langle T_-|)\right]$ and obtain:

$$\begin{aligned} H' &= \frac{\Omega_c}{2}\left(a^\dagger |-\rangle\langle T_+| + a^\dagger |+\rangle\langle T_-| + \text{h.c.}\right) + \frac{\Omega_l}{2}\left(|+\rangle\langle T_+| + |-\rangle\langle T_-|\right) + \text{h.c.}\right) \\ &\quad +\delta\, a^\dagger a + \Delta_{T_+}\,|T_+\rangle\langle T_+| + \Delta_{T_-}\,|T_-\rangle\langle T_-| + \omega_e S^z + H_{hf}, \end{aligned} \tag{2.7}$$

where $\Delta_{T_\pm} = \omega_{T_\pm} - \omega_l$ and $\delta = \omega_c - \omega_l$.

Choosing the cavity and laser frequencies, ω_c and ω_l, far detuned from the exciton transition and the splitting of the electronic states $\tilde{\omega}_e$ much larger than the hyperfine coupling g_n, such that conditions (2.4)-(2.6) are fulfilled, we can adiabatically eliminate the states $|T_\pm\rangle$ and $|+\rangle$. Adiabatic elimination yields a Hamiltonian, that describes an effective coupling between light and nuclear spins

$$\begin{aligned} H_{\rm el} = \; & \tfrac{\Omega_c\Omega_l A}{8\Delta'_{T_+}\tilde{\omega}_e}(aA^+ + \text{h.c.}) + \tfrac{\Omega_c\Omega_l A}{8\Delta'_{T_-}\tilde{\omega}_e}(aA^- + \text{h.c.}) + \omega_1 a^\dagger a - \tfrac{A}{2}\delta A^z \\ & - \tfrac{A^2}{4\tilde{\omega}_e}A^+A^- + T_{\rm nl}, \end{aligned} \tag{2.8}$$

where the energy of the photons $\omega_1 = \delta - \frac{\Omega_c^2}{4\Delta'_{T_+}} + \frac{\Omega_l^2}{4\Delta'^2_{T_-}}\delta$ and the energy of the nuclear spin excitations $\sim -\frac{A}{2N} - \frac{A^2}{4N\tilde{\omega}_e}$. By $T_{\rm nl}$ we denote the nonlinear terms

$$T_{\rm nl} = \frac{A^3}{8\tilde{\omega}_e^2}A^+\delta A^z A^- + \frac{A^2}{4\tilde{\omega}_e^2}\delta a^\dagger a A^+A^- + \frac{\Omega_c^2\delta}{4\Delta'^2_{T_+}}a^\dagger a^\dagger a a, \tag{2.9}$$

which are small ($\|T_{\rm nl}\| \ll \frac{\Omega_c\Omega_l A}{8\Delta'\tilde{\omega}_e}$) in the situation we consider ($\delta \ll \Omega_c, g_n/\tilde{\omega_z} \sim \Omega_l/\Delta'_{T_+,T_-} \ll 1$) and neglected in the following. We also neglect the nuclear Zeeman term which is of order 10^{-3} smaller than the Zeeman energy of the electron. In the bosonic description of the nuclear spins that we introduced in Eqn. (2.3), the Hamiltonian given by Eqn. (2.8) reads

$$H_{\rm eff} = g_1(ab^\dagger + \text{h.c.}) + g_2(ab + \text{h.c.}) + \omega_1 a^\dagger a + \omega_2 b^\dagger b, \tag{2.10}$$

with coupling strengths g_1 and g_2 given by

$$g_1 = \frac{\Omega_c \Omega_l g_n}{8\Delta'_{T_+}\tilde{\omega}_e}, \quad g_2 = \frac{\Omega_c \Omega_l g_n}{8\Delta'_{T_-}\tilde{\omega}_e}. \tag{2.11}$$

The energy of the nuclear spin excitations can now be written as $\omega_2 = -\frac{A}{2N} - \frac{g_n^2}{4\tilde{\omega}_e}$. The first term in the Hamiltonian is a beamsplitter type interaction $\sim (ab^\dagger + \text{h.c.})$ whereas the second term is a two-mode squeezing type interaction $\sim (ab + \text{h.c.})$. Both interactions can be made dominant by choosing the resonance condition to be either $\omega_1 = \omega_2$ or $\omega_1 = -\omega_2$. This will be discussed in detail in the following and illustrated numerically.

First, we validate the adiabatic elimination by a numerical simulation which compares the evolution of states Ψ_{20} (where the first subscript indicates the number of photons and the second the number of nuclear excitations) [under the condition $\omega_1 = \omega_2$, see Fig. 2.2] and Ψ_{00} [under the condition $\omega_1 = -\omega_2$, see Fig. 2.3] under the full Hamiltonian given by Eqn. (2.7) to the evolution under the eliminated Hamiltonian given by Eqn. (2.10). The solid lines show the evolution under the full Hamiltonian H', the dashed lines under the eliminated Hamiltonian H_{eff} and we find that H' is well approximated by H_{eff}, and that the nonlinear terms T_{nl} can indeed be neglected.

For the simulation, we choose the parameters as follows: we assume a hole g-factor $g_h = -0.31$ and an electron g-factor $g_e = 0.48$ [86]; the number of nuclei $N = 10^4$, the hyperfine coupling constant $A = 100\mu eV$, the laser and cavity Rabi frequency $\Omega_c = \Omega_l = 15\mu eV$, the detuning of the trion $\Delta' = 1000\mu eV$, the effective Zeeman splitting of the electronic states $\tilde{\omega}_e = 13.9\mu eV$ (the magnetic field in x-direction is 4T) and the Zeeman splitting of the hole $\omega_h = -71.8\mu eV$. With these parameters, the conditions given by (2.4)-(2.6) are fulfilled and values $g_1 = 2.1 \cdot 10^{-3}\mu$eV and $g_2 = 1.9 \cdot 10^{-3}\mu$eV are obtained. We assume full nuclear (spin-down) polarization and use the bosonic description.

As already mentioned, two distinct resonance conditions are chosen in Figs. 2.2 and 2.3, leading to different dynamics of the system:

For resonant exchange of excitations between the two systems, we choose $\omega_1 = \omega_2$, where the tuning can be done by changing $\delta = \omega_c - \omega_l$. Then H_{eff} describes a

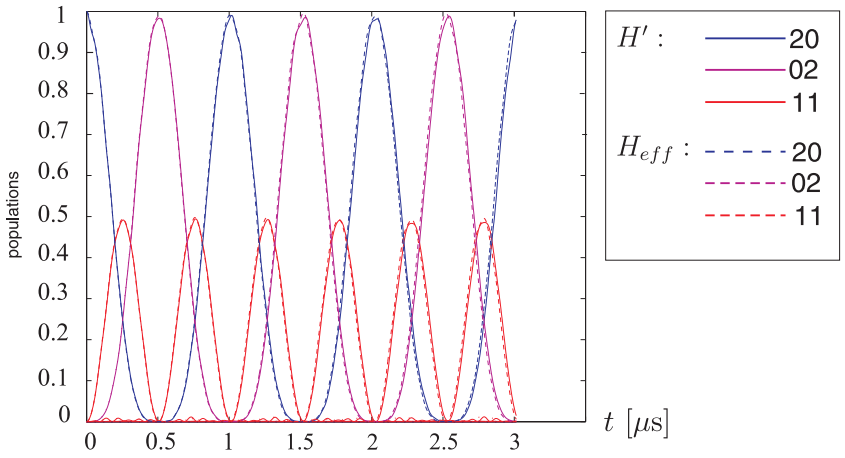

Figure 2.2: Evolution of the two-photon Fock state ψ_{20} under the full Hamiltonian H' (solid lines) and the eliminated Hamiltonian H_{eff} (dashed lines) tuning the energies such that $\omega_1 = \omega_2$ (beamsplitter-type interaction). Populations in the states ψ_{00}, ψ_{10}, ψ_{01}, ψ_{12}, ψ_{21}, ψ_{33} are plotted here but not mentioned in the plot legend as they are small.

beamsplitter-like coupling of the modes a and b and the effective interaction is described by

$$H_{\text{bs}} = g_1(ab^\dagger + \text{h.c.}) + \omega_1 a^\dagger a + \omega_2 b^\dagger b. \tag{2.12}$$

Processes in which absorption (or emission) of a cavity photon is accompanied by a nuclear spin excitation are resonant, whereas the squeezing interaction given by $g_2(a^\dagger b^\dagger + ab)$ is off-resonant. This can be seen going to a frame rotating with ω_1: g_2 is rotating with $2\omega_1$ and as $2\omega_1 \gg g_2$, the squeezing type interaction is off resonant.

Tuning the energies such that $\omega_1 = -\omega_2$, the creation of a nuclear spin excitation is accompanied by scattering of a laser photon *into* the cavity, i.e. the effective coupling becomes $g_2(a^\dagger b^\dagger + ab)$ and the beamsplitter-type interaction $g_1(ab^\dagger + a^\dagger b)$ is off-resonant. The driving laser now facilitates the *joint* creation (or annihilation) of a spin excitation and a cavity photon, realizing a two-mode squeezing Hamiltonian

$$H_{\text{sq}} = g_2(a^\dagger b^\dagger + ab) + \omega_1 a^\dagger a + \omega_2 b^\dagger b. \tag{2.13}$$

The plots in Figs. 2.2 and 2.3 illustrate that the dynamics of the system can indeed be approximated by Eqn. (2.12) and Eqn. (2.13). To simulate the beamsplitter type

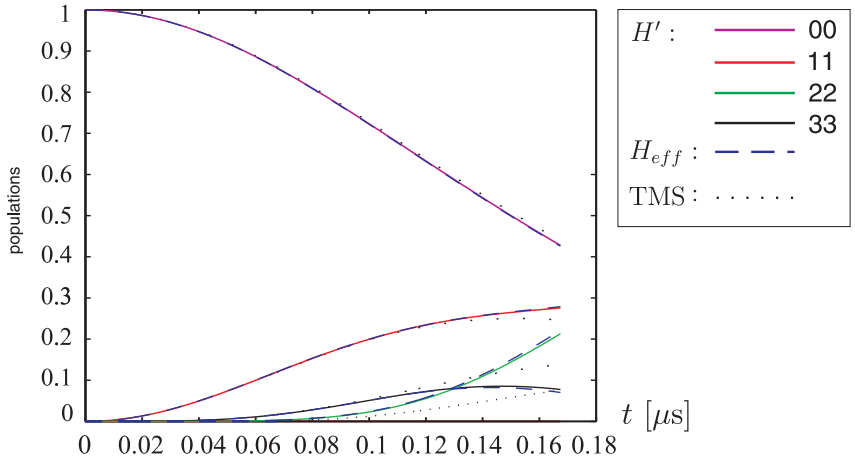

Figure 2.3: Evolution of the state ψ_{00} under the full Hamiltonian H' (solid lines) and the eliminated Hamiltonian H_{eff} (dashed blue lines) tuning the energies such that $\omega_1 = -\omega_2$ (squeezing interaction). The dotted black lines show the evolution under exact two-mode squeezing (TMS) (up to $n = 3$).

coupling given by Eqn. (2.12), we choose $\omega_1 = \omega_2$ and let the two-photon Fock state ψ_{20} evolve under the Hamiltonian given by Eqn. (2.10) [see dashed lines in Fig. 2.3]. Almost perfect Rabi-oscillations can be seen between the two-photon Fock state ψ_{20} and the state with two nuclear spin excitations ψ_{02}, showing that $g_2(a^\dagger b^\dagger + \text{h.c.})$ in Eqn. (2.10) can indeed be neglected. To simulate the squeezing-type interaction we choose $\omega_1 = -\omega_2$ and study the evolution of the state ψ_{00} under the Hamiltonian given by Eqn. (2.10) [see dashed blue lines in Fig. 2.3]. It can be seen that the state ψ_{00} evolves into the states ψ_{11}, ψ_{22} and ψ_{33} with coupling strengths $g_2\sqrt{n}$, depending on the number of excitations n. We have thus shown, that in this case, the beamsplitter-type interaction can indeed be neglected. For simplicity, we restricted the number of photons and nuclear excitations to 3 in our simulation, such that states ψ_{44} and higher excitation states do not occur and the evolution of the states ψ_{22} and ψ_{33} does only correspond to its evolution in a space with higher excitation numbers at very short times. This can be seen comparing the evolution to the exact two-mode squeezing which generates the state $\sqrt{1-\tanh^2(g_2 t)}\sum_{n=0}^{\infty}\tanh^n(g_2 t)\,|nn\rangle$ for which the populations up to $n = 3$ are plotted in Fig. 2.3 (dotted black lines).

2.3 Quantum interface

Now we will discuss how a quantum interface between light and nuclear spins can be realized with the physical system introduced so far. Note that the discussion in the following is also valid for a simplified toy model (and its physical implementation involving mixing of the trion states by a microwave field) as discussed in Appendix 2.A and 2.B, respectively. The toy model might be useful for the reader who is more interested in the quantum interface protocol than in the specific physical realization. The discussion in the following is valid for all three models introduced in Section 2.2 and the Appendixes 2.A and 2.B, as the Hamiltonians that are relevant for the quantum interface, H_{sq} and H_{bs}, given by Eqns. (2.13) and (2.59) and Eqns. (2.12) and (2.57) respectively, are of the same form for all three models. As the physical implementation that we discuss in Section 2.2 is significantly easier to realize in an experiment than the setup discussed in Appendix 2.B, we will in the following refer to this model.

The Hamiltonians H_{bs} and H_{sq} describe a direct coupling of light to the nuclear spins. Now, the obvious route to a quantum interface is via the beam-splitter Hamiltonian H_{bs}: acting for a time $t = \pi/g$ it maps $a \to ib$ and $b \to ia$ thus realizing (up to a phase) a swap gate between cavity and nuclear spins. This and related ideas are explored in my diploma thesis and in our publication [87]. There are two practical problems with this approach: Compared to the effective coupling, present-day cavities are "bad" with cavity life time $\tau_{\mathrm{cavity}} \ll 1/g$, i.e., the cavity field will decay before its state can be mapped to the nuclei. Moreover, it is notoriously difficult to couple quantum information into high-Q cavities, although proposals exist [63] that address this issue. Both problems can be circumvented for our system by two key ideas: (i) to include the field modes into which the cavity decays in the description and (ii) to realize write-in via quantum teleportation. We will show in the following that it is possible to create entanglement between nuclei and the traveling-wave *output* field of the cavity. Then, quantum teleportation can be used to write the state of another traveling-wave light field onto the nuclear spins (Fig. 2.4) [1]. This approach gives an active role to

[1] This maps the state up to a random (but known) displacement. It can be undone using H_{bs}, where the cavity is pumped with strong coherent light for a short time [88].

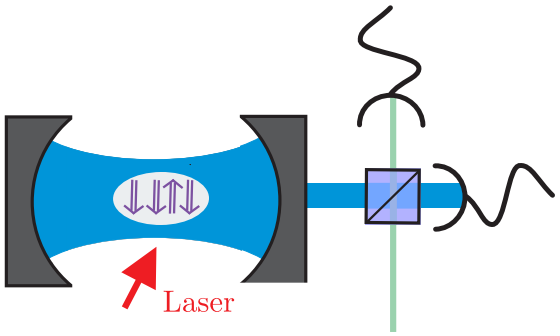

Figure 2.4: Quantum teleportation can be used to write the state of a traveling-wave light field onto the nuclei.

cavity decay in the interface and can tolerate a bad effective cavity as long as strong coupling is achieved in Eqn. (2.7). Moreover, it does not require to couple the quantum information into the cavity. Similarly $H_{\rm bs}$ [Eqn. (2.12)] enables read-out, by writing the state of the nuclei to the output field of the cavity. The entanglement between nuclear spins and output field can moreover be used to entangle nuclear spins in two distant cavities by interfering the output light of the cavities at a beamsplitter (Fig. 2.5).

2.3.1 Entangling nuclei with the output field

The Hamiltonian of the nuclear spin-cavity system tuned to the squeezing interaction in Eqn. (2.13) (and Eqn. (2.59) of the toy model which is of the same form) and coupled to the environment is given by

$$H = g_2(a^\dagger b^\dagger + ab) + ia\int\sqrt{\frac{\gamma}{2\pi}}c_\omega^\dagger\, d\omega + \text{h.c.} + \int \omega c_\omega^\dagger c_\omega d\omega, \tag{2.14}$$

where c_ω are the annihilation operators of the bath and γ the cavity decay constant. We have specialized (Eqn. (2.13)) to the case $\omega_1 = -\omega_2$ and transformed to an interaction picture[2] with $H_0 = \omega_1(a^\dagger a - b^\dagger b) + \omega_1\int c_\omega^\dagger c_\omega d\omega$ and performed the rotating-wave and Markov approximations in the description of the cavity decay [89]. The quantum

[2] As was already the case in (Eqn. (2.13)) all optical operators are also taken in a frame rotating with the laser frequency ω_l.

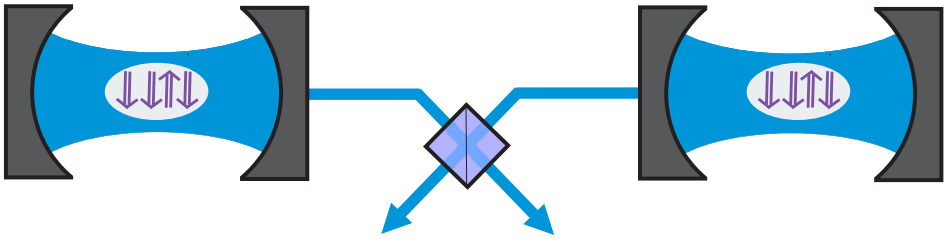

Figure 2.5: Nuclear spins of quantum dots in two distant cavities can be entangled by interfering the traveling wave output fields of the two cavities at a beamsplitter and measuring.

Langevin equations of cavity and nuclear operators read

$$\dot{a}(t) = -ig_2\, b^\dagger(t) - \frac{\gamma}{2}a(t) - \sqrt{\gamma}c_{\text{in}}(t) \tag{2.15}$$

$$\dot{b}(t) = -ig_2\, a^\dagger(t). \tag{2.16}$$

Here, c_{in} describes the vacuum noise coupled into the cavity and satisfies $[c_{\text{in}}(t), c_{\text{in}}^\dagger(t')] = \delta(t-t')$. The solutions of Eqn. (2.15) and Eqn. (2.16) are given (for $t \geq 0$) by

$$a(t) = p_-(t)a(0) + q(t)b^\dagger(0) + \sqrt{\gamma}\int_0^t p_-(t-\tau)c_{\text{in}}(\tau)d\tau \tag{2.17}$$

$$b(t) = q(t)a^\dagger(0) + p_+(t)b(0) + \sqrt{\gamma}\int_0^t q(t-\tau)c_{\text{in}}^\dagger(\tau)d\tau \tag{2.18}$$

where

$$p_\pm = e^{-\frac{1}{4}t\gamma}\left[\cosh(\nu t) \pm \tfrac{\gamma}{4\nu}\sinh(\nu t)\right], \tag{2.19}$$

$$q = -i\tfrac{g_2}{\nu}e^{-\frac{1}{4}\gamma t}\sinh\nu t, \tag{2.20}$$

with

$$\nu = \sqrt{\left(\frac{\gamma}{4}\right)^2 + g_2^2}. \tag{2.21}$$

While Eqns. (2.17) and (2.18) describe a non-unitary time-evolution of the open cavity-nuclei system, the overall dynamics of system plus surrounding free field given by the Hamiltonian in Eqn. (2.14) is unitary. Moreover, it is Gaussian (see Appendix 2.E), since all involved Hamiltonians are quadratic. Since all initial states are Gaussian

(vacuum), the joint state of cavity, nuclei, and output fields is a pure Gaussian state at all times as well. This simplifies the analysis of the dynamics and in particular the entanglement properties significantly: The covariance matrix [defined by Eqn. (2.82) in Appendix 2.E] of the system allows us to determine the entanglement of one part of the system with another one. In particular, we are interested in the entanglement properties of the nuclei with the output field.

The covariance matrix $\Gamma_{\text{ns-c-o}}$ of the pure Gaussian state of nuclear spins, cavity and output field and thus the covariance matrix $\Gamma_{\text{ns-o}}$ of the reduced nuclei-output field system can be found by analyzing the covariance matrix of the cavity-nuclei system $\Gamma_{\text{ns-c}}$.

The elements $\langle X \rangle$ of the covariance matrix $\Gamma_{\text{ns-c}}$ can be calculated by solving the Lindblad equation evaluated for the expectation values $\langle X \rangle$

$$\frac{d}{dt}\langle X\rangle = i\langle [H_{\text{sq}}, X]\rangle + \frac{\gamma}{2}\left(\left\langle 2a^\dagger X a\right\rangle - \left\langle X a^\dagger a\right\rangle - \left\langle a^\dagger a X\right\rangle\right). \tag{2.22}$$

We thus find the covariance matrix of the cavity-nuclei system to be

$$\Gamma_{\text{ns-c}} = \begin{pmatrix} m & 0 & 0 & k \\ 0 & m & k & 0 \\ 0 & k & n & 0 \\ k & 0 & 0 & n \end{pmatrix}, \tag{2.23}$$

where

$$m = e^{-\frac{\gamma t}{2}}\left[\frac{\gamma}{\nu}\sinh(2\nu t) + \left(\frac{g_2^2}{\nu^2} + \frac{\gamma^2}{8\nu^2}\right)\cosh(2\nu t) + \frac{g_2^2}{\nu^2}\right] - 1, \tag{2.24}$$

$$n = 1 + 32\frac{g_2^2}{\nu^2}e^{-\frac{\gamma t}{2}}\sinh(\nu t)^2, \tag{2.25}$$

$$k = e^{-\frac{\gamma t}{2}}\left[\frac{g_2\gamma}{2\nu^2}\sinh(\nu t)^2 + \frac{g_2}{\nu}\sinh(2\nu t)\right]. \tag{2.26}$$

According to [90] there exists a symplectic transformation S (see Appendix 2.E such that $\Gamma_{\text{D}} = S\Gamma_{\text{ns-c}}S^T = \text{diag}(\lambda_1^s, \lambda_1^s, \lambda_2^s, \lambda_2^s)$ where $\{\lambda_1^s, \lambda_2^s\}$ are the symplectic eigenvalues of $\Gamma_{\text{ns-c}}$. This allows us to calculate the covariance matrix of the pure nuclei-cavity-output field system

$$\Gamma_{\text{ns-c-o}} = S'\Gamma_{\text{D'}}(S'^{-1})^T \tag{2.27}$$

with $\Gamma_{\mathrm{D}'}$ in 2×2 block-matrix form

$$\Gamma_{\mathrm{D}'} = \begin{pmatrix} \cosh(2r_1)\mathbb{1}_2 & & \sinh(2r_1)\sigma_z & \\ & \cosh(2r_2)\mathbb{1}_2 & & \sinh(2r_2)\sigma_z \\ \sinh(2r_1)\sigma_z & & \cosh(2r_1)\mathbb{1}_2 & \\ & \sinh(2r_2)\sigma_z & & \cosh(2r_2)\mathbb{1}_2 \end{pmatrix}, \tag{2.28}$$

where $\cosh r_1 = \lambda_1^s$ and $\cosh r_2 = \lambda_2^s$ and $S' = \begin{pmatrix} S & \\ & \mathbb{1}_{4\times 4} \end{pmatrix}$. One of the symplectic eigenvalues $\{\lambda_1^s, \lambda_2^s\}$ is 1, indicating a pure - and therefore unentangled - mode in the system. That implies that there is a *single* "output mode" in the out-field of the cavity to which the cavity-nuclear–system is entangled and we can thus trace out the unentangled output mode.

The procedure for entangling the nuclei with the output field (write-in) is: let H_{sq} act for time t_1 to create a two-mode squeezed state $\psi(g_2, t_1)$: nuclei entangled with cavity and output field. To obtain a state in which the nuclei are only entangled to the output field, we switch the driving laser off ($g_2 = 0$) and let the cavity decay for a time $t_2 \gg \tau_{\mathrm{cav}}$, obtaining an almost pure two-mode squeezed state of nuclei and the output mode. We define the coupling as

$$g_t = \begin{cases} g_2, t < t_1 0, t \geq t_1 \end{cases} \tag{2.29}$$

For the parameters used in Section 2.2.1, $g_2 \sim 1.9 \cdot 10^{-3} \mu$eV.

The entanglement of the different subsystems can be quantified: We compute the Gaussian entanglement of formation (gEoF) [91] of the reduced covariance matrix of the nuclei-output field–system to quantify the entanglement of the nuclei with the output field (see Fig. 2.6). For a Gaussian state $\rho_{(\gamma,d)}$ the gEoF $E_G(\rho_{(\gamma,d)})$ is defined as the minimal amount of average entanglement in a decomposition of $\rho_{(\gamma,d)}$ *into Gaussian states*, i.e. $E_G(\rho_{(\gamma,d)}) = \min\{\int_{\gamma',d'} dp(\gamma', d') E(\rho_{(\gamma',d')}) : \rho_{(\gamma,d)} = \int_{\gamma',d'} dp(\gamma', d') \rho_{(\gamma',d')}\}$ [91]. Thus $E_G(\rho_{(\gamma,d)})$ measures how costly it is (in terms of entanglement) to prepare $\rho_{(\gamma,d)}$ by mixing Gaussian states and gives an upper bound to the Entangelement of Formation (EoF). In the present case, it coincides with the logarithmic negativity [92]. The entanglement of the pure cavity-nuclei-output mode–system can be quantified using

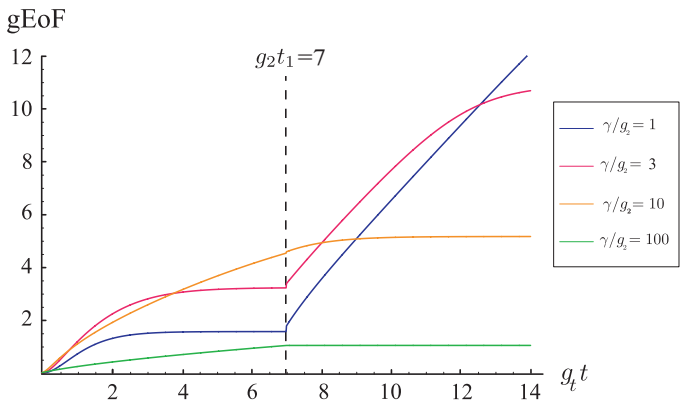

Figure 2.6: Plot of the Gaussian entanglement of formation (gEoF) of the nuclei with the output field vs t for different values of γ/g. At $g_2t_1 = 7$ the coupling is switched off. The curve saturates when all excitations have leaked out of the cavity.

the entanglement entropy S_E [93]. We plot S_E for the nuclei-cavity system with the output mode [see Fig. 2.7a)] and of the nuclei with the cavity-output mode–system [see Fig. 2.7b)]. The entanglement is plotted versus g_2t for different ratios of the cavity decay constants and the coupling, γ/g_2.

2.3.2 Write-in: Teleportation channel

The entangled state between nuclei and the cavity output field allows us to map a state of a traveling light field to the nuclei using teleportation (see Fig. 2.4) [42].

To realize the teleportation, a Bell measurement has to be performed on the output mode of the cavity and the signal state to be teleported. This is achieved by sending the two states through a 50:50 beam splitter and measuring the output quadratures [42]. To be able to do this, we need to know B_0, the output mode of the cavity. In the following, we derive an exact expression for this mode.

We fix a time t and denote by $B(y,t)$, $y \in \mathbb{N}$ a complete set of bath modes outside the cavity. $B(y,t)$ can be expressed as a superposition of bath operators $c(x,t)$

$$B(y,t) = \int z(y,x,t)c(x,t)dx \tag{2.30}$$

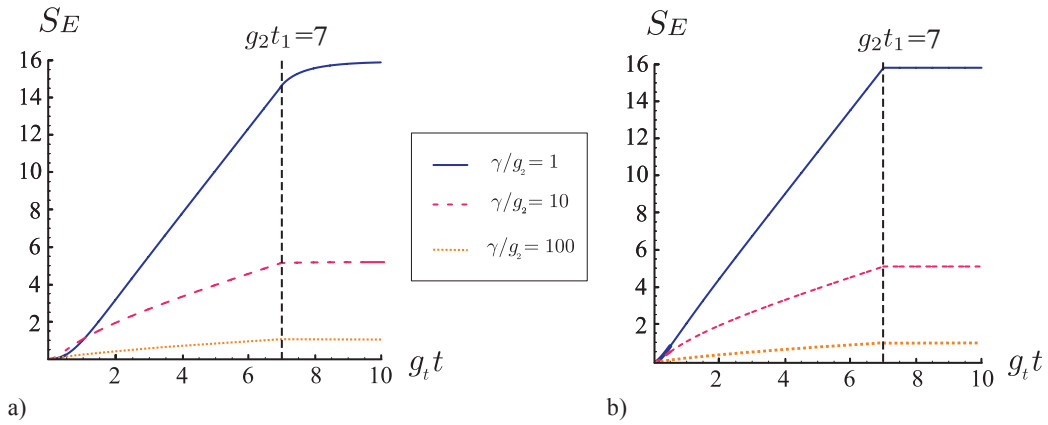

Figure 2.7: a) Plot of the entanglement entropy S_E of the nuclei+cavity with the output field vs t for different values of γ/g. At $g_2t_1 = 7$ the coupling is switched off. b) Plot of the entanglement entropy S_E of the nuclei with the cavity+output field vs g_2t for different values of γ/g_2.

where we introduce a complete set of orthonormal mode functions $z(y, x, t)$. The bath operators $c(x, t)$ are known from the input-output relations [89]

$$c(x,t) = \frac{\sqrt{\gamma}}{2} a(t-x)\chi_{[0,t]}(x), \tag{2.31}$$

where $a(t)$ is given by Eqn. (2.17) and

$$\chi_{[0,t]}(x) = \begin{cases} 1, & 0 \le x \le t \\ 0, & x < 0,\ x > t \end{cases} . \tag{2.32}$$

To calculate $B(y, t)$ we thus need to determine $z(y, x, t)$. This can be done, calculating the variance $\left\langle c^\dagger(x,t), c(x',t)\right\rangle = \left\langle c^\dagger(x,t)c(x',t)\right\rangle - \left\langle c^\dagger(x,t)\right\rangle \left\langle c(x',t)\right\rangle$ following two different pathways: With Eqn. (2.31) we find

$$\left\langle c^\dagger(x,t), c(x',t)\right\rangle = \frac{\gamma}{4} q(t-x')q(t-x)^*, \tag{2.33}$$

where $q(t)$ is given by Eqn. (2.20). Another way to express $c(x, t)$ follows from Eqn. (2.30):

$$c(x,t) = \sum_y z(y,x,t)^* B(y,t). \tag{2.34}$$

As shown in Section 2.3.1 there exists only one output mode which we label $y = 0$. This mode contains all the output photons. Therefore $\left\langle B(y,t)^\dagger B(y',t)\right\rangle = K\,\delta_{y0}\delta_{y'0}$ and the variance using Eqn. (2.34) reads

$$\left\langle c^\dagger(x,t), c(x',t)\right\rangle = K\, z(0,x,t)z(0,x',t)^*. \tag{2.35}$$

Comparing Eqn. (2.33) to Eqn. (2.35) we find

$$z(0,x,t) = \frac{q(t-x)^*}{\sqrt{\int |q(t-x)|^2 dx}} \tag{2.36}$$

and $K = \frac{\gamma}{4}\sqrt{\int |q(t-x)|^2 dx}$ and we have thus fully determined $B(0,t)$ (see Fig. 2.10). Note that the bath modes are given in a frame rotating with $\omega_1 + \omega_l$ to which we transformed in Section 2.2 (ω_l) and Section 2.2.1 (ω_1).

Therefore a state of a traveling light field can be teleported to the nuclear spins up to a random displacement that arises from the teleportation protocol [94, 42]. The random displacement can be undone, letting the beam-splitter interaction H_{bs} [given by Eqn. (2.12)] act for a short time, while pumping the cavity with intense coherent light as suggested in [88].

Next, we want to consider the quality of the teleportation. Whereas before (see Figs. 2.6 and 2.7) the time evolution of the system for a fixed switch-off time $g_2 t_1 = 7$ was considered, we now consider the "final" entangled state of nuclei and output field depending on $g_2 t_1$, where the cavity has decayed to the vacuum state while the nuclei are (still) stationary.

The fidelity with which a quantum state can be teleported onto the nuclei is a monotonic function of the two-mode squeezing parameter

$$r_1 = \frac{1}{2}\mathrm{arccosh}(m(t = t_1)) \tag{2.37}$$

with m defined in Eqn. (2.24). A typical benchmark [95] is the average fidelity with which an arbitrary coherent state can be mapped. This fidelity has a simple dependence on the two-mode squeezing parameter r_1 of the state used for teleportation and is given by [96]

$$F_{\mathrm{tel}} = \frac{1}{1 + e^{-2r_1}}. \tag{2.38}$$

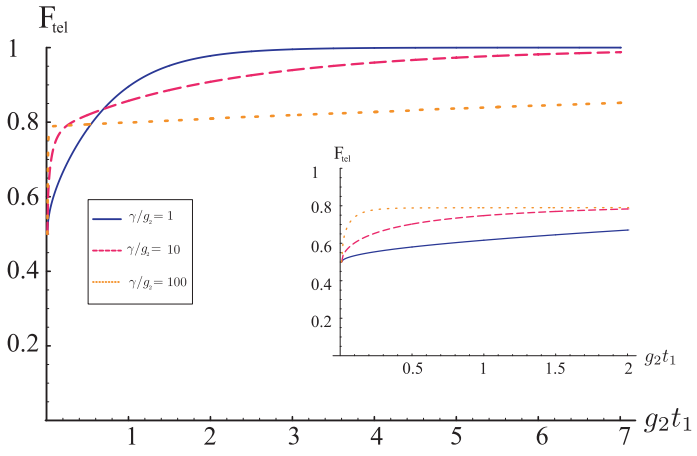

Figure 2.8: Plot of the teleportation fidelity vs $g_2 t_1$ for different values of γ/g_2.

We plot the teleportation fidelity dependent on the switch-off time t_1 (see Fig. 2.8).

Already for $r_1(t_1) \sim 1$ fidelities above 0.8 are obtained. After switching off the coupling we have to wait for the cavity to decay which typically happens on a nanosecond timescale and does not noticeably prolong the protocol.

2.3.3 Read-out

The beamsplitter Hamiltonian $H_{\rm bs}$ [given by Eqn. (2.12)] enables read-out of the state of the nuclei by writing it to the output field of the cavity. The quantum Langevin equations of cavity and nuclear operators lead to almost identical solutions as for $H_{\rm sq}$ [see Eqns. (2.17) and (2.18)]: of course, now $a(t)$ is coupled to $b(t)$ instead of $b^\dagger(t)$ but the only other change to Eqn. (2.17) and (2.18) is to replace ν by

$$\tilde{\nu} = \sqrt{(\gamma/4)^2 - g_1^2}. \tag{2.39}$$

This has the effect that all terms in Eqns. (2.17) and (2.18) show exponential decay with t. The decay of the slowest terms $\sim e^{-2\frac{g_1^2}{\gamma}t}$ sets the timescale for read-out. To calculate the read-out fidelity, we need to know the state of the output field at time $t = T$. We assume that the state we want to read-out is a coherent state with displacement $\alpha_{\rm ns}$ at time $t = 0$ fully described by its covariance matrix $\gamma_b(0) = \mathbb{1}$ and its displacement $d_b(0) = \langle b \rangle = \alpha_{\rm ns}$ (while cavity and output field are in the vacuum state at $t = 0$). As

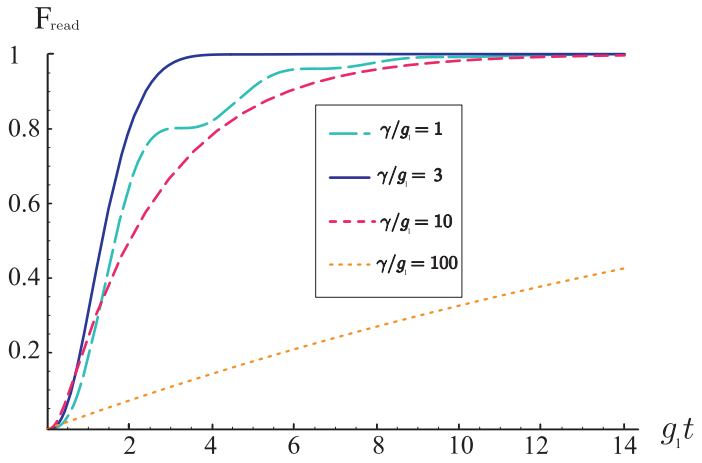

Figure 2.9: Plot of the read-out fidelity vs $g_1 t$ for different values of γ/g_1

the norm of the displacement $\|d(t)\|$ of the nuclei-cavity-output system

$$d(t) = \begin{pmatrix} d_a(t) \\ d_b(t) \\ d_{B_0}(t) \end{pmatrix} = \begin{pmatrix} \langle a(t) \rangle \\ \langle b(t) \rangle \\ \langle B_0(t) \rangle \end{pmatrix} \tag{2.40}$$

does not change under the beamsplitter transformation, the displacement of the output mode B_0 is given by

$$\begin{aligned} |d_{B_0}(t)| &= \sqrt{\|d(0)\|^2 - d_a(t)^2 - d_b(t)^2} \\ &= \sqrt{1 - (|q(t)|^2 + |p_+(t)|^2)}|\alpha_{\rm ns}| \end{aligned} \tag{2.41}$$

where $q(t)$ and $p_+(t)$ are defined by Eqn. (2.19) and (2.20) with ν replaced by $\tilde{\nu}$.

At finite times, the nuclear excitations and the cavity have not fully decayed which leads to a loss of amplitude of the mapped state. The loss is very small for sufficiently large T. To assure high fidelity even for states with large photon number, we can amplify the output field [97]. Then the state of the output field is $(\gamma_{B_0}, d_{B_0}) = (\kappa \mathbb{1}, \alpha_{\rm ns})$. This leads to a read-out fidelity (see Fig. 2.9) given by

$$F_{\rm read} = \ |\langle\, \mathbb{1}, \alpha_{\rm ns} \mid \kappa \mathbb{1}, \alpha_{\rm ns} \,\rangle|^2 = 1 - (|q|^2 + |p_+|^2),$$

where we have used relations for the transition amplitudes given by [98].

2.3.4 Output mode

In Fig. 2.10 we plot the output mode of the cavity given by Eqn. (2.30) for write-in and read-out, respectively, and for several choices of the parameters $g_{1,2}$ and γ. We are considering here only the idealized case of a one-sided and one-dimensional cavity. In general, the actual geometry of the cavity at hand has to be taken into account to determine B_0. In the following we briefly discuss the shape of the mode-function. It provides some insight into the dynamics of the mapping process, since due to (2.31) the weight of $c(x,T)$ in $B(0,t)$ reflects the state of the cavity mode at time $t-x$ in the past.

Write-in: Let us consider the two extreme cases of very strong and very weak cavity decay. In the former case ($\gamma \gg g_2$) the cavity mode can be eliminated, i.e., the nuclear spins couple directly and with constant strength $\sim g_2^2/\gamma$ to the output field: z_0 is a stepfunction which is 0 for $g_2 = 0$ and constant otherwise. This is reflected in Fig. 2.10, where for $\gamma = 100 g_2$ most of the excitations decay directly to the outputmode such that z_0 takes a "large" value at the time the squeezing is switched on and then increases only slowly in time. After switching the squeezing interaction off the cavity quickly decays to the vacuum. For $\gamma \ll g_2$, instead, two-mode squeezing builds up in the nuclei–cavity system as long as the squeezing interaction is on (3μs in Fig. 2.10) and after g_2 is switched off the cavity decays to its standard exponential output mode. The intermediate cases in Fig. 2.10a) show the shifting weight between "initial step-function" and subsequent exponential decay.

Read-out: In the case of the beamsplitter interaction, the same cases can be distinguished. For large γ/g_1, the cavity can be eliminated and the nuclear spins are mapped directly to the exponential output mode of a cavity decaying with an effective rate g_1^2/γ. For smaller γ, the output mode reflects the damped free evolution of the nuclei–cavity system, which in this case includes oscillations (excitations are mapped back and forth between nuclei and cavity at rate g_1) in absolute value and phase.

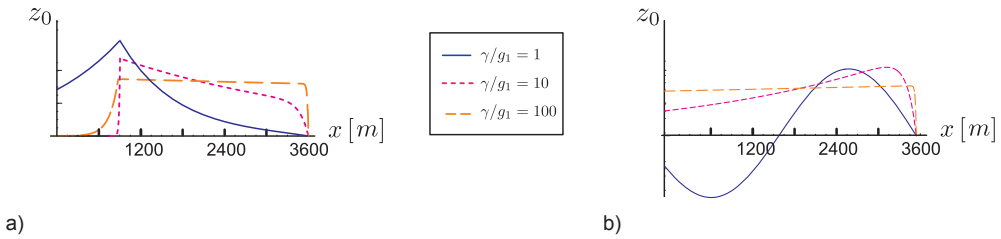

Figure 2.10: The output mode in one dimension: Plot of z_0 vs position x, where $x = 0$ is the position of the cavity a) Write-in: The squeezing interaction is "on" for 3μs and then switched off. b) Read-out: For $\gamma \gg g_2$ the excitations do not have fully decayed to the output mode after $t = 12\mu$s. The read-out fidelity given by Eqn. (2.42) corresponds to the probability that the excitations in the nuclear spins have decayed into the output mode of the cavity. For $\gamma/g_1 = 1$ and $\gamma/g_1 = 10$ the read-out fidelity is $F_{\text{read}} > 0.98$ after $t \approx 16 - 20\mu$s. For $\gamma/g_1 = 100$ however, it takes $\approx 200\mu$s to achieve $F_{\text{read}} > 0.98$. Note that for input and output modes to have similar shapes (e.g. for a network), it is best to consider the case where $\gamma/g_1 \gg 1$.)

2.4 Linear Optics with the nuclear spin mode

The interaction we have described can not only be used to **map** states to the nuclear spin ensemble but also for **state generation** and transformation. In fact, from a nuclear spin mode in the vacuum state, all single mode Gaussian states can be prepared. To see this, we have to show how any desired 2×2 correlation matrix Γ and displacement $d \in \mathbb{C}$ can be obtained.

As we remarked already when discussing the write-in via teleportation, the beam-splitter Hamiltonian H_{bs} can be used to realize displacements of the nuclear mode. Driving the cavity mode with a strong laser to a coherent state with amplitude α (and the same phase as d) and switching on H_{bs} for a time $t = |\beta|/(g_1|\alpha|)$ provides in the limit of large α a good approximation to the displacement operation by β [88].

Concerning the CM, we use that every CM of a pure Gaussian state is of the form $\Gamma = ODO^T$, where D is a positive diagonal matrix with determinant one and O is orthogonal and symplectic. O can be seen as the effect of time evolution under some

quadratic Hamiltonian acting on the single-mode squeezed state with CM D. In the single mode case, any O represents a phase shift and is obtained by letting the nuclear system evolve "freely" (without laser coupling, i.e. a polarized electron interacts off-resonantly with the nuclei) according to the Hamiltonian $\propto b^\dagger b$ for some time. Thus the state with CM Γ can be generated in a two-step process: first generate the state with $\Gamma = D$, then apply O.

While in the preceding paragraphs we could show how to realize *operations* that can act on any input state, no such possibility seems to exist for squeezing in our context. Instead we show how to obtain the pure single mode squeezed state with CM D from the vacuum state. Letting H_{sq} act on the vacuum results in a two-mode squeezed state with squeezing parameter r_2. Performing a homodyne measurement (of the X quadrature) on the optical part of this state projects the nuclear system into a squeezed state with squeezing $r_1 = \ln[\cosh(2r_2)]/2$ [99], thus given enough two-mode squeezing, any CM D can be produced.

One can go even further and *simulate* evolution according to any quadratic Hamiltonian on the nuclear-optical system: According to [100], the Hamiltonian given by Eqn. (2.10) with the interaction part $g_1 ab^\dagger + g_2 a^\dagger b^\dagger + \mathrm{h.c.}$ enables simulation of any Hamiltonian quadratic in $a, b, a^\dagger, b^\dagger$.

2.5 Remarks on internal nuclear dynamics and approximations

With regard to the realization of the proposed protocol and the applicability of the approximations leading to the Hamiltonians given by Eqns. (2.12) and (2.13) there are three aspects to consider: spontaneous emission of the quantum dot, the internal nuclear dynamics and errors in the bosonic description. We assume the strong coupling limit of cavity-QED and neglect spontaneous emission of the quantum dot. The other two aspects will be studied in the following. Note that the results on the internal nuclear dynamics are corroborated by independent work of Kurucz *et al.* [101]. They introduce the bosonic description to analyze the performance of a nuclear spin quantum

memory and show that the performance of the memory is enhanced due to a detuning between excitations in the mode b versus those in other modes $b_{k\neq 0}$ and that secular dipolar terms do not affect the memory.

2.5.1 Internal nuclear dynamics

Up to now, we have focused exclusively on the hyperfine interaction and neglected "internal" nuclear dynamics, dominated by dipolar and quadrupolar interactions. Moreover, the hyperfine coupling leads to a dipolar interaction between nuclei mediated by the electron. We study the dipolar interaction between nuclear spins which is significantly weaker than g_n, g_1 and g_2: the energy scale for dipolar interaction between two nuclei has been estimated $\sim 10^{-5}\mu$eV for GaAs [80]. However, since for $10^4 - 10^6$ nuclei there are many of these terms, they might play a role at the $10-50\mu$s time scales considered.

Dipolar interaction

The Hamiltonian of the direct dipolar interaction between N nuclei is given by [102]

$$H_{dd} = -\frac{\mu_0}{4\pi}\frac{1}{2}\sum_{i=1}^{N}\sum_{j\neq i=1}^{N}\frac{\mu_i\mu_j}{I_i I_j}\frac{1}{r_{ij}^3}\left(\frac{3(\mathbf{I}_i\mathbf{r}_{ij})(\mathbf{I}_j\mathbf{r}_{ij})}{r_{ij}^2} - \mathbf{I_i}\mathbf{I_j}\right), \tag{2.42}$$

where $\mathbf{r}_{ij}$ is the vector connecting spins i and j and $\boldsymbol{\mu}_i = (\mu_i/I_i)\mathbf{I}_i$ is the magnetic moment of the nuclear spin operator $\mathbf{I}_i$. H_{dd} can be written as

$$H_{dd} = \sum_{i=1}^{N}\sum_{j\neq i=1}^{N}\tilde{\gamma}_{ij}[A_{ij}I_i^zI_j^z + B_{ij}I_i^+I_j^- + (C_{ij}I_i^+I_j^+ + D_{ij}I_i^zI_j^- + \text{h.c.})] \tag{2.43}$$

where $A_{ij} = 1 - 3\cos^2\theta_{ij}$, $B_{ij} = -\frac{1}{2}(1 - 3\cos^2\theta_{ij})$, $C_{ij} = -\frac{3}{4}\sin^2\theta_{ij}e^{-2i\phi_{ij}}$, $D_{ij} = -\frac{3}{2}\sin\theta_{ij}\cos\theta_{ij}e^{i\phi_{ij}}$ and $\tilde{\gamma}_{ij} = \mu_0\mu_i\mu_j/4\pi r_{ij}^3$. In GaAs the nearest-neighbor dipolar interaction strength is around $\tilde{\gamma} = 10^{-5}\mu$eV [80]. We want to calculate the strength of the dipolar interaction between the main bosonic mode (that is defined as the mode that is coupled to the electron spin) and other bath modes (here, we no longer assume homogeneous coupling of the nuclei to the electron). We therefore write the Hamiltonian in terms of collective nuclear spin operators, use, in a next step, the bosonic approximation and finally separate the relevant terms (the ones which couple the main

bosonic mode to bath modes) and calculate the coupling strength of the main mode to the bath modes.

For highly polarized nuclear spins, the first term of H_{dd} can be written as

$$\sum_{i=1}^{N}\sum_{j\neq i=1}^{N}\tilde{\gamma}_{ij}A_{ij}I_i^zI_j^z \approx \frac{1}{2}\sum_{i=1}^{N}\sum_{j\neq i=1}^{N}\tilde{\gamma}_{ij}A_{ij}\left(\frac{1}{2}-I_i^+I_i^- - I_j^+I_j^-\right),$$

where we write $I_i^z = -1/2 + I_i^+I_i^-$ and neglect the second order term $I_i^+I_i^-I_j^+I_j^-$ which requires two excitations to be non-zero; thus in the highly polarized case the contribution from these terms is by a factor of $p = (1-P)/2$ smaller than the terms we keep. The last term is (for spin 1/2-nuclei)

$$\sum_{i=1}^{N}\sum_{j\neq i=1}^{N}\tilde{\gamma}_{ij}D_{ij}I_i^zI_j^- \approx -\frac{1}{2}\sum_{i=1}^{N}\sum_{j\neq i=1}^{N}\tilde{\gamma}_{ij}D_{ij}I_j^-,$$

neglecting higher order terms. In extension to the definition of the collective operators $A^{\pm}$ in Section 2.2, which we now label $A_0^{\pm}$, we introduce a complete set of collective operators $A_k^- = \sum_i \alpha_i^{(k)}I_i^-$ with $k = 0,..,N-1$ with an orthogonal set of coefficients $\alpha_i^{(k)}$ for which $\sum_i \alpha_i^k = 1$ for every collective mode k. Defining a unitary matrix U with columns $\boldsymbol{\alpha}^{(k)} = \left(1/\sqrt{\sum_i \alpha_i^{(k)2}}\right)\left(\alpha_1^{(k)},..,\alpha_N^{(k)}\right)^T$ we can write

$$(I_1^-,..,I_N^-)^T = U\mathbf{A}^- \tag{2.44}$$

where $\mathbf{A}^- = \mathrm{diag}\left(\frac{1}{\sqrt{\sum_i \alpha_i^{(0)^2}}},..,\frac{1}{\sqrt{\sum_i \alpha_i^{(N-1)^2}}}\right)(A_0^-,..,A_{N-1}^-)^T$. Writing H_{dd} in terms of the collective operators $A_k^{-,+}$ and neglecting higher order terms,

$$H_{dd} = \mathbf{A}^+U^\dagger SU\mathbf{A}^- + (\mathbf{A}^-U^\dagger MU\mathbf{A}^- - \frac{1}{2}DU\mathbf{A}^- + \mathrm{h.c.}). \tag{2.45}$$

Here, $M_{ij} = \tilde{\gamma}_{ij}C_{ij}$ for $i \neq j$, $M_{ij} = 0$ for $i = j$, $S_{ij} = \tilde{\gamma}_{ij}B_{ij}$ for $i \neq j$ and $S_{ii} = \sum_{l=1}^{N}\tilde{\gamma}_{il}A_{il}$ for $i = j$. D is a vector with entries $D_j = \sum_{i\neq j=1}^{N}\tilde{\gamma}_{ij}D_{ij}$. Next, we write H_{dd} in terms of bosonic operators, using the bosonic approximation introduced in Section 2.2, and map $\mathbf{A}^- \longrightarrow \mathbf{b} = (b_0,..,b_{N-1})^T$. This allows to separate relevant terms of H_{dd}, which couple the main bosonic mode b_0 to other (bath) modes b_k. Isolating the terms containing b_0, we find

$$\begin{aligned} b_0\left[\textstyle\sum_{k\neq 0}(U^\dagger 2MU)_{0k}b_k + (U^\dagger SU)_{0k}b_k^\dagger - \frac{1}{2}D_kU_{0k}\right] + \mathrm{h.c.} \\ +(U^\dagger SU)_{00}b_0^\dagger b_0 + (U^\dagger 2MU)_{00}b_0b_0 + \mathrm{h.c.}, \end{aligned} \tag{2.46}$$

where the notation $(U^\dagger SU)_{0l}$ denotes the element $(0,l)$ of the matrix $U^\dagger SU$. The first term describes the passive coupling of the main mode b_0 to other modes b_k and acquires a factor of two as the terms that describe the active coupling in Eqn. (2.46) can be written $b_l(U^\dagger MU)_{lk}b_k + b_k(U^\dagger MU)_{kl}b_l = b_l(U^\dagger 2MU)_{lk}b_k$ as $(U^\dagger MU)_{kl} = (U^\dagger MU)_{lk}$: the entries of U are real so that $(U^\dagger)^T = U$ and $M = M^T$, i.e., $M_{ij} = -\tilde{\gamma}_{ij}\frac{3}{4}\sin^2\theta_{ij}e^{-2i\phi_{ij}} = M_{ji}$ as $\phi_{ji} = \pi + \phi_{ij}$. The second term in Eqn. (2.46) describes the passive coupling of b_0 to the modes $b_k^\dagger$ and the third term displaces the main mode. The last two terms describe a constant energy shift ($\sim b_0^\dagger b_0$) and a squeezing term ($\sim b_0 b_0 + \text{h.c.}$), respectively.

The terms that couple the main mode b_0 to bath modes can be written as

$$\begin{aligned} & b_0\left(\textstyle\sum_{k\neq 0}(U^\dagger 2MU)_{0k}b_k + (U^\dagger SU)_{0k}b_k^\dagger - \frac{1}{2}D_kU_{0k}\right) + \text{h.c.} \\ & \quad = b_0\left(c_1\tilde{b}_1 + c_2\tilde{b}_2^\dagger - \tfrac{1}{2}\textstyle\sum_{k\neq 0}D_kU_{0k}\right) + \text{h.c.} \end{aligned} \tag{2.47}$$

where the linear combinations of bosonic modes b_k, $b_k^\dagger$ can be transformed to bosonic modes $\tilde{b}_1$ and $\tilde{b}_2^\dagger$. The coupling strength of b_0 to the first term in Eqn. (2.47) is given by

$$\begin{aligned} [c_1\tilde{b}_1, (c_1\tilde{b}_1)^\dagger] \quad & = |c_1|^2 = \textstyle\sum_{k\neq 0}|(U^\dagger 2MU)_{0k}|^2 \\ & = (U^\dagger 4MM^\dagger U)_{00} - |(U^\dagger 2MU)_{00}|^2 = (\Delta M_0)^2, \end{aligned} \tag{2.48}$$

and $|c_2|^2 = (\Delta S_0)^2$ for the second term. ΔM_0 and ΔS_0 depend only on the electron wave function and the lattice geometry. To numerically calculate ΔM_0 and ΔS_0 and the effect of the last two terms in Eqn. (2.46), we consider the case where the nuclei lie in a 2-dimensional square plane with length $R = \sqrt{N}r_0$ of each side on a grid with equal spacings r_0 (=0.24nm in GaAs [80]) [see Fig. 2.11a)]. Consequently, $\theta_{ij} = \pi/2$, which simplifies many expressions in H_{dd}. These assumptions can be made as the height of the QD is small compared to its diameter, so that the variation of θ that is dependent of the height of the QD is small, $\theta_{ij} \approx \pi/2$.

To illustrate our results we consider two simple choices for the electron wavefunction such that $\alpha_l^{(0)} = \frac{1}{\sum_l f_{1/2}(\mathbf{r}_l)}f_{1/2}(\mathbf{r}_l)$ with $\mathbf{r}_l = (x_l, y_l)$,

$$f_1(\mathbf{r}_l) = \cos\left(\frac{\pi}{2}\frac{x_l}{R}\right)^2 \cdot \cos\left(\frac{\pi}{2}\frac{y_l}{R}\right)^2, \tag{2.49}$$

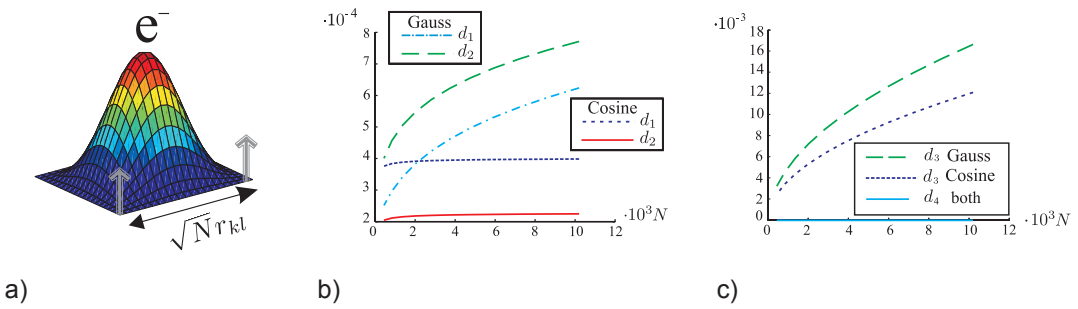

a) b) c)

Figure 2.11: a) Cosine-shaped wavefunction of the electron on a 2-dimensional square grid with the nuclear spins located at the vertex points, b) plot of the ratios $d_1 = \frac{\tilde{\gamma}(\Delta M_0)}{g_2}$ and $d_2 = \frac{\tilde{\gamma}(\Delta S_0)}{g_2}$ for a cosine and a Gaussian shaped wave function. For $N = 10^4$, both ratios d_1 and d_2 are on the order of 10^{-4}, together with c), we see that the dipolar interaction is negligible. c) plot of the ratios $d_3 = \frac{\tilde{\gamma}(U^\dagger SU)_{00}}{g_2}$ and $d_4 = \frac{\tilde{\gamma}(U^\dagger 2MU)_{00}}{g_2}$ for a cosine and a Gaussian shaped wave function. For $N = 10^4$, d_3 is on the order of 10^{-2} and d_4 is zero due to the symmetry of the electron wavefunction.

and

$$f_2(\mathbf{r}_l) = \exp\left(-\sqrt{2}r_l^2/R^2\right). \tag{2.50}$$

To show that the direct dipolar interaction is a weak effect compared to the optical-nuclear coupling g, we calculate the ratios

$$d_1 = \frac{\tilde{\gamma}(\Delta M_0)}{g_2} = \frac{\tilde{\gamma}(\Delta M_0)}{\frac{\Omega_c\Omega_l g_n}{8\Delta'_{T_-}\tilde{\omega}_e}} = \frac{8\Delta'_{T_-}\tilde{\omega}_e}{\Omega_c\Omega_l}\frac{\tilde{\gamma}}{A}\frac{(\Delta M_0)}{\sqrt{\sum_{i=1}^N \alpha_i^{(0)2}}}. \tag{2.51}$$

and $d_2 = \frac{\tilde{\gamma}\Delta S_0}{g_2}$. For the parameters used for the simulation in Section 2.2.1, $\frac{8\Delta'_{T_-}\tilde{\omega}_e}{\Omega_c\Omega_l}\frac{\tilde{\gamma}}{A} \approx 4\cdot 10^{-5}$ with $\tilde{\gamma}$ for GaAs [80]. A plot of d_1 and d_2 is shown in Fig. 2.11b). d_1 and d_2 are both on the order of $10^{-4} - 10^{-5}$, for $N > 1000$ nuclear spins and increase slowly with N. The last two terms in Eqn. (2.46), $(U^\dagger SU)_{00}b_0^\dagger b_0$ and $(U^\dagger 2MU)_{00}b_0 b_0$ are small and zero, respectively, as can be seen in Fig. 2.11c): The ratio of $d_3 = \frac{\tilde{\gamma}(U^\dagger SU)_{00}}{g_2}$ is on the order of $10^{-3} - 10^{-2}$ for $N > 1000$ nuclear spins and the ratio $d_4 = \frac{\tilde{\gamma}(U^\dagger 2MU)_{00}}{g_2}$ is zero due to the symmetry of the electron wavefunction in this setting. Shifting the electron wavefunction such that it is not longer symmetric with respect to the coordinate origin, d_4 is on the order of 10^{-4}. We assume that the nuclei lie in a plane, so there is no

displacement of b_0 as $D_{ij} = 0$ for $\theta_{ij} = \frac{\pi}{2}$. Therefore, we have shown, that direct dipolar coupling is an effect that does not affect our protocol.

The hyperfine coupling between electron spin and nuclear spins leads to a *mediated* dipolar interaction between nuclear spins [103]. In the bosonic description, the electron couples solely to the b_0 mode, thus, the mediated coupling leads only to an energy shift

$$\frac{g_n^2}{4\tilde{\omega}_e} b_0^\dagger b_0 \tag{2.52}$$

that depends on the Zeeman splitting $\tilde{\omega}_e$ and the number of nuclear excitations. This was already present in Eqn. (2.10) and is not affecting the protocol, in fact it can help as Kurucz et al. [104] showed.

For spin-1/2 systems, as considered here, the quadrupolar interaction is not present. For large spin I (e.g. 3/2 or 9/2) nuclei present in GaAs, there is a significant quadrupolar term. Depending on the strain, up to $g_q \lesssim 10^{-2}\mu$eV have been measured [38]. Therefore, for $I > 1/2$, dots with small strain have to be considered. The quadrupolar interaction [102] can be treated on a similar footing as the dipolar coupling.

2.5.2 Errors in the bosonic picture

We have relied on a simple bosonic description of the collective nuclear excitations and neglected all corrections to that simplified picture. For homogeneous coupling (α_j =const) this is the well-known Holstein-Primakoff approximation [82] and for systems cooled to a dark state [105] at moderate polarization ($\langle A^z \rangle$ on the order of $-1/2$) spin, replacing the collective spin operators by bosonic operators is accurate to $o(1/N)$. The generic inhomogeneous case is discussed in detail in [84]. In that case, the Hamiltonian given by Eqn. (2.3) can be seen as a zeroth order approximation in a small parameter $\sim q(1-P)$, where $q \geq 1/2$ and $q = 1/2$ for a homogeneous wave function. The first-order correction analyzed in [84] contains two contributions: (i) a polarization dependent scaling of the coupling-strength g_n which has negligible effect on the adiabatic transfer we consider and (ii) an effective coupling of b to bath modes due to the inhomogeneity of the A^z term. This correction can be computed similarly to the one in the preceding subsections by rewriting A^z in terms of bosonic operators. The

coupling strength of the leading term is found to be $\sim A/N = g_n/\sqrt{N}$ and is thus much weaker than $g_{1/2}$. Since $g_{1/2}$ also characterizes the energy splitting between different excitation-manifolds in the Jaynes-Cummings system, this term is further suppressed by energy considerations.

2.6 Summary and Conclusions

We have shown how to realize a quantum interface between the polarized nuclear spin ensemble in a singly charged quantum dot and a traveling optical field. The coupling is mediated by the electron spin and the mode of a high-Q optical cavity to which the quantum dot is strongly coupled. Our proposal exploits the strong hyperfine and cavity coupling of the electron to eliminate the electronic degree of freedom and obtain an effective coupling between cavity and nuclei. We have presented an interface between light and nuclear spins which is robust to cavity decay. Read-out is achieved via cavity decay while write-in is based on the generation of two-mode squeezed states of nuclei and output field and teleportation. For typical values of hyperfine interaction and cavity lifetimes, several ebit of entanglement can be generated before internal nuclear dynamics becomes non-negligible. All proposed schemes take advantage of the bosonic character of the nuclear system at high polarization, which implies that all the relevant dynamics of nuclei, cavity and output field is described by quadratic interactions. This allows the analytical solution of the dynamics and a detailed analysis of the entanglement generated. We show that apart from mapping a light state to the nuclei, the couplings described enable the preparation of arbitrary Gaussian states of the nuclear mode.

For highly polarized nuclear spin systems the bosonic description provides a very convenient framework for the discussion of (dipolar and quadrupolar) "internal" nuclear dynamics. It is seen that these processes do not appreciably affect the performance of the interface.

Our results give further evidence that nuclear spins in quantum dots can be a useful system for quantum information processing. In view of the recent impressive experimental progress in both dynamical nuclear polarization of quantum dots and quantum dot cavity-QED, their use for QIP protocols may not be too far off.

2.A System: Toy model

Here, we present a simplified model of the system that also allows for the realization of a quantum interface as discussed in Section 2.3. Note that the selection rules in QDs often make it necessary to consider more complicated level schemes than the simplified Λ-system described by the toy model. One example for a more complicated level scheme is the setup discussed in Section 2.2. The toy model is a simplified model for the reader who is interested more in the quantum interface protocol in general than in the specific physical system. In Section 2.B we present a physical implementation of the toy model, that is, however, more difficult to realize experimentally than the scheme discussed in Section 2.2. Note, that the Hamiltonians describing the effective couplings between light and nuclear spins are the same for all three setups in Section 2.2 and in the Appendixes 2.A and 2.B. Therefore the quantum interface protocol applies to all three setups.

Here, we consider a self-assembled QD charged with a single conduction-band electron, whose spin-states $|\uparrow\rangle, |\downarrow\rangle$ are split in a magnetic field. For clarity we consider a simplified model, in which both electronic states are coupled by electric dipole transitions to the same charged exciton (trion) state $|X\rangle$ in a Λ-configuration, see Fig. 2.12. We assume that the QD is strongly coupled to a high-Q nano-cavity [76]. The two transitions are, respectively, off-resonantly driven by the cavity mode (frequency ω_c) and a laser of frequency ω_l, see Fig. 2.12, described by the Hamiltonian

$$H_{\text{opt}} = \left(\frac{\Omega_c}{2}\, a^\dagger \; |\downarrow\rangle\langle X| + \frac{\Omega_l}{2}\, e^{+i\omega_l t}\, |\uparrow\rangle\langle X| + \text{h.c.} \right) + \omega_c\, a^\dagger a + \omega_X\, |X\rangle\langle X| + \omega_z S^z, \quad (2.53)$$

where $\hbar = 1$, Ω_l, Ω_c are the Rabi frequencies of laser and cavity fields, $a^\dagger$, a are the cavity photons, ω_X denotes the trion energy, ω_z the Zeeman splitting of the electronic states and $S^z = 1/2(|\uparrow\rangle\langle\uparrow| - |\downarrow\rangle\langle\downarrow|)$.

As explained in detail in Section 2.2 the electron spin in a QD has a strong hyperfine interaction with the lattice nuclear spins given by Eqn. (2.2). As previously discussed, the highly polarized nuclear spins with homogeneous coupling to the electron spin can be mapped to bosonic operators. The coupling of the electron spin to the collective nuclear bosonic mode is described by H_{hf} given by Eqn. (2.3).

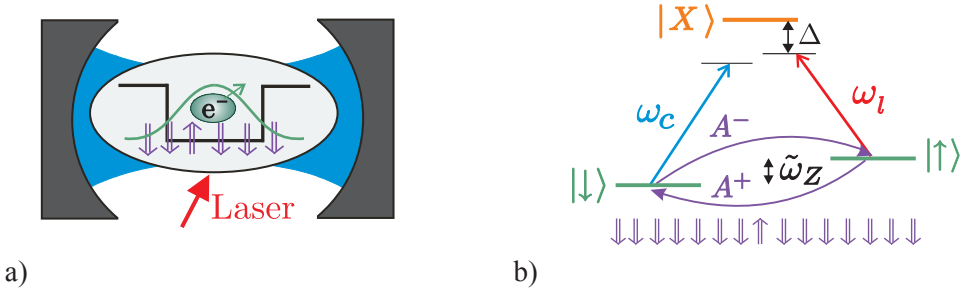

a) b)

Figure 2.12: a) Singly charged QD coupled to high-Q optical cavity. b) Level scheme of the QD. Optical and hyperfine transitions.

2.A.1 Coupling cavity and nuclear spins

The excitonic levels can again be eliminated (as explained in Section 2.2.1) to obtain an effective Hamiltonian that describes a direct coupling between nuclear spins and light. This can be achieved if the couplings (the Rabi frequency of the laser/cavity, the hyperfine coupling, respectively) are much weaker than the detunings to the corresponding transition:

$$\Delta' \gg \Omega_l, \Omega_c\sqrt{n}, \tag{2.54a}$$

$$\sqrt{\Delta'\,\tilde{\omega}_z} \gg \Omega_l, \Omega_c\sqrt{n}, \tag{2.54b}$$

$$\tilde{\omega}_z \gg g_n\sqrt{m}. \tag{2.54c}$$

Here, $\Delta' = \omega_X - \omega_l + \tilde{\omega}_z/2$ is the detuning, n is the number of cavity photons, and m the number of nuclear excitations. Note that typically $\tilde{\omega}_z < \Delta'$ such that condition (2.54a) becomes redundant. In addition to (2.54a-2.54c), we choose the adjustable parameters such that all first order and second order processes described by H are off-resonant, but the (third order) process in which a photon is scattered from the laser into the cavity while a nuclear spin is flipped down (and its converse) is resonant. This leads to the desired effective interaction.

The starting point is the Hamiltonian $H = H_{\text{opt}} + H_{\text{hf}}$ given by Eqns. (2.53) and (2.2). In order to get a time-independent Hamiltonian, we go to a frame rotating with

$U^\dagger = \exp\left[-i\omega_l t(a^\dagger a + |X\rangle\langle X|)\right]$:

$$H' = \frac{\Omega_c}{2}(a^\dagger |\downarrow\rangle\langle X| + \text{h.c.}) + \frac{\Omega_l}{2}(|\uparrow\rangle\langle X| + \text{h.c.}) + \delta a^\dagger a + \tilde{\omega}_z S^z + \frac{A}{2}(A^+S^- + S^+A^-) + AS^z\delta A^z + \Delta\,|X\rangle\langle X|\,, \tag{2.55}$$

with detunings $\Delta = \omega_X - \omega_l$ and $\delta = \omega_c - \omega_l$.

Choosing the cavity and laser frequencies, ω_c and ω_l, far detuned from the exciton transition and the splitting of the electronic states $\tilde{\omega}_z$ much larger than the hyperfine coupling g_n, such that conditions (2.54a-2.54c) are fulfilled, we can adiabatically eliminate the states $|X\rangle$, $|\downarrow\rangle$. A detailed derivation of the adiabatic elimination can be found in Appendix 2.C. This yields a Hamiltonian, that describes an effective coupling between light and nuclear spins

$$H_{el} = \frac{\Omega_c\Omega_l A}{8\Delta'\tilde{\omega}_z}(aA^+ + \text{h.c.}) + \omega_1 a^\dagger a + \omega_2 N\delta A^z + T_{nl}, \tag{2.56}$$

where the energy of the photons $\omega_1 = \delta - \frac{\Omega_c^2}{4\Delta'}$ and the energy of the nuclear spin excitations $\omega_2 = -\frac{A}{2N} - \frac{A^2}{4N\tilde{\omega}_z}$. By T_{nl} we denote the nonlinear terms $T_{nl} = \frac{A^3}{8\tilde{\omega}_z^2}A^+\delta A^z A^- + \frac{\Omega_c^2 A}{8\Delta'^2}a^\dagger a\delta A^z + \frac{A^2}{4\tilde{\omega}_z^2}\delta a^\dagger a A^+A^- + \frac{\Omega_c^2\delta}{4\Delta'^2}a^\dagger a^\dagger aa$, which are small ($\|T_{nl}\| \ll \frac{\Omega_c\Omega_l A}{8\Delta'\tilde{\omega}_z}$) in the situation we consider ($\delta \ll \Omega_c, g_n/\tilde{\omega}_z \sim \Omega_l/\Delta' \ll 1$) and neglected in the following. In the bosonic description of the nuclear spins that we introduced in Eqn. (2.3) the Hamiltonian given by Eqn. (2.56) then reads

$$H_{bs} = g(ab^\dagger + \text{h.c.}) + \omega_1 a^\dagger a + \omega_2 bb^\dagger, \tag{2.57}$$

with coupling strength g given by

$$g = \frac{\Omega_c\Omega_l g_n}{8\Delta'\tilde{\omega}_z}. \tag{2.58}$$

The energy of the nuclear spin excitations can now be written as $\omega_2 = -\frac{A}{2} - \frac{g_n^2}{4\tilde{\omega}_z}$. For resonant exchange of excitations between the two systems, we choose $\omega_1 = \omega_2$. Then H_{bs} describes a beamsplitter-like coupling of the modes a and b. Processes in which absorption (or emission) of a cavity photon is accompanied by a nuclear spin flip are resonant, and we have thus derived the desired effective interaction between light and nuclear spins. Since $\sqrt{\Omega_c\Omega_l/(\Delta'\tilde{\omega}_z)} \ll 1$ the effective coupling g is typically $2-3$ orders of magnitude smaller than the hyperfine coupling g_n.

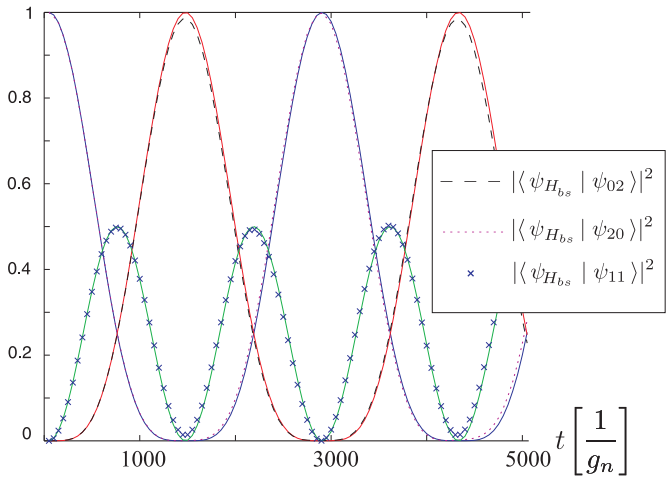

Figure 2.13: Evolution of the two-photon Fock state ψ_{20} under the full Hamiltonian H' (solid lines) and Hamiltonian H_{bs} ($\times$, dashed and dotted lines), where the trion and the electronic spin-up state have been eliminated.

To illustrate the validity of the adiabatic elimination and the approximations leading to Eqn. (2.57), we have simulated the evolution of the two-photon Fock state ψ_{20} (the first subscript denotes the number of photons, the second the number of nuclear spin excitations) under the full Hamiltonian H' given by Eqn. (2.55) and compared it to the evolution under the Hamiltonian H_{bs} given by Eqn. (2.57). We assume full nuclear spin-down polarization and the validity of the bosonic description. In the simulation, we choose $\Omega_l = \Omega_c$, $\Omega_l/\Delta = 1/10$, $\Omega_l^2/(\Delta\tilde{\omega}_z) = 1/100$ and $g_n/\tilde{\omega}_z = 1/50$, such that the conditions given by Eqns. (2.54a)-(2.54b) are fulfilled. Fig. 2.13 shows, that H' is well approximated by H_{bs}, and that the nonlinear terms T_{nl} can be neglected. Almost perfect Rabi-oscillations between the two-photon Fock state ψ_{20} and the state with two nuclear spin excitations ψ_{02} can be seen in Fig. 2.13. For ψ_{01}, the adiabatic elimination is an even better approximation to the full Hamiltonian as the nonlinear terms T_{nl} and the conditions (2.54a)-(2.54c) depend on the excitation number.

In the process leading to the beamsplitter coupling, a photon is scattered from the cavity into the laser mode while a nuclear spin excitation is created (and vice versa). If we interchange the role of laser and cavity field (i.e., the laser drives the $|\downarrow\rangle \leftrightarrow |X\rangle$ transition and the cavity couples to $|\uparrow\rangle$) then creation of a nuclear spin excitation is

accompanied by scattering of a laser photon *into* the cavity, i.e. the effective coupling becomes $a^\dagger b^\dagger + ab$. Tuning the energies such that $\omega_1 = -\omega_2$, the driving laser now facilitates the *joint* creation (or annihilation) of a spin excitation and a cavity photon, realizing a two-mode squeezing effective Hamiltonian

$$H_{\mathrm{sq}} = g(a^\dagger b^\dagger + ab) + \omega_1 a^\dagger a + \omega_2 b b^\dagger. \tag{2.59}$$

Here, the energy of the photons is $\omega_1 = \delta\left(1 + \frac{\Omega_c^2}{4\Delta'^2}\right)$, the energy of the nuclear spin excitations is $\omega_2 = -\frac{A}{2N} - \frac{g_n^2}{4\tilde{\omega}_z}$, and the nonlinear terms are now given by $T_{nl} = \frac{g_n^2}{4\tilde{\omega}_z^2}\frac{A}{2N} b^\dagger b^\dagger b b + \frac{g_n^2}{4\omega_z^2}\delta a^\dagger a b^\dagger b$. As before, they are much smaller than g and can be neglected for low excitation number. To be able to freely switch between H_{bs} and H_{sq} simply by turning on and off the appropriate lasers, both the "driven" and the empty mode should be supported by the cavity.

2.B Physical implementation of the toy model

Here, we discuss a physical implementation of the toy model and its performance as a quantum interface. Quantum dots generally have a richer level structure than the Λ scheme of the toy model depicted in Fig. 2.12. This and the applicable selection rules imply that H_{opt} is not exactly realized. Here, we take this into account and discuss a setting that allows to realize the desired coupling. In contrast to the physical setup discussed in Section 2.2, the setup in the following requires a microwave field to mix the states of the trion. The setup explained in Section 2.2 avoids the need of an additional microwave field at the expense of additional couplings (which have to be kept off-resonant) as explained in Section 2.2.

We now consider the two spin states $|\Downarrow\rangle, |\Uparrow\rangle$ of the trion in addition to the two electronic spin states. We focus on a setup where these states are Zeeman split by an external magnetic field in growth/z-direction (Faraday geometry). The electronic state $|\uparrow\rangle$ is coupled to $|\Uparrow\rangle$ (with angular momentum $+3/2$) by σ^+ circularly polarized light (and $|\downarrow\rangle$ to $|\Downarrow\rangle$ with σ^--polarized light). We can stimulate these transitions by a σ^+-polarized cavity field and a σ^--polarized classical laser field, respectively, but this will not lead to a Λ scheme, see Fig. 2.14a. The cleanest way to obtain the desired coupling

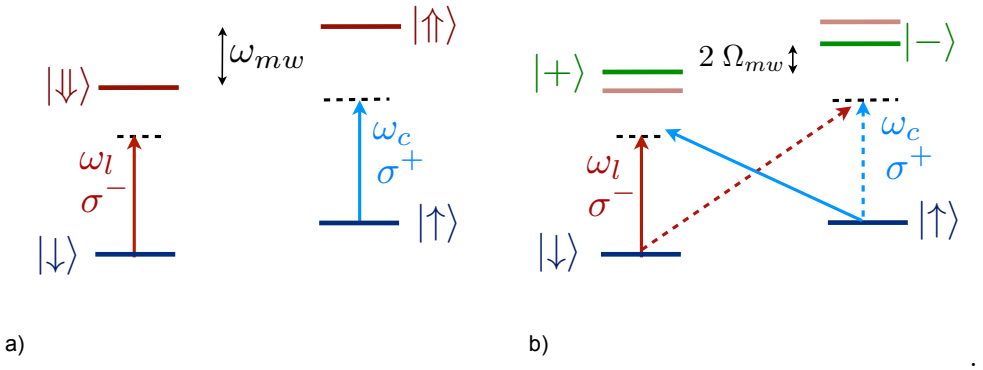

Figure 2.14: Level scheme of the QD a) Electronic and trion states split in an external magnetic field in growth direction (Faraday geometry). They are coupled by a σ^--polarized laser and a σ^+-polarized cavity field with frequencies ω_l, ω_c, respectively. b) Additional to the setting in a), a microwave field resonant with the splitting of the trion states in the magnetic field ($\omega_{\Uparrow} - \omega_{\Downarrow} = \omega_{mw}$) mixes the trion states. Laser and cavity couple both electronic states to the trion states $|+\rangle$ and $|-\rangle$.

is to mix the trion states with a resonant microwave field. The electronic eigenstates are unchanged (being far detuned from the microwave frequency) and are now both coupled to the new trion eigenstates $|-\rangle = 1/\sqrt{2}(|\Uparrow\rangle - |\Downarrow\rangle)$ and $|+\rangle = 1/\sqrt{2}(|\Uparrow\rangle + |\Downarrow\rangle)$, see Fig. 2.14b in a double Λ system.

The Hamiltonian of the system is now given by

$$H = \frac{\Omega_c}{2}\, a^\dagger\, |\downarrow\rangle\langle\Uparrow| + \frac{\Omega_l}{2}\, e^{i\omega_l t}\, |\uparrow\rangle\langle\Downarrow| + \Omega_{mw}\, e^{i\omega_{mw} t}\, |\Downarrow\rangle\langle\Uparrow| + \text{h.c.} + \omega_c\, a^\dagger a + \omega_{\Uparrow}\, |\Uparrow\rangle\langle\Uparrow| + \omega_{\Downarrow}\, |\Downarrow\rangle\langle\Downarrow| + \tilde{\omega}_z S^z + H_{\text{hf}}, \tag{2.60}$$

where $\omega_{\Uparrow}, \omega_{\Downarrow} = \omega_X \pm \omega_{zh}/2$ include the hole Zeeman splitting $\omega_{zh} = \omega_{mw}$ and H_{hf} is given by Eqn. (2.2). In a frame rotating with

$$U^\dagger = \exp[-i(\omega_{mw} + \omega_l)t(|\Uparrow\rangle\langle\Uparrow| + a^\dagger a) - i\omega_l t\, |\Downarrow\rangle\langle\Downarrow|)],$$

the Hamiltonian reads

$$H = \frac{\Omega_c}{2\sqrt{2}}\, (a^\dagger\, |\downarrow\rangle\langle +| + a^\dagger\, |\downarrow\rangle\langle -|) + \frac{\Omega_l}{2\sqrt{2}} (|\uparrow\rangle\langle +| - |\uparrow\rangle\langle -|) + \delta' a^\dagger a + \Delta_+\, |+\rangle\langle +| + \Delta_-\, |-\rangle\langle -| + \tilde{\omega}_z S^z + H_{\text{hf}}, \tag{2.61}$$

where $\delta' = \omega_c - \omega_l - \omega_{mw}$ and $\Delta_\pm = \omega_\Downarrow - \omega_l \pm \Omega_{mw}$. We adiabatically eliminate $|\pm\rangle$ and $|\uparrow\rangle$ as explained in Section 2.A.1 and Appendix 2.C. This yields

$$H_{el} = g'(aA^+ + \text{h.c.}) + \omega_1' a^\dagger a + \omega_2' N A^- A^+ + T_{nl}'. \tag{2.62}$$

This Hamiltonian is of exactly the same form as the Hamiltonian of our toy model given by Eqn. (2.56). By replacing $\frac{\Omega_l^2}{4\Delta} \longrightarrow \frac{\Omega_l^2}{8}\left(\frac{1}{\Delta_+} + \frac{1}{\Delta_-}\right)$, and $\frac{\Omega_l^2}{4\Delta^2} \longrightarrow \frac{\Omega_l^2}{8}\left(\frac{1}{\Delta_+^2} + \frac{1}{\Delta_-^2}\right)$ in the Hamiltonian given by Eqn. (2.62), ω_1', ω_2', and T_{nl}' correspond to ω_1, ω_2, and T_{nl} in Eqn. (2.56). As before, the nonlinear terms T_{nl}' are small and are neglected in the following. Using the bosonic description, we then obtain again a beam splitter Hamiltonian as given by Eqn. (2.57), where the coupling is now given by

$$g' = \frac{\Omega_c \Omega_l g_n}{16\tilde{\omega}_z}\left(\frac{1}{\Delta_+} - \frac{1}{\Delta_-}\right). \tag{2.63}$$

Compared to Eqn. (2.58) the effective coupling g is reduced by a factor $\Delta'(\Delta_+^{-1} - \Delta_-^{-1})$, i.e., $\approx 2\Omega_{mw}/\Delta'$ for $\Omega_{mw} \ll \Delta'$. Now we want to estimate the strength of the coupling. We choose the parameters as follows: we assume a hole g-factor $g_h = 2.2$ and an electron g-factor $g_e = 0.48$; the number of nuclei $N = 10^4$, the hyperfine coupling constant $A = 100\mu eV$, the laser and cavity Rabi frequency $\Omega_c = \Omega_l = 5\mu eV$, the detuning of the trion $\Delta = 600\mu eV$, the effective Zeeman splitting $\tilde{\omega}_z = 50\mu eV$ and the microwave Rabi frequency $\Omega_{mw} = 50\mu eV$. With these parameters, a value of $g' \sim 5 \cdot 10^{-5}\mu$eV is obtained. This leads to times of ~ 10 microseconds for an operation of the interface that will be discussed in Section 2.3.

To illustrate that H_{el}, in the bosonic description, which we denote by H_{bs}, provides a good approximation to H and allows to implement a good quantum interface, we consider a maximally entangled state $\sum_k |k\rangle_R |k\rangle_c$ of cavity and some reference system R and then use the interface to map the state of the cavity to the nuclei. If a maximally entangled state of R and nuclei is obtained, it shows that the interface is perfect for the whole subspace considered. The fidelity of the state $\mathbb{1}_R \otimes U(t) \sum_{k=1}^2 |k\rangle_R |k\rangle_c |0\rangle_n$ with the maximally entangled state $\sum_k |k\rangle_R |0\rangle_c |k\rangle_n$ fully quantifies the quality of the interface. In Fig. 2.15 we plot this fidelity for the evolutions $U(t)$ generated by the two Hamiltonians H and H_{el} of Eqns. (2.62) and (2.61) to show that a high-fidelity mapping is possible with the chosen parameters and that the simple Hamiltonian H_{el}

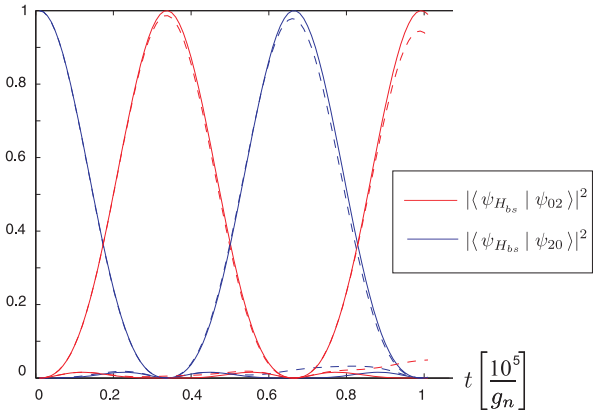

Figure 2.15: Performance of the quantum interface. One half of the maximally entangled state $\sum_{k=1}^{2} |k\rangle_R |k\rangle_c$ (subscript c indicates the cavity) is sent through the interface. The fidelity of the reduced state of R and nuclei with the maximally entangled states $\sum_{k=1}^{2} |k\rangle_R |k\rangle_n$ and $\sum_{k=1}^{2} (-1)^k |k\rangle_R |k\rangle_n$ is plotted. Solid lines refer to the evolution under H_{bs}, dashed lines to H.

well describes the relevant dynamics. Since $U(\pi/g)aU(\pi/g)^\dagger = ib$ some care must be taken concerning the phases of the number state basis vectors in the nuclear spin mode ($|k\rangle_c \mapsto (i)^k |k\rangle_n$) and different phases at $t = 3\pi/g$. For the numerical simulation, we chose the parameters as follows: we assume a hole g-factor $g_h = 2.2$ and an electron g-factor $g_e = 0.48$; the number of nuclei $N = 10^4$, the hyperfine coupling constant $A = 100\mu eV$, the laser and cavity Rabi frequency $\Omega_c = \Omega_l = 5\mu eV$, the detuning of the trion $\Delta = 600\mu eV$, the effective Zeeman splitting $\tilde{\omega}_z = 50\mu eV$ and the microwave Rabi frequency $\Omega_{mw} = 50\mu eV$. With these parameters, a value of $g \sim 5 \cdot 10^{-5}\mu$eV is obtained, leading to times of ~ 10 microseconds for an interface operation.

2.C Adiabatic elimination

In this Section, we give a detailed derivation of the adiabatic elimination that yields the Hamiltonian that describes the effective interaction between light and nuclei, given by Eqn. (2.56). Here, we discuss the adiabatic elimination for the toy model discussed in Appendix 2.A as it involves less terms. The adiabatic elimination for the system

discussed in Section 2.2 follows identical lines.

The starting point is the Hamiltonian given by Eqn. (2.55). Choosing the cavity and laser frequencies, ω_c and ω_l, far detuned from the exciton transition and the splitting of the electronic states $\tilde{\omega}_z$ much larger than the hyperfine coupling g_n, such that conditions (2.54a-2.54c) are fulfilled, we can adiabatically eliminate the states $|X\rangle$, $|\downarrow\rangle$: denote by $\mathbb{Q} = |X\rangle\langle X| + |\uparrow\rangle\langle\uparrow|$ and $\mathbb{P} \equiv \mathbb{1} - \mathbb{Q} = |\downarrow\rangle\langle\downarrow|$ the projectors on the eliminated subspace and its complement, respectively. Then the Schrödinger equation in the two subspaces reads

$$E\mathbb{P}\,|\Psi\rangle = \mathbb{P}H'(\mathbb{P}+\mathbb{Q})\,|\Psi\rangle\,, \tag{2.64a}$$

$$E\mathbb{Q}\,|\Psi\rangle = \mathbb{Q}H'(\mathbb{P}+\mathbb{Q})\,|\Psi\rangle\,. \tag{2.64b}$$

Our goal is to derive an approximation of the Hamiltonian in the $\mathbb{P}$-subspace which we denote by H_{el}. From Eqn. (2.64b) we obtain

$$\mathbb{Q}\,|\Psi\rangle = \frac{1}{E - \mathbb{Q}H'\mathbb{Q}}\mathbb{Q}H'\mathbb{P}\,|\Psi\rangle\,. \tag{2.65}$$

Inserting Eqn. (2.65) into (2.64a), we arrive at the (still exact) equation

$$E\mathbb{P}\,|\Psi\rangle = \left(\mathbb{P}H'\mathbb{P} + \mathbb{P}H'\mathbb{Q}\frac{1}{E - \mathbb{Q}H'\mathbb{Q}}\mathbb{Q}H'\mathbb{P}\right)\mathbb{P}\,|\Psi\rangle\,, \tag{2.66}$$

for the wavefunction in the electron spin-down subspace, with the unknown E appearing both on the right hand side (rhs) and the left hand side (lhs) of Eqn. (2.66).

Now we use that (i) the range of (unperturbed) energies in the $\mathbb{P}$-subspace is small compared to the energy difference between the $\mathbb{P}$- and $\mathbb{Q}$-subspaces and (ii) the coupling term $\mathbb{P}H'\mathbb{Q}$ is small compared to this difference, i.e.,

$$\| \frac{1}{E - \mathbb{Q}H'\mathbb{Q}}\mathbb{Q}H'\mathbb{P} \| \ll 1. \tag{2.67}$$

Then the second part on the rhs of Eqn. (2.66) is small and E can be approximated by E^0, an eigenvalue of $\mathbb{P}H'\mathbb{P} = -\left(\frac{\tilde{\omega}_z}{2} + \frac{A}{2}\delta A^z - \delta a^\dagger a\right)|\downarrow\rangle\langle\downarrow|$, which is here given by $E^0 \approx -\tilde{\omega}_z/2$. Since for our purposes the energy of the nuclear excitations [$\sim g_n^2/(4\tilde{\omega}_z)$] and cavity photons ($\delta$) are chosen equal and are $\ll \tilde{\omega}_z$, and $\|\frac{A}{2}\delta A^z\|$ is of order $\frac{A}{2N}$ and $\ll \tilde{\omega}_z$, condition (i) is fulfilled. Condition (ii) given by Eqn. (2.67) is satisfied

if the conditions of Ineq. (2.54a) hold. This yields the effective Hamiltonian in the electron-spin down subspace:

$$H_{el} = \left(\mathbb{P}H'\mathbb{P} - \mathbb{P}H'\mathbb{Q}\frac{1}{\tilde{\omega}_z + \mathbb{Q}H'\mathbb{Q}}\mathbb{Q}H'\mathbb{P} \right) \mathbb{P}. \tag{2.68}$$

To simplify the second term in H_{el} (the denominator is an operator containing $a, a^\dagger, A^-, A^+$), we split it into two parts: $\tilde{\omega}_z + \mathbb{Q}H'\mathbb{Q} = B_1 + B_2$, where

$$B_1 = \tilde{\omega}_z \left|\uparrow\right\rangle\!\left\langle\uparrow\right| + (\Delta + \tilde{\omega}_z/2) \left|X\right\rangle\!\left\langle X\right| \tag{2.69}$$

contains the energetically large part and is easy to invert, and

$$B_2 = \frac{\Omega_l}{2}(\left|\uparrow\right\rangle\!\left\langle X\right| + \text{h.c.}) + \delta a^\dagger a\, \mathbb{Q} + \frac{A}{2}A^+A^- \left|\uparrow\right\rangle\!\left\langle\uparrow\right|. \tag{2.70}$$

contains the Rabi frequency of the laser field Ω_l that couples the spin-up state and the trion and the energies of photons and nuclear spins. From the conditions in Eqn. (2.54a) follows that the cavity field is weak and the energies of photons and nuclear spins are small compared to the energy scale given by Δ' and $\tilde{\omega}_z$, therefore

$$\| \frac{1}{\sqrt{B_1}} B_2 \frac{1}{\sqrt{B_1}} \| \ll 1, \tag{2.71}$$

and we can approximate the denominator in Eqn. (2.66) by

$$\frac{1}{B_1 + B_2} \approx \frac{1}{B_1} - \frac{1}{B_1}B_2\frac{1}{B_1}. \tag{2.72}$$

Thus, inserting Eqn. (2.72) in Eqn. (2.66) and assuming the conditions given by Eqns. (2.54a) to be fulfilled, we can write the Hamiltonian in the electron spin-down subspace as

$$H_{el} = \mathbb{P}H'\mathbb{P} + \mathbb{P}H'\mathbb{Q}\left(\frac{1}{B_1} - \frac{1}{B_1}B_2\frac{1}{B_1}\right)\mathbb{Q}H'\mathbb{P}, \tag{2.73}$$

with $\mathbb{P}H'\mathbb{Q} = \frac{\Omega_c}{2}a^\dagger \left|\downarrow\right\rangle\!\left\langle X\right| + AA^+ \left|\downarrow\right\rangle\!\left\langle\uparrow\right|$, which yields

$$H_{el} = \frac{\Omega_c\Omega_l A}{8\Delta'\tilde{\omega}_z}(aA^+ + \text{h.c.}) + \omega_1 a^\dagger a + \omega_2 N A^+A^- + T_{nl}, \tag{2.74}$$

where the energy of the photons $\omega_1 = \delta - \frac{\Omega_c^2}{4\Delta'}$, the energy of the nuclear spin excitations $\omega_2 = -\frac{A}{2N} - \frac{A^2}{4N\tilde{\omega}_z}$. By T_{nl} we denote the nonlinear terms $T_{nl} = \frac{A^3}{8\tilde{\omega}_z^2}A^+A^+A^-A^- + \left(\frac{\Omega_c^2 A}{8\Delta'^2} + \frac{A^2}{4\tilde{\omega}_z^2}\delta\right)a^\dagger a A^+A^- + \frac{\Omega_c^2\delta}{4\Delta'^2}a^\dagger a^\dagger aa$, which are small ($\|T_{nl}\| \ll \frac{\Omega_c\Omega_l A}{8\Delta'\tilde{\omega}_z}$) in the situation we consider ($\delta \ll \Omega_c, g_n/\tilde{\omega}_z \sim \Omega_l/\Delta' \ll 1$) and neglected in the following.

2.D Bosonic description of nuclear spins

The description of collective spin excitations in a large, highly polarized system of N spins $\sigma_j\pm, z$ as bosonic excitations out of the vacuum states goes back at least to the introduction of the Holstein-Primakoff transformation [82].

If the collective spin operators involved are $A^{\pm,z} \equiv J^{\pm,z} = \sum_j \sigma_j^{\pm,z}$ and the system is initialized in the symmetric fully polarized state $|\downarrow\downarrow \ldots \downarrow\rangle$ then the symmetric space spanned by the Dicke states [106] $|J = N/2, m\rangle$ is never left under the action of $A^{\pm,z}$ and up to a n-dependent correction the matrix elements of J^- in the basis $|N/2, n - N/2\rangle$ coincide with the matrix elements of the bosonic annihilation operator b in the Fock basis $|n\rangle$. In fact we have

$$\langle J, n - J| \, J^- \, \big|J, n' - J\big\rangle = \sqrt{2J}\sqrt{1 - \frac{n-1}{2J}}\sqrt{n}\delta_{n,n'-1}. \tag{2.75}$$

As long as $n \ll 2J$ (in the whole subspace significantly populated throughout the evolution) the factor $\sum_n \sqrt{1 - n/(2J)}P_{|J,n-J\rangle} \approx \mathbb{1}$ and the association

$$J^+ \to \sqrt{2J}b \tag{2.76a}$$

$$|J, n - J\rangle \to |n\rangle \tag{2.76b}$$

$$J^z \to -J\mathbb{1} + b^\dagger b. \tag{2.76c}$$

is accurate to $o(n_{\max}/(2J))$. To obtain a more accurate description, we can even express the factor $\sum_n \sqrt{1 - \frac{n-1}{2J}}$ in Eqn. (2.75) in bosonic terms, i.e., as $\sqrt{1 - b^\dagger b/(2J)}$ leading to an *exact* mapping between the spin and bosonic operators.

The intuition we are following is that this association still is useful if we are dealing with (i) *not fully polarized* systems (i.e., $2J < N$) and (ii) the collective spin operators appearing in the dynamics are *inhomogeneous*, i.e. $A^{\pm,z} = \sum_j \alpha_j \sigma_j^{\pm,z}$.

Let us first discuss the two issues separately. If the system is homogeneous and $J < N/2$ but known, e.g., by measuring J_z and J^2, then by Eqn. (2.75) compared to the fully polarized case only the parameter $2J$ has to be adapted and the bosonic description is still good as long as $n_{\max} \ll 2J$.

If J is not precisely known, we get an inhomogeneous broadening of the coupling constants appearing in front of $A^\pm$ [due to the scaling factor $\sqrt{2J}$ in Eqn. (2.76a)] and

of the constant in Eqn. (2.76c).

If $A^{\pm,z}$ are inhomogeneous, the three operators no longer form a closed algebra and the dynamics cannot be restricted to the symmetric subspace even if starting from the fully polarized state. However, it is still possible to associate A^- to an annihilation operator $A^- \to (\sum_j \alpha_j^2)^{1/2}(1+f)b$ where the correction factor $1+f$ is close to one for highly polarized systems ($\|f\| \sim 1-P$) and depends on the excitation number not only of the mode b but also of other bosonic modes, associated with collective spin operators different from $A^{\pm}$. These can be introduced, e.g., by choosing a complete orthonormal set of coupling vectors $\{\vec{\alpha}^{(k)}\}$ with $\alpha^{(0)} \propto \vec{\alpha}$ and defining a complete set $\{A_k^{\pm} = \sum_j \alpha_j^{(k)} \sigma_j^{\pm}, k = 0, \ldots, N-1\}$ of collective spin operators. We refer to the modes $b_{k\neq 0}$ as "bath modes".

Generalizing the single-mode case discussed before, an exact mapping $A_k^- \to (1+f_k)b_k$ and $A^z \to -\frac{1}{2} + \frac{1}{N}\sum_k b_k^\dagger b_k + C_z$, with operators f_k, C_z describing corrections to the ideal case can be obtained. It was shown in [84] that the corrections f_k, C_z are of order $1-P$ for high polarization. Thus the mapping used in our analysis of the quantum interface is correct to zeroth order in $1-P$.

Corrections to that description can be obtained by including the corrections $1-f_k$ and C_z. The analysis is simplified by the fact that coupling between the mode b and the bath modes is weak (first order in the small parameter $1-P$) and we are interested only in the mode b. Thus by the replacements [84]

$$A^- \to (\sum \alpha_j^2)^{1/2}(1-f)b, \tag{2.77a}$$

$$A_k^- \to b_k, \tag{2.77b}$$

$$A^z \to -\frac{1}{2} - \frac{1}{N}\sum_{k=0}^{N-1} b_k^\dagger b_k + C_z, \tag{2.77c}$$

with quadratic hermitian operators $f = \sum_{kk'} \tilde{F}_{kk'} b_k^\dagger b_{k'}$ and $C_z = \sum_{k,k'} C_{kk'} b_k^\dagger b_k$ we obtain a first order description of the dynamics of the mode b (and the electron and photons coupled to it). Here $C = U\mathrm{diag}(\alpha_j - 1/N)U^\dagger$ and $F = \left(\sum_j \alpha_j^2\right) U\mathrm{diag}(\alpha_j^2)U^\dagger$ and and U transforms from the canonical basis to $\left\{\vec{\alpha}^{(k)}\right\}$. The matrix $\tilde{F}$ is obtained from F by multiplying F_{00} by $1/2$ and F_{k0}, F_{0k} by $2/3$. The operators f, D have been chosen such that the commutation relations of $A^{\pm}$ are preserved to first order. And

while $A_k^{\pm}, k > 0$ are not as accurately preserved, this affects the dynamics of $A^{\pm,z}$ only to second order [84]. From Eqn. (2.56) we see that there are three main effects of the corrections: (i) inhomogeneous broadening of $\tilde{\omega}_z, g_n$ (and consequently ω_2 and g) due to the finite variance in P; (ii) inhomogeneous broadening of g due to the variance of the correction factor $1 - f$; and (iii) losses of excitations from the b mode to baths modes due to inhomogeneity.

Since $\tilde{\omega}_z \gg g_n$, the broadening due to the variance of the Overhauser field is $\ll \tilde{\omega}_z$ and thus has only a small effect. Similarly, the broadening of g affects the form of the output mode $z(0, x, t)$ [see Eqn. (2.36)], but since it appears there only via the parameter $\nu = \sqrt{(\gamma/4)^2 \pm g^2}$ the effect is negligible since $g \ll \gamma$. However, the effective energy of the nuclear excitations, $\omega_2 = g_n^2/(4\tilde{\omega}_z)$, can be more strongly affected: e.g., a standard deviation of 10% in P translates to a 10% variation in ω_2. It must be assured that this variation is small compared to g so that the resonance condition is maintained.

Concerning leakage, the strongest term is the one arising from A^z and it is not necessarily small compared to g. However, as was pointed out in [101] the mode b is detuned from the others due to the "AC Stark shift" arising from the off-resonant interaction with the electron [the term $\sim A^2/(4\tilde{\omega}_z)A^+A^-$]. As long as this energy shift is large compared to leakage, losses are suppressed and the mode b is only coupled dispersively to the bath (via the inhomogeneous broadening). To work in that regime, $\tilde{\omega}_z$ must not be too large, i.e., external and Overhauser field should partially compensate each other while still keeping $\Omega_l \ll \sqrt{\Delta' \tilde{\omega}_z}$.

2.E Gaussian states and operations

Gaussian states and operations play a central role in quantum information with continuous variable systems [107]. To make this work self-contained we briefly summarize here the main properties of Gaussian states and operations with particular regard to their entanglement.

Gaussian states are a family of states occurring very frequently in quantum optics, e.g., in the form of coherent, squeezed, and thermal states. Despite being defined on an infinite dimensional Hilbert space [$\mathcal{F}_+(\mathbb{R}^{2N})$, the symmetric Fock space over $\mathbb{R}^{2N}$] they

are characterized by a finite number of real parameters, namely the first and second moments of N pairs of canonically conjugate observables $(Q_1, P_1, \ldots, Q_N, P_N) \equiv \vec{R}$.

One way to define them is that their *characteristic function*, i.e., the expectation values $\chi(\xi) = \mathrm{tr}(W_\xi \rho)$ of the displacement operators $W_\xi = \exp(i\xi^T \vec{R}), \xi \in \mathbb{R}^{2N}$ is a Gaussian function [108]:

$$\chi(\rho) = \exp(-i\xi^T d - 1/4 \xi^T \gamma \xi). \tag{2.78}$$

The displacement vector $d \in \mathbb{R}^{2N}$ and the $2N \times 2N$ real positive covariance matrix (CM) γ are given by the expectations and (co)variances of the R_k:

$$d_k = \mathrm{tr}[\rho R_k], \tag{2.79}$$

$$\gamma_{kl} = \langle R_i R_j + R_j R_i \rangle - 2\langle R_i \rangle \langle R_j \rangle. \tag{2.80}$$

All $d \in \mathbb{R}^{2N}$ are admissible displacement vectors and any real positive matrix γ is a valid CM if it satisfies $\gamma \geq i\sigma_N$ when the symplectic matrix σ_N is

$$\sigma_N = \oplus_{l=1}^{N} \sigma_1 \text{ with } \sigma_1 = \begin{pmatrix} 0 & -1 \\ 1 & 0 \end{pmatrix}. \tag{2.81}$$

The last condition summarizes all the uncertainty relations for the canonical operators R_j. These operators are related to the creation and annihilation operators $a_j^\dagger, a_j$ by the relations $Q_j = (a_j + a_j^\dagger)/\sqrt{2}$ and $P_j = -i(a_j - a_j^\dagger)/\sqrt{2}$.

An example for a one-mode Gaussian state is a coherent state $|\alpha\rangle$, with covariance matrix $\gamma = \mathbb{1}$ and displacement $d = (\mathrm{Re}|\alpha|, \mathrm{Im}|\alpha|)/\sqrt{2}$.

Entanglement: All information about the entanglement properties of Gaussian states is encoded in the CM. Given a CM, there are efficient criteria to decide whether a Gaussian state is entangled or not.

To apply these criteria, it is useful to write the CM of a bipartite $N \times M$ Gaussian states in the following form,

$$\gamma = \begin{pmatrix} A & C \\ C^T & B \end{pmatrix}, \tag{2.82}$$

where the $2N \times 2N$ ($2M \times 2M$) matrix A (B) refers to the covariances of the quadrature operators associated with the first (second) system and C contains the covariances

between the two systems. A (B) are the CM of the reduced state in the first (second) system only.

In the case of a two-mode system the criteria [109, 110] are necessary and sufficient for separability: a state with CM γ is entangled if and only if $\det\gamma + 1 - \det A - \det B + 2\det C \not\geq 0$. In this case, entanglement is necessarily accompanied by a non-positive partial transpose (npt) [111]. For more modes, entangled states with positive partial transpose exist [112] and more general criteria to decide entanglement have to be used [113, 114].

For pure states, the analysis of entanglement properties becomes particularly easy since all such states can be transformed to a simple standard form, namely a collection of two-mode squeezed states (TMSS) and vacuum states, by local unitaries [115], hence the entanglement of such a state is fully characterized by the vector of two-mode squeezing parameters. This also shows that for a $1 \times M$ system in a pure state one can always identify a single mode such that only it (and not the $M-1$ other modes) is entangled with the first system.

For many Gaussian states it is also possible to make *quantitative* statements about the entanglement, i.e. to compute certain entanglement measures. For pure $N \times M$ states, the entropy of entanglement can be computed from the symplectic eigenvalues of the reduced CM A (or, equivalently, B). These are given by the modulus of the eigenvalues of $\sigma_N A$ [92]. All symplectic eigenvalues $\lambda \geq 1$ correspond to a TMSS with squeezing parameter $\operatorname{acosh}(\lambda)/2$ in the standard form of the state at hand and contributes $\lambda^2 \log_2 \lambda^2 - (\lambda-1)^2 \log_2(\lambda^2-1)$ to the entanglement entropy of the system.
For mixed states, it is possible to compute the negativity [92] for any $N \times M$ system from the symplectic eigenvalues of the CM of the partially transposed state (which is related to the CM obtained by replacing all momenta P_j in the second system by $-P_j$). Every symplectic eigenvalue $\lambda < 1$ contributes $-\log_2 \lambda$ to the negativity.
For 1×1 Gaussian states with $\det A = \det B$ (so-called symmetric states), the entanglement of formation (EoF) can be computed [116] and for more general states a Gaussian version of EoF is available [91]. Even if the states are not certain to be Gaussian, several of the Gaussian quantities can serve as lower bounds for the actual amount of

entanglement [117].

Gaussian operations: Operations that preserve the Gaussian character of the states they act on are called Gaussian operations [99]. Like the Gaussian states they are only a small family (in the set of all operations) but play a prominent role in quantum optics, since they comprise many of the most readily implemented state transformations and dynamics. With Gaussian operations and Gaussian states many of the standard protocols of quantum information processing such as entanglement generation, quantum cryptography, quantum error correction and quantum teleportation can be realized [107].

Of particular interest for us are the Gaussian unitaries, i.e. unitary evolutions generated by Hamiltonians that are at most quadratic in the creation and annihilation operators. Unitary displacements W_ξ are generated by the linear Hamiltonian $\xi^T \vec{R}$. All other Gaussian unitaries can be composed of three kinds [118], named according to their optical incarnations. The *phase shifter* ($H = a^\dagger a$) corresponds to the free evolution of an harmonic system. The *beam splitter* ($H = ab^\dagger + a^\dagger b$) couples two modes. Both generators do not change the total photon number and are therefore examples of *passive* transformations. The remaining type of Gaussian unitary is *active*: the (single-mode) *squeezer* is generated by the squeezing Hamiltonian $H = a^2 + (a^\dagger)^2$, which, when acting on the vacuum state decreases the variance in one quadrature (Q) by a factor $f < 1$ and increases the other one by $1/f$. Combining these building blocks in the proper way, all other unitaries generated by quadratic Hamiltonians, e.g. the two-mode squeezing transformation ($H = ab + a^\dagger b^\dagger$) can be obtained.

Both active and passive transformations map field operators to a linear combination of field operators (disregarding displacements caused by linear parts in the Hamiltonians, which can always be undone by a further displacement), i.e. for all Gaussian unitaries we have in the Heisenberg picture

$$U\vec{R}U^\dagger = S\vec{R} \equiv \vec{R}'. \tag{2.83}$$

Here S is a symplectic map on $\mathbb{R}^{2N}$, i.e. S preserves the symplectic matrix σ_N, assuring that R_i and R_i' satisfy the same commutation relations. We denote by U_S the unitary corresponding to the symplectic transformation S. Passive operations correspond to

symplectic transformations that are also orthogonal.

In the Schrödinger picture, U_S transforms the Gaussian state with CM γ and displacement d such that $(\gamma, d) \mapsto (S\gamma S^T, Sd)$. The two-mode squeezing transformations

$$T(r) = \begin{pmatrix} \cosh(r)\mathbb{1} & \sinh(r)\sigma_x \\ \sinh(r)\sigma_x & \cosh(r)\mathbb{1} \end{pmatrix} \tag{2.84}$$

is an important example of a active symplectic transformation.

Besides Gaussian unitaries, *Gaussian measurements* are another important and readily available tool. Gaussian measurements are generalized measurements represented by a positive-operator-valued measure $\left\{|\gamma, d\rangle\langle\gamma, d|\, \gamma, d, d \in \mathbb{R}^{2N}\right\}$ that is formed by all the projectors obtained from a pure Gaussian state $|\gamma, 0\rangle\langle\gamma, 0|\, \gamma, 0$ by displacements. The most important example is a limiting case of the above: the quadrature measurements (von Neumann measurements which project on the (improper, infinitely squeezed) eigenstates of, e.g., Q). In quantum optics, these are well approximated by *homodyne detection*. For example, the "Bell- or "EPR-measurement" that is part of the teleportation protocol is a measurement of the commuting quadrature operators $Q_1 + Q_2$ and $P_1 - P_2$.

Chapter 3

Asymmetric optical nuclear spin pumping in a single quantum dot

In this Chapter we present an experimental and theoretical investigation of asymmetric unidirectional nuclear spin pumping in an uncharged self-assembled InGaAs quantum dot. The experiment was carried out by Florian Klotz under the supervision of Prof. Finley at the Walter-Schottky Institute of the TU Munich. In the experiment, highly asymmetric dynamic nuclear spin pumping is observed in a quantum dot subject to resonant optical pumping of the neutral exciton transition leading to a large maximum polarization of 54%. The theoretical model gives new insights into the mechanism leading to the observed DNP effect. It can be understood in terms of electron-nuclear spin flip-flop processes exchanging the orientation of an electron and nuclear spin and transferring the exciton from an optically active bright into an optically inactive dark state which then decays non-radiatively. The model allows to perform numerical calculations that simulate the actual measurement procedure and quantitatively reproduce the experimentally observed characteristic features of the achievable steady state nuclear polarization.

3.1 Introduction

Nuclear spin effects in semiconductor quantum dot (QD) nanostructures have attracted much attention over recent years [119, 39, 120, 121, 122, 123, 124, 125, 126, 127, 128, 129, 38, 130]. The hyperfine (hf) interaction of the 10^4-10^5 nuclear spins within the dot and the spin of an individual electron that is electrically or optically generated is key to address and control the nuclear spin system. This may provide opto-electronic access to the mesoscopic nuclear spin system with strong potential for future applications in quantum information technologies [39]. The hf interaction limits the electron spin coherence in QDs [120, 23] making reliable strategies to control the nuclear field highly desirable [121, 122]. From both perspectives, a highly polarized ensemble of nuclear spins would be advantageous. To date, the vast majority of experiments on dynamical nuclear polarization (DNP) (for a review see [36]) have been carried out on charged QDs containing a resident electron [123, 124, 131]. However, this system is subject to fast depolarization effects that are typically mediated by the residual electron in the dot [123]. Neutral QDs are particularly interesting [126, 132, 128, 129, 38, 130] since for them stable polarization of the nuclear spin system over timescales exceeding one hour has been demonstrated [38].

The experiment demonstrates pumping of the nuclear spin system in an InGaAs QD via resonant optical excitation of the neutral exciton X^0. Most surprisingly, a strong asymmetry in the DNP efficiency is found for excitation of the two transitions of the bright neutral exciton states of the dot with DNP predominantly occurring for pumping of the higher energy Zeeman level. To gain a better understanding of the mechanisms and processes involved, a detailed theoretical model of the driven neutral QD was developed that allows to perform numerical calculations simulating the actual experimental procedure used in our measurements. The observed asymmetric DNP effects can be understood in terms of hf-mediated spin flip transitions between dark and bright exciton states. We treat the hyperfine coupling in second order perturbation theory and eliminate the subspace of the fast dynamics of the excitonic decay. Under the semiclassical approximation that the nuclear state is separable, we obtain an equation of motion for the nuclear polarization. The simulations of the steady state population

in the excitonic subspace quantitatively reproduce the experimental results.

3.1.1 Reader's guide

In Section 3.2 the experimental setup is explained. Experimental results of nuclear spin pumping are presented in Section 3.3. More experimental details can be found in our joint publications [43] and [37]. In Section 3.4 the physical mechanisms that account for the observed asymmetric nuclear spin polarization are explained. First, the principal idea is sketched, and then details of the physical mechanism leading to DNP as observed in the numerical simulations are explained in a comprehensive manner. In Section 3.5, a detailed analysis of the theoretical description, that treats the hyperfine coupling perturbatively, can be found. This description allows to perform numerical calculations (work done by Geza Giedke) that are discussed in Section 3.6.

3.2 The system

The investigated structure is depicted in the inset of Fig. 3.1 consisting of a single layer of molecular beam epitaxy grown InGaAs QDs embedded within the intrinsic region of a Schottky photodiode formed by a heavily n^+-doped back contact and a 3nm thick semitransparent Ti top contact. This device geometry allows the application of DC electric fields along the growth direction of the QDs. The Ti top contact is covered with an opaque Au layer in which 1μm wide circular apertures are opened to facilitate optical access to single QDs. Photocurrent (PC) measurements were carried out on this structure at 10K for different magnetic fields B_{ext} using linearly polarized light from a tunable laser. The quantum confined Stark effect (QCSE) is employed to tune the transitions of the QD into resonance with the laser by sweeping the applied electric field whilst keeping the laser energy fixed. Fig. 3.1 shows the DC Stark shift of the examined X^0 state measured at $B_{\text{ext}} = 0$T in both PC at high (> 30kV/cm) and photoluminescence at lower electric fields (< 30kV/cm) which can be well described using a second order polynomial fit allowing a direct conversion of applied electric field into transition energy [133].

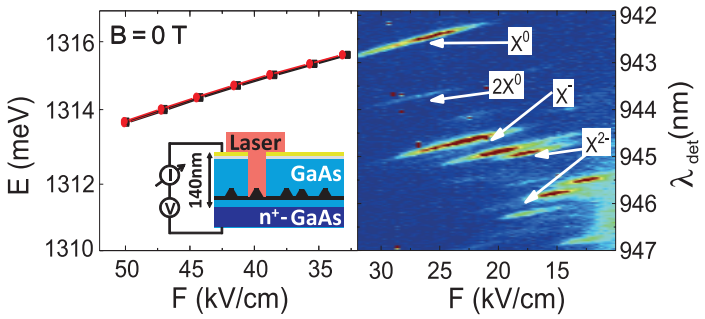

Figure 3.1: Combined PC and PL measurements at $B_{\text{ext}} = 0$T. Inset: Schematic of the structure investigated consisting of a single layer of self assembled QDs is embedded in the intrinsic region of Schottky photodiode.

3.3 Experimental observation of DNP

Fig. 3.2 shows an example of an electric field sweep PC measurement performed at $B_{\text{ext}} = 5$T. The measurement clearly reveals the two optically active (bright) s-shell states of X^0, denoted $|E_1\rangle$ and $|E_2\rangle$, as they are tuned into and out of resonance with the laser by the QCSE. The levels $|E_1\rangle$ and $|E_2\rangle$ are separated by an energy gap $\Delta E = \sqrt{E_Z^2 + {\delta_1^b}^2}$ in an externally applied magnetic field, where E_Z is the Zeeman energy and δ_1^b the fine structure splitting due to anisotropic exchange coupling [134]. For $E_Z \gg \delta_1^b$, the states $|E_{1,2}\rangle$ correspond to the bright excitons with angular momentum projection $J_z = +1$ ($|{\downarrow}{\Uparrow}\rangle$) and $J_z = -1$ ($|{\uparrow}{\Downarrow}\rangle$), respectively, where $\uparrow, \downarrow$ ($\Uparrow, \Downarrow$) denote the electron (hole) spin orientation, respectively. A clear difference is observed between the two measurements performed with opposing sweeping directions of the electric field; from low to high values ('sweep up' - blue trace on Fig. 3.2) and high to low values ('sweep down' - red trace on Fig. 3.2). These observations are shown to arise from DNP and the resulting effective Overhauser magnetic field B_N. Partial polarization of the nuclear spin bath in the QD arises from hf coupling to the spins of the electrons pumped through the dot during the measurement and introduces an Overhauser energy shift $\delta_n = g_e \mu_B B_N$, where μ_B is the Bohr magneton and g_e the electron g-factor.

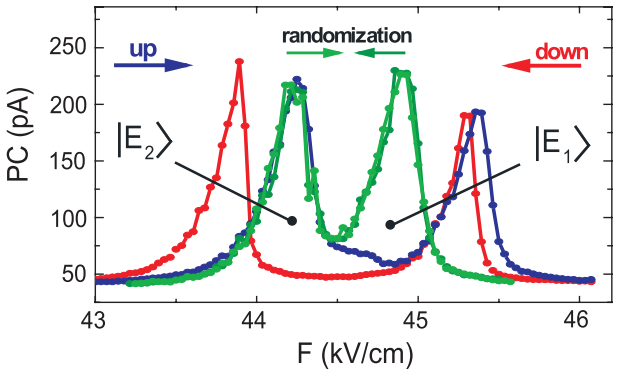

Figure 3.2: Both X^0 s-shell states measured in PC electric field sweeps at $B_{\text{ext}} = 5\text{T}$. The individual curves were measured as described in the text.

3.3.1 Reference measurement: randomizing nuclear spins

To study DNP it is important to obtain a reference measurement for an unpolarized state of the QD nuclear spin system. We obtain such a reference PC spectrum by randomizing the nuclear spins prior to every measurement point recorded during an electric field sweep and ensuring that our measurement does not induce significant DNP. To achieve this, the sample was tuned close to flatband and excited non resonantly in the wetting layer for 10 s with linearly polarized light. This procedure pumps randomly oriented electron spins through the QD, whereupon hf interactions efficiently depolarize the nuclear spin system. This expectation is confirmed by the observations presented in Fig. 3.2; when applying this randomization procedure the sweep direction is found to have no influence on the measured resonance curves, the light and dark green traces in Fig. 3.2 corresponding to sweep up and sweep down directions, respectively. We note that the observed insensitivity to sweep direction when employing the randomization procedure is in strong contrast to the results obtained without randomization during the sweep (red and blue traces on Fig. 3.2). For all measurements without randomization, as discussed below the electric field sweep was performed at a speed that was slow compared to the time required to reach the steady state polarization of the nuclear spin system. Therefore, each of these measurement point presented in Fig. 3.2 represents the steady state situation of the nuclear spin system. However, before every sweep we

applied the randomization process once to ensure a well defined initial state without residual DNP.

3.3.2 Observation of asymmetric DNP

Fig. 3.2 reveals an asymmetric behavior of DNP upon pumping of the two bright exciton states of X^0. For the up-sweep, first $|E_2\rangle$ comes into resonance with the laser as the energies of the states are shifted via the QCSE. No significant DNP effects are observed upon exciting $|E_2\rangle$ since the measured PC signal coincides exactly with the reference curve recorded without DNP effects. However, as $|E_1\rangle$ is tuned into resonance with the excitation laser, the nuclear spin bath is clearly subject to DNP since a shift of the $|E_1\rangle$ resonance to higher energies is observed. When the electric field is swept in the opposite direction, first the $|E_1\rangle$ state is tuned into resonance with the laser leading to a buildup of B_N. After the $|E_1\rangle$ state has been tuned through the laser, the energetically lower $|E_2\rangle$ state approaches the laser energy. The measurements presented in Fig. 3.2 clearly show that the $|E_2\rangle$ peak in the PC signal is now red shifted as compared to the reference measurement. This observation unequivocally shows that the nuclear field created by optical pumping of $|E_1\rangle$ is still present.

A systematic investigation of δ_n^s as a function of the applied magnetic field is presented in Fig. 3.3 b). For $B_\mathrm{ext} = 0 - 6\mathrm{T}$, δ_n^s created via resonant excitation of $|E_1\rangle$ increases with increasing B_ext and then decreases monotonically for $B_\mathrm{ext} \geq 6\mathrm{T}$. The maximum observed Overhauser shift of $\delta_n^\mathrm{s} \approx 135\mu\mathrm{eV}$ obtained for $B_\mathrm{ext} \approx 6\mathrm{T}$ corresponds to a nuclear bath polarization of $P = 54\%$ [124] and an Overhauser field of $B_\mathrm{N} = 3.8\mathrm{T}$ (using $g_\mathrm{e} = -0.6$ calculated for our InGaAs QDs [135] and similar to values found in the literature [136, 137]). In strong contrast, resonant excitation of $|E_2\rangle$ does not result in any pumping of the nuclear spin bath for $B_\mathrm{ext} \geq 4\mathrm{T}$. For $B_\mathrm{ext} \leq 4\mathrm{T}$ a small Overhauser shift is observed. However, the magnitude of δ_n^s is always significantly smaller than that induced by pumping of $|E_1\rangle$ at the same B_ext. Most remarkably, the direction of B_N with respect to B_ext is found to be identical for excitation of both $|E_1\rangle$ and $|E_2\rangle$, since in both cases δ_n is found to result in an increase in ΔE over the value measured without DNP effects.

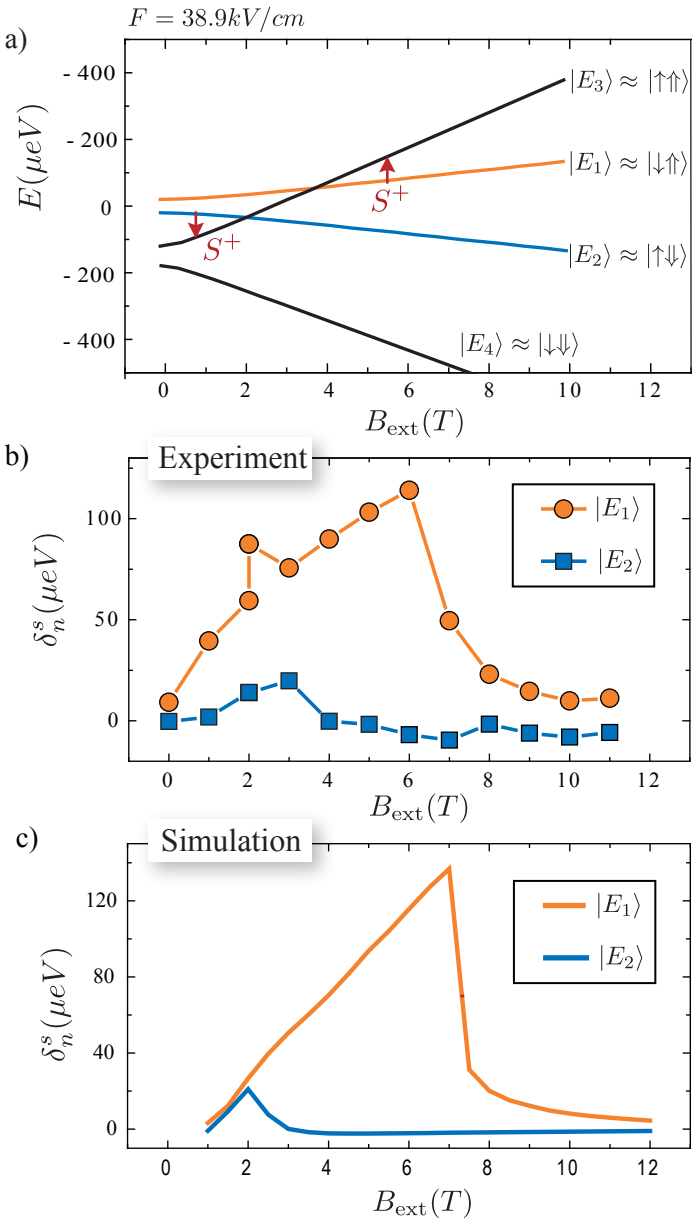

Figure 3.3: a) Calculated Breit-Rabi diagram for the bright ($|E_{1,2}\rangle$) and dark ($|E_{3,4}\rangle$) exciton states. b) Experiment: Steady state Overhauser shift δ_n^{s} created by resonant excitation of either of the two X^0 states $|E_1\rangle$ and $|E_2\rangle$ as a function of B_{ext}. c) Theory: Overhauser shift calculated from the lineshift displayed in Fig. 3.4. System parameters as in Tab. 3.1. A constant phenomenological nuclear depolarization rate $f_{\mathrm{depol}} = 10^{-9}$ was assumed.

3.4 The physical mechanism

Different mechanisms can lead to DNP in a optically pumped quantum dot [105, 138, 139, 140, 141]. Most rely on the flip-flop terms in the hyperfine interaction, but differ with regard to the active quantum dot states, the means by which an imbalance in the up and down polarization rates is achieved, and which process provides the energy for the typically off-resonant hyperfine flip-flop process. In our treatment, we focus on a mechanism that is related to the neutral exciton in the QD. In the following the physical mechanism that leads to the observed nuclear spin polarization is explained. After sketching the main idea in Section 3.4.1, a detailed explanation of the physical mechanism is given. This is done using results of the numerical simulation that is introduced at a later stage (in Section 3.6). For now, the results can be understood without explaining details of the numerical model, as the numerical results reflect the already explained experimental results.

3.4.1 Principal idea of the mechanism

The pumping of the nuclear spin bath can be explained via hf-mediated electron-nuclear spin flip-flop processes that exchange the orientation of the electron and a nuclear spin. This process is described by the hf Hamiltonian

$$H_{\mathrm{ff}} \sim S^{+}\sum_{j} I_{j}^{-} + S^{-}\sum_{j} I_{j}^{+}$$

[80], where $S^{\pm}, I_{j}^{\pm}$ are the raising and lowering operators for the electron and j^{th} nuclear spin, respectively. To understand the principle characteristics of the DNP curve in Fig. 3.3 b) and c) we consider the exciton level structure shown in Fig. 3.3 a). The two bright exciton states $|E_{1,2}\rangle$ are split from the two optically inactive (dark) excitons $|E_{3,4}\rangle$ by the large isotropic exchange splitting ($\sim 150\mu$eV [134]). Bright and dark doublets are also split by anisotropic exchange δ_1^{b} (with $\delta_1^{\mathrm{b}} = 40\mu$eV determined from measurements at $B_{\mathrm{ext}} = 0$T) and are, therefore, a superposition of the pure spin states with a mixing ratio that decreases with increasing B_{ext}.

The hf interaction couples different excitonic levels: the laser driving only populates the bright excitons, but these are coupled to dark exciton states by the electron spin-flip

terms in the hyperfine Hamiltonian,

$$|\uparrow\Downarrow\rangle \leftrightarrow |\downarrow\Downarrow\rangle \qquad \text{and} \qquad |\downarrow\Uparrow\rangle \leftrightarrow |\uparrow\Uparrow\rangle\,.$$

For the large magnetic fields considered in the present experiment, the dark exciton eigenstates of the Hamiltonian $|E_3\rangle$ and $|E_4\rangle$ are (approximately) spin eigenstates,

$$|E_3\rangle \approx |\uparrow\Uparrow\rangle \qquad \text{and} \qquad |E_4\rangle \approx |\downarrow\Downarrow\rangle\,.$$

Thus transitions into $\left|E_{3(4)}\right\rangle$ require an electron spin flip $S^+(S^-)$ which is accompanied by an opposite flip of the nuclear spin. As can be seen from the energy level diagram in Fig. 3.3 a), for the magnetic field values investigated, the dark exciton with dominant electron spin-up character $|E_3\rangle$ is closer in energy to the bright excitonic states. This makes hyperfine flip-flop transitions into $|E_3\rangle$ more likely than those into $|E_4\rangle$, since the flip rate scales with the inverse of the energy difference squared (and the matrix elements between the two states) [142]. The ensuing imbalance in hyperfine spin flip rates can lead to a net polarization of the nuclei even if the optically excited electrons are not polarized – the bias is provided by the difference in rates for the two flip-flop processes.

As will be explained in detail in the next subsection, there are two different second order processes involving hf flip-flops:

1. If the laser is resonant with the bright exciton $|E_1\rangle \approx |\downarrow\Uparrow\rangle$, a second order process which involves hf flip-flops can occur in which a nuclear spin is flipped down and an electron spin is flipped up:

$$|E_1\rangle \approx |\downarrow\Uparrow\rangle \xrightarrow{S^+} |E_3\rangle \approx |\uparrow\Uparrow\rangle\,.$$

2. The hyperfine assisted excitation of the dark exciton. It occurs when the laser is resonant with the dark exciton $|E_3\rangle$ but detuned from the resonance with the bright exciton $|E_1\rangle$. Then, the dark exciton is excited in a second order process involving virtual excitation of the bright exciton and hf flip-flops. This process is very efficient as each such exciton is accompanied by a nuclear spin flip. Note however that in contrast to the process described in 1., the photocurrent here is very weak.

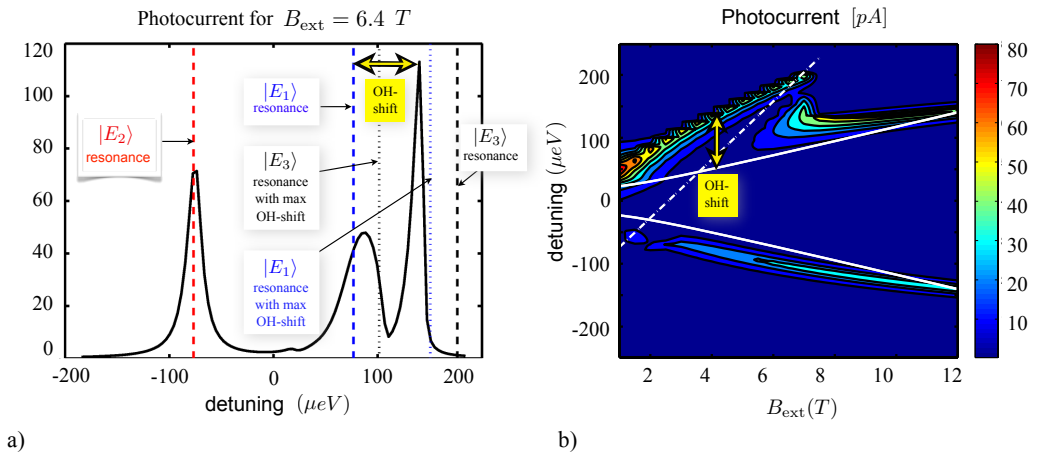

Figure 3.4: a) Simulated polarization dynamics at $B_{\text{ext}} = 6.4$T. Photocurrent as a function of laser detuning. b) Simulated photocurrent as a function of magnetic field and DC Stark detuning. The peaks in the current display the Zeeman shift and the effect of DNP. The Overhauser field shifts the resonance to larger detunings up to $B_{\text{ext}} \sim 8$T, when DNP is no longer efficient. White lines indicate the bright exciton resonances (solid) and the dark blue exciton (dashed), all without Overhauser effect.

In the next Section these two mechanisms will be explained on the basis of the calculated full PC trace obtained from the numerical simulation presented in Section 3.6.

Both processes have the result that nuclear spins are predominantly flipped to align *anti-parallel* with B_{ext}. This qualitatively explains why we observe *unidirectional* nuclear polarization independent of the net polarization of the electrons pumped through the dot.

3.4.2 Detailed explanation of the physical mechanism

In this Section the physical mechanism that leads to DNP is explained in more detail. This is done on the basis of the calculated full PC trace obtained from the numerical simulation shown in Fig. 3.4 a). Details of the numerical simulation are presented at a later stage in Section 3.6. However, for the following, it is not necessary to understand details of the simulation. The simulated PC trace corresponds to an actual steady state PC bias sweep as carried out in experiment (see Fig. 3.2). To understand the

detailed mechanism that leads to nuclear spin polarization, we consider a numerically simulated PC trace at a fixed external magnetic field $B_{\text{ext}} = 6.4\text{T}$ in Fig. 3.4 a) . The level scheme of the excitonic states is found by making a vertical cut through the Breit-Rabi diagramm in Fig. 3.3 a) at $B_{\text{ext}} = 6.4\text{T}$. Now we follow a laser sweep from red to blue detuning in the PC trace in Fig. 3.4 a) at $B_{\text{ext}} = 6.4\text{T}$. When the laser hits the red exciton resonance (see Fig. 3.4 a), dashed red line), the photocurrent peaks but no nuclear polarization is built up since all hyperfine interactions are suppressed (energetically or by spin selection rules) for the red bright exciton $|E_2\rangle$.

When the laser reaches the blue resonance, PC increases and nuclear polarization begins to build up (see Fig. 3.4 a), around the dashed blue vertical line). As the Overhauser field and the external magnetic field point in the same direction, the total magnetic field increases. Note, that the bright and dark excitons couple to the external magnetic field with a total g factor of $g^b_{\text{ex}} = 0.4$ for the bright exciton and $g^d_{\text{ex}} = -1.6$ for the dark excitons (as given in Tab. 3.1). In contrast, the Overhauser field is only seen by the electron and not by the hole, such that the bright exciton $|E_1\rangle$ couples mainly with a spin down electron $|\downarrow\rangle$ and the dark exciton $|E_3\rangle$ couples mainly with an electron spin up $|\uparrow\rangle$ to the Overhauser field, both with g factor $g_e = -0.6$.

Now two counteracting effects come into play: the nuclear polarization that builds up shifts the bright exciton $|E_1\rangle$ to higher energies (as the electron $|\downarrow\rangle$ couples to the Overhauser field with negative g factor). Thus the bright exciton gets detuned which reduces the PC and the polarization rate. In contrast, the dark exciton $|E_3\rangle$ is moved to lower energies (as the electron $|\uparrow\rangle$ couples to the Overhauser field with negative g factor), i.e., closer to the bright exciton $|E_1\rangle$. Thereby the hyperfine coupling between them is enhanced. At first, the first effect prevails, PC increases and only little nuclear polarization is built up. But as the blue dark exciton $|E_3\rangle$ (and the laser) move closer to $|E_1\rangle$ a new process becomes resonant, namely the hyperfine-assisted excitation of dark excitons (see point 2 in Section 3.4.2). This process leads to a very low photocurrent, but it is very efficient (each such exciton is accompanied by a nuclear spin flip) and it is self-enhancing: as nuclear polarization is increased, the dark exciton line shifts to lower energies, towards resonance with the laser. At the same time, $|E_1\rangle$ is further *detuned*,

which explains the deep trough in the PC curve. The doubly peaked structure is not seen in experiment, probably due a combination of additional broadening of the lines, lower nuclear polarization (which reduces the separation of the peaks), and different ratio of the dark and bright exciton g factors. The asymmetric shape of the blue exciton line might be related to this effect. Eventually, the energy of $|E_3\rangle$ falls below the laser energy, so the process becomes less efficient (and is no longer self-enforcing). However, now the Overhauser-shifted $|E_1\rangle$ comes into resonance again, resulting in the final sharp peak in PC and a small revival in polarization rate. As the laser is tuned further to the blue, all excitons become off resonant, the nuclear polarization processes are no longer efficient and the base depolarization rate takes over. The process described above requires $|E_3\rangle$ close and to the blue of $|E_1\rangle$. This is only the case for intermediate B_{ext}. For too high fields, the gap between the two is too big. For too low magnetic fields, $|E_3\rangle$ is still below $|E_1\rangle$ and the hyperfine-assisted excitation of $|E_3\rangle$ is a self-detuning process.

3.5 The theoretical model

3.5.1 Properties of the system

We consider a neutral QD in a magnetic field in Faraday configuration; resonantly driven and strongly tunnel-coupled to the leads. As evidenced by the photocurrent at saturation ($\sim 10^{10}$ excitons per second), most excitons decay non-radiatively via tunneling on a timescale $\lesssim$ns (see below). The hyperfine coupling is much slower than these tunnel processes and we have a clear separation of time scales: the excitonic system reaches a (quasi-)steady state ρ_s^e quickly and the nuclear spins evolve "driven" by an excitonic system in this state. The hyperfine flip-flop terms can then change the nuclear polarization and ρ_s^e adiabatically follows these changes.

We only consider the subspace of a neutral quantum dot with zero or one exciton. This is the simplest model capturing the effects important for the setting we have in mind. Multiple excitons are not expected at the pump rates and detunings the experiment investigates (far from saturation). We expect the singly charged states of

the QD to have little effect on the nuclear polarization since the (much lighter) electron is expected to tunnel faster and thus mostly hole states are populated, which do not exchange spin with the nuclei. Therefore, we neglect these states in the following and model tunneling by a Lindblad master equation that describes direct transitions from excitonic states to the empty QD.

3.5.2 Theoretical description

Let us now describe the model and simulation in detail. We use the basis states $|k\rangle, k = 0, \ldots, 4$ where $|0\rangle$ denotes the empty QD, and the spin eigenstates $|1\rangle = |\uparrow\Downarrow\rangle$ and $|2\rangle = |\downarrow\Uparrow\rangle$ span the bright exciton space (the first arrow characterizes the electron spin, the second one the hole spin), and $|3\rangle = |\uparrow\Uparrow\rangle$ and $|4\rangle = |\downarrow\Downarrow\rangle$ the dark exciton space. By P_X, P_B, P_D we denote the projectors on the exciton, bright-exciton, and dark-exciton subspaces respectively. The electron and hole spin operators in the exciton subspace are given by $S^z_{\mathrm{e}} = (|\uparrow\rangle\langle\uparrow| - |\downarrow\rangle\langle\downarrow|)/2$ and $S^z_{\mathrm{h}} = (|\Uparrow\rangle\langle\Uparrow| - |\Downarrow\rangle\langle\Downarrow|)/2$.

Hamiltonian Master Equation

The system dynamics is governed by a quantum master equation

$$\dot{\rho} = \mathcal{L}\rho \equiv -i[H, \rho] + \mathcal{L}_d\rho,$$

where $\mathcal{L}_d$ is the dissipative part of the master equation that is explained later. The Hamiltonian takes into account (i) the energy levels of the excitonic system including Zeeman and exchange energies ($H_{\mathrm{z}} + H_{\mathrm{x}}$), (ii) the driving laser (H_{l}), and (iii) the hyperfine interaction of the electron (H_{hf}). Written in a frame rotating with the laser frequency we have the time-independent QD Hamiltonian $H = H_{\mathrm{x}} + H_{\mathrm{z}} + H_{\mathrm{l}} + H_{\mathrm{hf}}$ with

$$H_{\mathrm{x}} = \omega_{\mathrm{x}} P_X + \delta_0(P_B - P_D)/2 + \delta_1^{\mathrm{b}}(|1\rangle\langle 2| + |2\rangle\langle 1|)/2 + \delta_1^{\mathrm{d}}(|3\rangle\langle 4| + |4\rangle\langle 3|)/2 \tag{3.1}$$

$$H_{\mathrm{z}} = g_{\mathrm{e}}\mu_{\mathrm{B}} B_{\mathrm{ext}} S^z_{\mathrm{e}} + g_h \mu_{\mathrm{B}} B_{\mathrm{ext}} S^z_{\mathrm{h}}, \tag{3.2}$$

$$H_{\mathrm{l}} = \Omega_+ |1\rangle\langle 0| + \Omega_- |2\rangle\langle 0| + \mathrm{h.c.}, \tag{3.3}$$

$$H_{\mathrm{hf}} = \vec{S}_{\mathrm{e}} \cdot \vec{A} \equiv S^z_{\mathrm{e}} A^z + \frac{1}{2}(S^+ A^- + S^- A^+). \tag{3.4}$$

Here, $\vec{A} = \sum_i A_i \vec{I}_i$ is the sum of the individual nuclear spin-I operators weighted by their respective coupling A_i to the electron spin and $A = I \sum_i A_i$ is the total hyperfine interaction [1]; ω_x contains the laser detuning from the bare exciton energy and the DC Stark shift of the excitons (the latter is changed in the experiment used to perform the sweeps). δ_0 denotes the splitting between dark and bright excitons, $\delta_1^{b(d)}$ the bright (dark) exciton exchange splitting, and $\Omega_\pm$ denotes the Rabi frequency of the $\sigma^\pm$-circularly polarized laser components.

It is useful to express the electron and hole spin operators in terms of the excitonic spin eigenstates

$$S_\mathrm{e}^z = \frac{1}{2}\left(|1\rangle\langle 1| - |2\rangle\langle 2| + |3\rangle\langle 3| - |4\rangle\langle 4|\right), \tag{3.5}$$

$$S_\mathrm{e}^+ = |1\rangle\langle 4| + |3\rangle\langle 2|, \tag{3.6}$$

$$S_\mathrm{h}^z = \frac{1}{2}\left(|3\rangle\langle 3| - |1\rangle\langle 1| + |2\rangle\langle 2| - |4\rangle\langle 4|\right). \tag{3.7}$$

We also separate the zz-part of the hyperfine coupling into the (potentially large) Overhauser term $\langle A^z\rangle S_\mathrm{e}^z$ which is added to H_Z and the rest $(A^z - \langle A^z\rangle)S_\mathrm{e}^z$.

As the experiment uses linearly polarized light, we usually consider $\Omega_+ = \Omega_-$. There is, however, little qualitative dependence on the polarization of the light, even using σ_- light the asymmetric polarization effect persists (though it will be significantly weaker especially for large magnetic fields).

The decay of the excitons is described by a Lindblad master equation with jump operators $J_k^-, k = 1, \ldots 4$

$$J_k^- = |0\rangle\langle k| \tag{3.8}$$

and associated rates Γ_k. The excitonic–nuclear quantum master equation then reads

$$\frac{d}{dt}\rho = \mathcal{L}\rho \equiv (\mathcal{L}_0 + \mathcal{L}_1)\rho, \tag{3.9}$$

with

$$\mathcal{L}_0\rho = \sum_k \Gamma_k \left(2J_k^-\rho J_k^+ - \left\{J_k^+ J_k^-, \rho\right\}_+\right) - i\left[H_0, \rho\right], \tag{3.10}$$

[1] We found that including a *hole* hyperfine interaction (of $\sim 10\%$ of electronic coupling) does not lead to relevant changes of the observed behaviour and therefore do not include it in our simulations.

where $H_0 = H_x + H_z + H_l$ contains all Hamiltonian terms except the hyperfine interaction. The decay rates Γ_k include radiative and non-radiative processes and satisfy $\Gamma_3 \equiv \Gamma_4 = \Gamma_{\rm nr}$ and $\Gamma_1 \equiv \Gamma_2 = \Gamma_{\rm nr} + \Gamma_{\rm r}$. The time scale of $\mathcal{L}_0$ is set by the decay rates, as long as $\Gamma_k \gg \|H_{\rm hf}\|$ the QD decays to its steady state $\rho_{\rm s}^e$ before hyperfine dynamics appreciably changes the nuclear state, thus the dynamics of the nuclei is determined by the instantaneous steady state of the QD (excitonic degree of freedom), and this steady state, in turn, follows adiabatically the slow evolution of the nuclei (build-up of nuclear polarization).

Nuclear Spin Dynamics

This intuition can be formalized by adiabatic elimination of the "fast" non-steady-state subspace of $\mathcal{L}_0$. Let $\rho_{\rm ss}$ denote the steady state of the Liouvillian $\mathcal{L}_0(\langle A^z\rangle)$, i.e., the instantaneous steady state of the QD at fixed Overhauser field $\langle A^z\rangle$. Define the projector on the electronic steady state ("slow subspace") by

$$\mathcal{P} : \rho \mapsto \rho_{\rm ss} \otimes {\rm tr}_{\rm qd}(\rho) \equiv \rho_{\rm ss} \otimes \mu, \tag{3.11}$$

($\mathcal{H} = \mathcal{H}_{\rm qd} \otimes \mathcal{H}_{\rm nuc}$ is the Hilbert space of the composite system; ${\rm tr}_{\rm qd}$ denotes the trace over the QD degrees of freedom and $\mu = {\rm tr}_{\rm qd}(\rho)$ denotes the reduced state of the nuclear system) and its complement $\mathcal{Q} = \mathbb{1} - \mathcal{P}$.

The master equation Eqn. (3.9) leads to two coupled equations for $\mathcal{P}\rho$ and $\mathcal{Q}\rho$. Setting $\frac{d}{dt}\mathcal{Q}\rho = 0$ (as the electronic system quickly reaches $\rho_{\rm ss}$) we obtain for $\mathcal{P}\rho$ the equation

$$\frac{d}{dt}\mathcal{P}\rho = \mathcal{P}\mathcal{L}_1\mathcal{P}\rho - \mathcal{P}\mathcal{L}_1\mathcal{Q}\left(\mathcal{Q}\mathcal{L}_0\mathcal{Q}\right)^{-1}\mathcal{Q}\mathcal{L}_1\mathcal{P}\rho, \tag{3.12}$$

which describes (to second order in $\mathcal{L}_1$) the dynamics on the slow subspace, i.e. the evolution of the nuclear spin system. Note that $\mathcal{L}_0$ is invertible on the subspace $\mathcal{Q}$. Inserting $\mathcal{L}_1(\rho) = -i[H_{\rm hf}, \rho]$ and writing the hyperfine Hamiltonian $H_{\rm hf} = \sum_{r=\pm,z} h_r S^r (A^r)^\dagger$ as $\sum_r h_r(\Delta S^r + \langle S^r\rangle_{\rm ss})A^r$ we obtain

$$\begin{aligned}\frac{d}{dt}{\rm tr}_{\rm qd}(\mathcal{P}\rho) = &-i[\sum_r h_r\langle S^r\rangle_{\rm ss}A^r, \mu] + \sum_{r,s} h_r h_s [c_{rs}^{(1)} A^r A^s \mu - c_{rs}^{(1)} A^r \mu A^s \\ &- c_{rs}^{(2)} A^s \mu A^r + c_{rs}^{(2)} \mu A^r A^s],\end{aligned} \tag{3.13}$$

where

$$c_{rs}^{(1)} = \mathrm{tr}_{\mathrm{qd}}(\Delta S^r \mathcal{L}_{0,Q}^{-1}(\Delta S^s \rho_{\mathrm{ss}})),$$
$$c_{rs}^{(2)} = \mathrm{tr}_{\mathrm{qd}}(\Delta S^r \mathcal{L}_{0,Q}^{-1}(\rho_{\mathrm{ss}} \Delta S^s)),$$

and $\mathcal{L}_{0,Q} = \mathcal{Q}\mathcal{L}_0\mathcal{Q}$; $h_\pm = 1/2, h_z = 1$.

Eqn. (3.13) contains (among others) the spin pumping terms responsible for DNP. Note that $c_{\pm\mp}^{(2)} = (c_{\mp\pm}^{(1)})^*$, which ensures that the (spin pumping) master equation for the nuclear spins is of Lindblad type. For the polarization rates (prefactors of the terms $A^+\mu A^-$ and $A^-\mu A^+$) we find

$$\gamma_+ = -\mathrm{Re}(\mathrm{tr}_{\mathrm{qd}}\left[\mathcal{L}_0^{-1}(\Delta S_e^+ \rho_{\mathrm{ss}}) S_e^-\right])/2, \tag{3.14}$$
$$\gamma_- = -\mathrm{Re}(\mathrm{tr}_{\mathrm{qd}}\left[\mathcal{L}_0^{-1}(\Delta S_e^- \rho_{\mathrm{ss}}) S_e^+\right])/2, \tag{3.15}$$

respectively. All the other terms in Eqn. (3.13) ($\propto A^+A^+, A^zA^+, A^zA^z$ etc.) are either very small or do not contribute to DNP and are therefore neglected. The imaginary part of $\mathrm{tr}_{\mathrm{qd}}\left[\mathcal{L}_0^{-1}(\Delta S_e^+ \rho_{\mathrm{ss}}) S_e^-\right]$ yields the electron-mediated nuclear spin interaction $\propto \{A^+, A^-\}_+$, which we also neglect.

Even after all these simplifications, solving Eqn. (3.13) is still difficult due to the exponentially large size of the Hilbert space of the N nuclear spins. It is significantly simplified by invoking factorization assumptions [143, 144, 145], neglecting some (or all) correlations between nuclear spins. Since we are interested here in long times on which nuclear coherences are likely to play no role (due to inhomogeneities and dipolar interaction), we use the semiclassical approximation that the nuclear spin state is separable and diagonal in the z-basis at all times. Then we obtain the equation of motion for the lth nuclear spin as

$$\frac{d}{dt}\mu_l = \gamma_+ A_l^2 \left(I_l^+ \mu_l I_l^- - \{I_l^- I_l^+, \mu_l\}_+/2\right) + \gamma_- A_l^2 \left(I_l^- \mu_l I_l^+ - \{I_l^+ I_l^-, \mu_l\}_+/2\right). \tag{3.16}$$

Assuming spin-I nuclei and states that are diagonal in the I^z-basis, Eqn. (3.16) yields a rate equation for the probabilities $p_{i,m}$ of the ith nuclear spin to be in state $|I, m\rangle$:

$$\begin{aligned}\frac{d}{dt}p_{i,m} = &-\left[\gamma_{i,+}(I-m)(I+m+1) + \gamma_{i,-}(I+m)(I-m+1)\right]p_{i,m} \\ &+ \gamma_{i,+}(I-m+1)(I+m)p_{i,m-1} + \gamma_{i,-}(I+m-1)(I-m)p_{i,m+1}.\end{aligned} \tag{3.17}$$

From this the steady state nuclear populations (for given $\gamma_{i,\pm}$) can be easily found as $p_{i,m} = \frac{1-x}{1-x^{2I+1}} x^{I+m}$ with $x = \gamma_{i,+}/\gamma_{i,-}$ and $m = -I, \ldots, I$. E.g., for spin-1/2 nuclei the steady state population in the $I^z = +1/2$ state is $p^{\mathrm{ss}}_{i,+1/2} = \frac{\gamma_{i,+}}{\gamma_{i,+}+\gamma_{i,-}}$. Since the rates $\gamma_\pm$ depend (nonlinearly) on the nuclear polarization we have to integrate the model numerically to find the nuclear steady state at given magnetic field and laser detuning (see Section 3.5.2). For simplicity, we will in this work only consider homogeneously coupled nuclei ($\gamma_{i,\pm} = \gamma_\pm$) and omit the index i henceforth.

3.6 Numerical simulation

3.6.1 The idea behind

We use the model described above to simulate the polarization process during the DC-Stark sweeps performed in the experiment: for each value of external magnetic field, the nuclear spins start in the maximally mixed stated (fully depolarized). Then, for a given DC Stark shift (fixing the detuning ω_{x} of the laser frequency from the exciton resonance), we numerically determine the electronic steady state and the associated coefficients $c^{(i)}_{rs}$ in the nuclear master equation Eqn. (3.16). This yields the instantaneous DNP rates $\gamma_\pm$ and the associated nuclear steady state. We repeat the steps (i) evolve nuclear state by Eqn. (3.17) and (ii) determine $\gamma_\pm$ that correspond to the changed nuclear polarization until the nuclear steady state is reached. Then nuclear polarization $P(B_{\mathrm{ext}}, \omega_x) = \langle I^z \rangle_{\mu^n_s}$ and the exciton population $\langle P_X \rangle_{\rho^e_s}$ are recorded. The latter is proportional to the steady state photocurrent, which is the observable from which the Overhauser shift is deduced in the experiment. Now ω_{x} is changed (without changing μ^n_s) and the same calculation is repeated for the whole sweep.

3.6.2 Result: PC curve and determination of the Overhauser shift

As already mentioned in Section 3.4.2, a calculated full PC trace obtained this way is presented in Fig. 3.4 a) simulating an actual steady state PC bias sweep as carried out in the experiment (see Fig. 3.2. For each pair of parameters $(B_{\mathrm{ext}}, \omega_{\mathrm{x}})$ this yields a steady state photocurrent. The results are plotted in Fig. 3.4 b). For fixed B_{ext} we

obtain a (typically) doubly-peaked curve, the peaks corresponding to the two bright exciton levels. We numerically determine the peaks and deduce the Overhauser shift by comparing the location of the blue and red peaks with and without nuclear polarization[2] and solving

$$\Delta\omega_b(B_{\text{ext}}) = \frac{1}{2}\left[\sqrt{(\delta_1^b)^2 + (\omega_z(B_{\text{ext}}) + \delta_n(B_{\text{ext}}))^2} - \sqrt{(\delta_1^b)^2 + \omega_z(B_{\text{ext}})^2}\right], \quad (3.18)$$

$$\Delta\omega_r(B_{\text{ext}}) = -\frac{1}{2}\left[\sqrt{(\delta_1^b)^2 + (\omega_z(B_{\text{ext}}) + \delta_n(B_{\text{ext}}))^2} - \sqrt{(\delta_1^b)^2 + \omega_z(B_{\text{ext}})^2}\right], \quad (3.19)$$

for δ_n. Here, ω_z denotes the Zeeman splitting. This yields, for every value B_{ext} of the external field an Overhauser shift of the exciton lines. These values are plotted in Fig. 3.3 c) and reproduce the qualitative behavior seen in the experiment: an *increased* splitting (Overhauser field enhancing the external field) independent of whether the blue or red exciton is pumped. However, the increase is much more pronounced and extended for the blue exciton line. For a discussion of the physical mechanisms that we believe account for the shape of the full PC trace in Fig. 3.4, see Section 3.4.2.

3.6.3 Remark on the parameters

The parameters describing the system are not known precisely from experiment, in particular, the exchange splittings $\delta_1^{\text{d}}, \delta_0$, the depolarization rate f_{depol}, the Rabi frequency $\Omega_\pm$ or the sign of g_{e}. We use typical values found in similar systems for our simulation, since our objective is only to indicate that the proposed mechanism can reproduce qualitatively the observed behavior. The values used in our simulations are collected in Tab. 3.1. To reproduce the qualitative features of the polarization process no fine-tuning of the parameters is required, but a few broad features seem necessary, in particular that the dark excitons have lower energy than the bright ones ($\delta_0 > 0$) and that the g factor of the dark excitons is larger than the g factor of the bright excitons. An important ad-hoc ingredient in the simulation is a small nuclear depolarization rate, without which the simulation would predict too much polarization. The possible origin of such a rate is discussed in the next Section.

[2] if a peak is split as in Fig. 3.4 a) the higher one is used to determine δ_n

parameter	value	
δ_0	120 μeV	dark–bright splitting
δ_1^{b}	40 μeV	bright exciton exchange splitting
δ_1^{d}	10 μeV	dark exciton exchange splitting
g_{e}	-0.6	electron g factor
g_{h}	1	heavy hole g factor
$g_{\mathrm{ex}}^{\mathrm{b}}$	$g_{\mathrm{e}} + g_{\mathrm{h}}$	bright exciton g factor
$g_{\mathrm{ex}}^{\mathrm{d}}$	$g_{\mathrm{e}} - g_{\mathrm{h}}$	dark exciton g factor
$\Omega_{\pm}$	0.3 μeV	Laser Rabi frequencies (linear polarization)
A	150μeV	hyperfine interaction
N	30 000	number of nuclei
Γ_{nr}	15 μeV	non-radiative decay rate
Γ_{r}	1 μeV	radiative decay rate

Table 3.1: System parameters used in the simulation

3.6.4 Depolarization Rate

Given how many system parameters have not been measured directly (see Tab. 3.1) and the stark simplifications (homogeneously coupled, factorizing spin-1/2 nuclei without dipolar or quadrupolar interaction; neglect of singly-charged states of the QD) used, we do not attempt to fit the measured data. The purpose of the model is only to achieve qualitative agreement to corroborate the proposed mechanism as the likely reason for the observed effect. To obtain the peaked Overhauser shift (as a function of B_{ext}) shown in Fig. 3.3 c) the introduction of a phenomenological nuclear depolarization rate f_{depol} is necessary. If the latter is set to zero, an almost constant Overhauser shift corresponding to maximal nuclear polarization is obtained from the simulation. The rate f_{depol} needs to be much larger than the nuclear depolarization rate observed when the QD is empty and the laser is off. Therefore, we have to look for a laser-induced (or exciton-induced) depolarization process. One such mechanism was proposed and studied as DNSP mechanism in [141]: laser-induced nuclear spin flips enabled by the non-collinear terms of the nuclear quadrupolar interaction arising from strain in the QD. In [141] it was shown that nuclear spin polarization rates

$$\gamma_{\pm}^{q} = \left(\frac{\Omega A_{\text{nc}}}{4\omega_{nz}}\right)^2 \frac{\Gamma}{4\delta_{\pm}^2 + \Gamma^2 + \Omega^2/2} \tag{3.20}$$

are induced, where A_{nc} is the effective strength of the non-collinear quadrupolar terms (that arise from a small non-zero angle between the directions of growth and strain), Ω the laser Rabi frequency and Γ the decay rate of the optically excited state, and $\delta_{\pm}$ is the detuning of the laser from the exciton. In [141] almost resonant lasers and only radiative decay were considered. Then the *difference* between these two rates (which is related to the difference between δ_+ and δ_- given by the Zeeman energy of a single nucleus) is non-zero, leading to a net nuclear polarization rate explaining the dragging effects seen in many optical DNSP experiments [146]. In contrast, we consider a QD that is strongly coupled to the leads and through much of the sweep strongly detuned so that the tiny difference between $\delta_{\pm}$ can be neglected ($|\delta_+ - \delta_-| \ll |\delta_+ + \delta_-|, \Gamma$) in our setting, leaving us with a purely depolarizing process with a rate

$$f_{\text{depol}} = \left(\frac{\Omega A_{\text{nc}}}{4\omega_{nz}}\right)^2 \frac{\Gamma_{\text{nr}} + \Gamma_{\text{r}}}{4\Delta^2 + (\Gamma_{\text{nr}} + \Gamma_{\text{r}})^2}, \tag{3.21}$$

where $\Delta = (\delta_+ + \delta_-)/2$ is the laser detuning. Throughout most of the sweep, Δ is the largest value in the denominator. Taking $A_{\mathrm{nc}} = 1.3 \cdot 10^{-4}\mu$eV as in [141], the depolarizing rate is too small to balance DNP. Thus the question of the depolarization mechanism remains open.

3.7 Conclusions

In summary, we have presented an experimental and theoretical investigation of asymmetric unidirectional nuclear spin pumping in an uncharged self-assembled InGaAs quantum dot via resonant optical excitation of the neutral exciton states in the photocurrent regime. The model allows to perform numerical calculations that simulate the actual measurement procedure and quantitatively reproduce the experimentally observed characteristic features of the achievable steady state nuclear polarization δ_n^s. From the theoretical model, new insights into the mechanism leading to the observed DNP effect are gained. It can be understood in terms of electron-nuclear spin flip-flop processes exchanging the orientation of an electron and nuclear spin and transferring the exciton from a optically active bright into an optically inactive dark state which then decays non-radiatively. The efficiency of these processes are determined by the detuning of bright and dark energy levels as well as the mixed character of the states which both are magnetic field dependent. Taking this into account, empirically found effects like the pronounced asymmetry in DNP upon excitation of the two X^0 Zeeman states and the dependence on the magnetic field applied appear naturally in our simulations.

Chapter 4

One-dimensional spin chain under dissipation with cold atoms

We propose a quantum optical implementation of a class of dissipative spin systems with ultra-cold atoms in optical lattices using detuned Raman transitions in the Lamb-Dicke regime. We show that using the *motional* degrees of freedom of cold bosonic atoms described by the two-band Mott insulator model, different spin models like the XXZ or the Ising model can be realized. Optical driving and decay of internal atomic levels leads to engineerable dissipation and a tunable magnetic field. This system comprises an interesting toy model for one-dimensional spin chains under dissipation studied in Chapter 5.

4.1 Introduction

Quantum spin models play a fundamental role for the theoretical and experimental study of quantum many-body effects. They represent paradigmatic systems exhibiting, e.g., quantum phase transitions [147] and peculiar forms of matter. They also provide toy models for the description of many solid-state systems. Ultra-cold atoms in optical lattices [148] have emerged as a system that is especially suited to study the low-energy sector of quantum spin systems with the promise to eventually simulate theoretical

models in large, controlled quantum systems.

To observe these effects, coupling to uncontrolled degrees of freedom has to be kept to a minimum, since it leads to dissipation and decoherence [149, 150] which can mask or destroy the quantum effects. But in recent years, it has been shown how the coupling to an environment can be harnessed to generate useful quantum states [14, 15, 16, 20, 17] or perform quantum information tasks [17, 18].

We propose a scheme to realize a quantum spin system using ultra-cold atoms in an optical lattice in which both coherent interaction and dissipation can be engineered and controlled. Considering a two-band Mott insulator model, we show how a spin Hamiltonian (Ising, XXZ) can be implemented. Coupling to optical fields, we derive an effective Master equation and show how to implement an effective transverse magnetic field. This system enables the study the non-equilibrium and steady state physics of open and driven spin systems. As studied in Chapter 5, we find that for such systems, surprisingly, peaks occur in the steady state expectation values of the collective spin operators for weak dissipation.

4.1.1 Reader's guide

In Section 4.2.1, we introduce the setup and explain qualitatively how a spin chain under engineerable dissipation in a tunable magnetic field can be realized with cold atoms in optical lattices. In Sections 4.2.2-4.2.5 we give details of the derivation. In Section 4.2.2, we study how engineerable dissipation can be realized with optical driving (and decay) of internal atomic levels. Then, in Section 4.2.3, we show how a magnetic field in x-direction can be realized with detuned Raman transition between internal atomic levels. The derivation of the spin Hamiltonian (which is tunable and can describe the Ising or the XXZ model) is explained in Section 4.2.4. In Section 4.2.5, we combine and discuss the results from the previous Sections.

4.2 Physical implementation of a one-dimensional spin chain under dissipation

Ultra-cold bosonic atoms in optical lattices are ideal candidates to simulate spin Hamiltonians. Different theoretical and experimental approaches [151] have been employed to simulate quantum spin chains in optical lattices, for example by optical driving of two hyperfine levels of cold bosons in the Hubbard regime [152]. Recently, a one-dimensional chain of interacting Ising spins has been implemented experimentally using a Mott-Insulator of spinless bosons in a tilted optical lattice [60].

In the following, we add engineered dissipation to the toolbox of these systems [153, 154]. Specifically, we show how to implement a system with the following properties: [i] dissipative dynamics of Lindblad form, [ii] a tunable magnetic field in x-direction and [iii] an effective spin Hamiltonian such as, e.g., the XXZ, Heisenberg or Ising model. In the next subsections, we first introduce the setup and explain qualitatively how such a one-dimensional spin chain in a tunable magnetic field under engineerable dissipation can be realized with cold atoms in optical lattices. In the subsequent subsections we give specific requirements and parameters and details of the derivation for [i]-[iii].

4.2.1 Setup and qualitative description

The system we consider is an optical lattice that is populated with a single atomic bosonic species. We assume to be in the Mott-insulator regime with filling factor 1, where the on-site interaction is much larger than the tunneling (hopping) between neighboring lattice sites. In this regime, the atoms are localized such that each lattice potential is occupied with one atom. We aim to use the motional ground and first excited state $\{|0\rangle, |1\rangle\}$ of the atom to realize an effective spin-1/2 system in each lattice site. To access the motional degree of freedom optically, we work in the Lamb-Dicke regime where the motion of the atom is restricted to a region small compared with the laser wavelength. We make use of the anharmonicity of the lattice potential and, as explained in the following, of decay of the atoms that leads to cooling of the system, to restrict the dynamics to the two-dimensional subspace of $\{|0\rangle, |1\rangle\}$ [155] (see Fig. 4.1).

For the optical manipulation, we assume that the atoms have internal degrees of freedom that can be addressed optically with laser fields. We consider a Λ-scheme with ground states $|g\rangle$ and $|r\rangle$ (both trapped by the same optical lattice potential) and an excited state $|e\rangle$. The level scheme of the internal states of the atoms is shown in Fig. 4.1. Off-resonant laser fields drive transitions between the two ground states $|g\rangle$ and $|r\rangle$ and the excited state $|e\rangle$. The system decays fast into the ground states, and as we will see later, effectively decays into the state $|g\rangle$. Therefore the atoms are optically pumped to the state $|g\rangle \otimes |0\rangle$ and the states $|r\rangle$ and $|e\rangle$ can be adiabatically eliminated. Eliminating the excited state $|e\rangle$ leads to the effective two-level system in the lower part of Fig. 4.1 with designable decay rates. Further elimination of the state $|r\rangle$ leads to an effective description in the internal ground state $|g\rangle$. The optical couplings by laser fields give rise to effective Hamiltonians and effective dissipation (cooling) in the ground state $|g\rangle$ at each lattice site. Details will be given in Section 4.2.2.

Therefore, we have an effective two-level system at each lattice site. As explained before, the atoms are effectively in the internal ground state $|g\rangle$, and occupy the external, motional degrees $|g\rangle \otimes |0\rangle$ and $|g\rangle \otimes |1\rangle$, i.e., the effective two-level system is given by $|0\rangle$ and $|1\rangle$ as depicted in Fig. 4.3.

In the following Sections, we show that the optical couplings of the internal levels of the atoms can be engineered such that we get an effective master equation for the two-level system $|0\rangle$, $|1\rangle$ that [i] describes dissipation of Lindblad form and [ii] an effective magnetic field in x-direction. In the Mott insulator regime, tunnel couplings between neighboring lattice wells can be treated as a perturbation, which [iii] leads to an effective spin Hamiltonian. The resulting master equation[1] is given by

$$\dot{\rho}_t = \sum_k A^- (2\sigma_k^- \rho_t \sigma_k^+ - \{\sigma_k^+ \sigma_k^-, \rho_t\}_+) - i\,[H, \rho_t]\,. \tag{4.1}$$

Here, $\sigma_k^+ = |1\rangle\langle 0|_k$ is the operator that excites an atom at lattice site k from state $|0\rangle$ to state $|1\rangle$. The sum runs over all N sites of the optical lattice potential. The first part in Eqn. (4.1) describes decay from state $|1\rangle$ into state $|0\rangle$ as depicted in Fig. 4.3. The decay parameter A^- can be tuned by changing the Rabi frequencies of the lasers and

[1] for details see Eqn. (4.15)

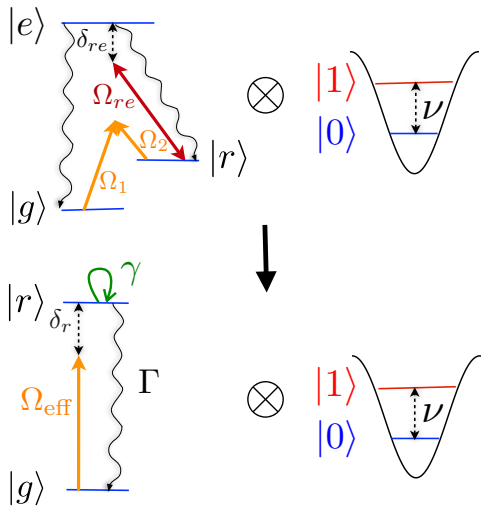

Figure 4.1: Upper Figure: Left: Internal levels of the atom: Λ system $|g\rangle$, $|r\rangle$, $|e\rangle$, off-resonantly driven by lasers. Right: Motional states of the optical lattice potential. Lower Figure: After adiabatic elimination of the excited level: effective two-level system with designable decay rates Γ and γ.

the detunings and is given by Eqn. (4.13) in Section 4.2.5. The Hamiltonian is given by $H = H_B + H_{\text{spin}}$ where H_B describes the magnetic field in x-direction given by

$$H_B = \sum_k B_x(\sigma_k^+ + \sigma_k^-), \tag{4.2}$$

where B_x is proportional to an effective magnetic field in x-direction. It is derived in Section 4.2.3. The Hamiltonian H_{spin} describes the spin Hamiltonian

$$H_{\text{spin}} = \sum_k \alpha_1(\sigma_k^x\sigma_{k+1}^x + \sigma_k^y\sigma_{k+1}^y) + \alpha_2\sigma_k^z\sigma_{k+1}^z, \tag{4.3}$$

as derived in Section 4.2.4. The parameters α_1 and α_2 depend on the properties of the optical lattice potential and can be tuned. Therefore, the Hamiltonian H_{spin} describes the XXZ model, the Ising Model or the Heisenberg Model. In the following three Sections, we employ a perturbative approach to derive a master equation comprising dissipation of Lindblad form [i] as in Eqn. (4.1), a magnetic field in x-direction [ii] as in Eqn. (4.2) and an effective spin Hamiltonian [iii] as in Eqn. (4.3). For the sake of clarity, we derive [i]-[iii] in three separate steps employing the approximation of independent rates of variation as explained in [156].

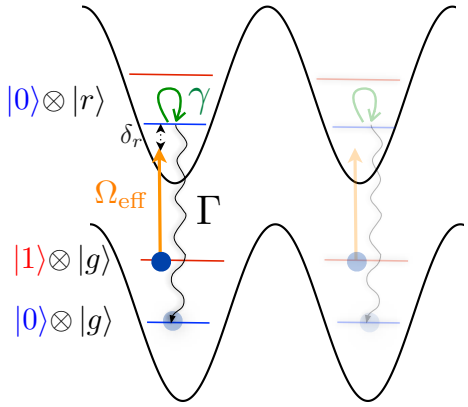

Figure 4.2: Effective two-level system $|g\rangle$-$|r\rangle$ in the optical lattice potential with motional states $|0\rangle$ and $|1\rangle$. Choosing resonance conditions as explained in Section 4.2.2, the atoms are selectively excited from $|g\rangle\otimes|1\rangle$ to the state $|r\rangle\otimes|0\rangle$ and spontaneously decay into $|g\rangle\otimes|0\rangle$.

4.2.2 Dissipation of Lindblad form

In this Section, we show that optically addressing the atoms with suitably tuned lasers allows to engineer dissipation of Lindblad form as in Eqn. (4.1).

We consider the internal levels $|g\rangle$, $|r\rangle$, $|e\rangle$ of an atom at site k. The ground states $|g\rangle$ and $|r\rangle$ can be coupled via the excited state $|e\rangle$ by a detuned Raman transition of two standing wave laser fields with Rabi frequencies Ω_1 and Ω_2. Eliminating the excited state $|e\rangle$ leads to an effective coupling between $|g\rangle$ and $|r\rangle$ (see Fig. 4.1) with $\Omega_{\text{eff}} = \Omega_1\Omega_2/\delta_{re}$ where δ_{re} is the detuning with respect to $|e\rangle$ (for details see Appendix 4.A). As shown in Fig. 4.1, $|r\rangle$ and $|e\rangle$ are coupled by another laser field (denoted by a red arrow). Adiabatic elimination of the excited state $|e\rangle$ leads to an effective two-level system (as shown in the lower part of Fig. 4.1) with states $|r\rangle$ and $|g\rangle$ which has designable decay rates Γ and γ as derived in [157] (see also Appendix 4.A). Thereby, the excited state $|e\rangle$ that is broadened by spontaneous emission is eliminated, and the effective two-level system $|g\rangle$-$|r\rangle$ allows to resolve the motional states $|0\rangle$ and $|1\rangle$ of the lattice potential (note that we are in the Lamb-Dicke regime), as can be seen in Fig. 4.2. Under appropriate resonance conditions that will be specified in the following, the atoms are excited from state $|1\rangle\otimes|g\rangle$ to state $|0\rangle\otimes|r\rangle$ and spontaneously decay

into the state $|0\rangle \otimes |g\rangle$ as shown in Fig. 4.2. Adiabatically eliminating the state $|r\rangle$, this corresponds to an effective decay from state $|1\rangle \otimes |g\rangle$ into $|0\rangle \otimes |g\rangle$. Thus the atoms effectively remain in the internal ground state $|g\rangle$, such that the decay can be written as an effective decay from state $|1\rangle$ to $|0\rangle$ as depicted in Fig. 4.3.

In Appendix 4.A, we derive in a perturbative approach (that corresponds to an adiabatic elimination of the state $|r\rangle$) a master equation that describes the dynamics of the two-level system $|0\rangle$, $|1\rangle$ of the atom. Assuming that the driving of level $|r\rangle$ is sufficiently weak such that the condition

$$\Gamma, \gamma, \nu, \delta_r \gg |\Omega_{\text{eff}}|$$

is fulfilled, and that the level broadening remains small

$$\Gamma + \gamma < \nu,$$

the master equation is given by

$$\dot{\rho}_t = \sum_k A^- \left(2\sigma_k^- \rho_t \sigma_k^+ - \{\sigma_k^+ \sigma_k^-, \rho_t\}_+\right) + A^+ \left(2\sigma_k^+ \rho_t \sigma_k^- - \{\sigma_k^- \sigma_k^+, \rho_t\}_+\right) - i[H_{\text{eff}}^{(1)}, \rho_t] \quad (4.4)$$

Here, A^+ determines the strength of the heating terms and A^- the strength of the decay terms. For simplicity, $A^\pm$ are chosen to be independent of the lattice site k. $A^\pm$ can be made dependent on the lattice site k by choosing different phases of the driving lasers as explained in Appendix 4.A. Note that $A^- \gg A^+$ is required for the validity of the approximation that only the motional levels $|0\rangle$ and $|1\rangle$ are considered. A^- and A^+ are given by

$$A^\pm = \Omega_{\text{eff}}^2 \eta_1^2 \frac{(\Gamma + \gamma)}{(\Gamma + \gamma)^2 + (\delta_r \pm \nu)^2}. \quad (4.5)$$

Here, δ_r is the effective detuning given by Eqn. (4.20) in Appendix 4.A, $\eta_1 = k_1/\sqrt{2M\nu}$ is the Lamb-Dicke parameter where k_1 is the wave number of the laser with Rabi frequency Ω_1, M the atomic mass, and ν denotes the energy difference between the motional state $|0\rangle$ and $|1\rangle$ of the lattice potential. As mentioned before, $\sigma_k^+ = |1\rangle\langle 0|_k$ is the operator that excites the atom in lattice site k from the motional ground state $|0\rangle$ to the first excited motional state $|1\rangle$ (while the atom remains in the internal ground state $|g\rangle$). The Hamiltonian $H_{\text{eff}}^{(1)}$ in the last part in Eqn. (4.4) is given by

$$H_{\text{eff}}^{(1)} = \sum_k \nu \, |1\rangle\langle 1|_k + H_S \quad (4.6)$$

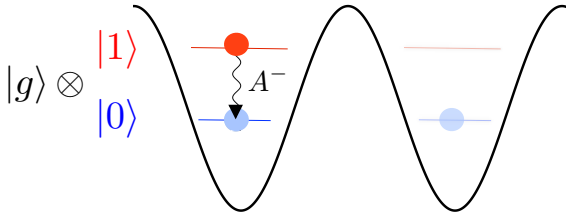

Figure 4.3: Decay of the effective two-level system $|0\rangle$, $|1\rangle$ described by the effective master equation given by Eqn. (4.7) that we derive in Section 4.2.2. The dissipation strength A^- is given in Eqn. (4.5).

where H_S describes AC Stark shifts on the motional levels that are $\ll \nu$ and are given in more detail in Appendix 4.A. Now, we have everything at hand to implement dissipation. If

$$\delta_r \approx \nu,$$

which can be achieved by choosing the laser frequency ω_l in $\delta_r = \omega_r - \omega_l$ accordingly, the strength of the dissipation is much larger than the strength of the heating:

$$A^- \gg A^+.$$

Then, the master equation has only decaying terms and is of the form

$$\dot{\rho}_t = \sum_k A^- (2\sigma_k^- \rho_t \sigma_k^+ - \{\sigma_k^+ \sigma_k^-, \rho_t\}_+) - i \left[H_{\text{eff}}^{(1)}, \rho_t\right]. \tag{4.7}$$

It describes dissipation of the atoms from state $|1\rangle$ into $|0\rangle$, while the atoms effectively remain in the internal state $|g\rangle$. By adiabatic elimination of the internal state $|r\rangle$, we have thus shown that a master equation can be derived that can be tuned such that it describes pure decay. Note that while we have shown here how to derive local dissipation assuming that each atom couples to its environment independently, the derivation of *collective* dissipation follows identical lines under the assumption that the atoms either couple all to the same mode (of an optical cavity) or that the atoms are restricted to a volume smaller than the optical wavelength.

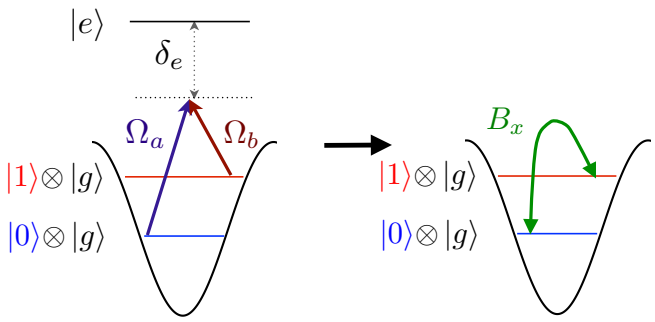

Figure 4.4: Left: A detuned Raman transition couples the internal ground state $|g\rangle$ and the excited state $|e\rangle$ of the atom. Right: Adiabatic elimination of the excited state $|e\rangle$ leads to an effective magnetic field in x-direction (see Section 4.2.3) which drives transitions between the motional states $|0\rangle$ and $|1\rangle$.

4.2.3 Effective magnetic field in x-direction

To derive the effective magnetic field in x-direction, we consider a detuned Raman transition. Two standing wave laser fields with Rabi frequencies Ω_a and Ω_b couple the internal ground state $|g\rangle$ and the excited state $|e\rangle$ of the atoms as depicted in Fig. 4.4. The coupling is described by the Hamiltonian

$$H_{ab} = \sum_k \Omega_a \cos(k_a x_k) |e\rangle\langle g|_k + \Omega_b \sin(k_b x_k) |e\rangle\langle g|_k + \text{h.c.}, \tag{4.8}$$

where k_a, k_b denote the wave numbers of the lasers and x_k the displacement from the equilibrium position of the atom at lattice site k. As we are in the Lamb-Dicke regime, $\sin(k_b x_k) \approx \eta_b(\sigma_k^- + \sigma_k^+)$ [2] and $\cos(k_a x_k) \approx 1$. Under the condition

$$|\Omega_a|, |\Omega_b| \ll |\delta_e|,$$

where δ_e is the detuning of the driving lasers as depicted in Fig. 4.4, the excited state $|e\rangle$ can be adiabatically eliminated and we get an effective Hamiltonian

$$H_{\text{eff}}^{(2)} = H_B = \sum_k B_x(\sigma_k^+ + \sigma_k^-), \tag{4.9}$$

[2] Note, that $\sin(k_b x_k) \approx \eta_b(c_k + c_k^\dagger)$ where $c_k, c_k^\dagger$ are bosonic operators that describe the harmonic oscillator states of the trapping potential. As explained before, we work in the truncated subspace of $|0\rangle$ and $|1\rangle$ due to the anharmonicity of the trapping potential and the cooling to the ground state. Therefore, we can write $\eta_b(c_k + c_k^\dagger) = \eta_b(\sigma_k^- + \sigma_k^+)$.

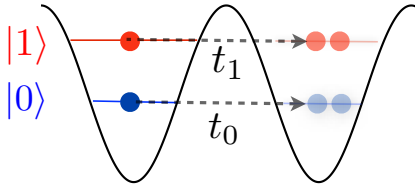

Figure 4.5: Tunneling between neighboring lattice wells with tunnel amplitudes t_0 and t_1. States with two atoms per lattice well are treated in perturbation theory in Section 4.2.4, as the on-site interaction is much larger than the tunneling amplitudes.

that describes a tunable magnetic field in x-direction where B_x is proportional to the magnetic field strength in x-direction is given by

$$B_x = \frac{\Omega_a \Omega_b \eta_b}{\delta_e}.$$

Thus, we have derived an effective magnetic field in x-direction that drives transitions between the motional states $|0\rangle$ and $|1\rangle$ (as depicted in Fig. 4.4 on the right), while the atoms remain effectively in the ground internal state $|g\rangle$.

4.2.4 Effective spin Hamiltonian

In the Mott-Insulator regime, bosonic atoms trapped by a lattice potential with two motional states are described by the two-band Bose-Hubbard model (see Appendix 4.B). We denote the on-site interaction by U_{01}, U_0 and U_1 [3] and by t_0 (t_1) the amplitudes for atoms in state $|0\rangle$ ($|1\rangle$) to tunnel to neighboring lattice sites. We assume that the on-site interaction U_{01}, U_0, $U_1 \gg t_0$, t_1 such that tunneling between neighboring wells that leads to states with two atoms in one lattice well can be treated as a perturbation (see Fig. 4.5). Using second order perturbation theory [156] (for a detailed derivation see Appendix 4.B), we derive an effective spin Hamiltonian H_{spin} given by:

$$H_{\text{eff}}^{(3)} = H_{\text{spin}} + B_z \sum_k |1\rangle\langle 1|_k \,, \tag{4.10}$$

[3] $U_{xx'}$ is the on-site repulsion of two atoms on lattice site k, where one atom is in motional state $|x\rangle$ and the other one in $|x'\rangle$ with $x, x' = 0, 1$, respectively

with

$$H_{\text{spin}} = \sum_k \alpha_1(\sigma_k^x \sigma_{k+1}^x + \sigma_k^y \sigma_{k+1}^y) + \alpha_2 \sigma_k^z \sigma_{k+1}^z, \tag{4.11}$$

where $\alpha_1 = -2t_0 t_1/U_{01}$, $\alpha_2 = (t_0^2 + t_1^2)/(2U_{01}) - t_0^2/U_0 - t_1^2/U_1$, the magnetic field in z-direction

$$B_z = t_1^2/U_1 - t_0^2/U_0,$$

and the Pauli spin matrices σ_k^x, σ_k^y with $\sigma_k^x = |0\rangle\langle 1|_k + |1\rangle\langle 0|_k$. The Hamiltonian given by Eqn. (4.11) is an effective spin Hamiltonian that is tunable by changing the lattice properties. If $\alpha_1, \alpha_2 > 0$, $H_{\text{eff}}^{(3)}$ corresponds to the XXZ model with a magnetic field in z-direction. If the lattice properties can be tuned such that one of the tunneling constants t_0 or $t_1 \to 0$, H_{spin} is an Ising Hamiltonian with a magnetic field in z-direction.

4.2.5 Dissipative one-dimensional spin chain in a magnetic field

In the previous Sections, we showed that optical couplings of the internal levels can be engineered such that we get a master equation of Lindblad form [Eqn. (4.4)] and an effective magnetic field in x-direction [Eqn. (4.9)]. Then we derived the spin Hamiltonian given by Eqn. (4.10) in perturbation theory. Now, we would like to combine all these results to get a one dimensional spin chain described by the XXZ, Ising or Heisenberg Model [iii] under dissipation of Lindblad form [i] in an effective magnetic field in x-direction [ii]. This system is discussed in Section 4.1 and is described by Eqn. (4.1). Now, we want to discuss it in more detail.

In the previous Sections we derived [i]-[iii] in separate steps for the sake of clarity. Combining these results, one has to carefully consider the order of magnitude of each term. Doing so, we find that the magnetic field in z-direction B_z in Eqn. (4.10) and Stark shifts in Eqn. (4.6) can be of the same order of magnitude as ν. B_z and Stark shifts lead to an effective energy difference between the motional states $|0\rangle$ and $|1\rangle$ given by

$$\tilde{\nu} = \nu + B_z + s_- - s_+,$$

where B_z is defined in Eqn. (4.11) and s_-, s_+ are the AC Stark shifts in Eqn. (4.6). Therefore, combining all results, the laser detuning δ_r that enters in the $A^{\pm}$ has to be

adjusted to $\tilde{\delta}_r$ such that $\tilde{\delta}_r - \nu = \delta_r - \tilde{\nu}$ which means that $\tilde{\delta}_r = \delta_r \pm (B_z + s_- - s_+)$.

Then, the master equation combining results from Eqns. (4.4), (4.9) and (4.10) reads

$$\dot{\rho}_t = \sum_k A^+(2\sigma_k^+\rho_t\sigma_k^- - \{\sigma_k^-\sigma_k^+, \rho_t\}_+) + A^-(2\sigma_k^-\rho_t\sigma_k^+ - \{\sigma_k^+\sigma_k^-, \rho_t\}_+) \\ -i[H, \rho_t], \tag{4.12}$$

where the rates $A^\pm$ are modified

$$A^\pm = \Omega_{\text{eff}}^2\eta_1^2\frac{(\Gamma+\gamma)}{(\Gamma+\gamma)^2 + (\tilde{\delta}_r \pm \nu)^2}. \tag{4.13}$$

and the Hamiltonian part of the master equation is given by

$$H = \quad H_{\text{spin}} + H_B + \tilde{\nu}\sum_k |1\rangle\langle 1|_k\,, \tag{4.14}$$

where H_{spin} is given by Eqn. (4.11) and H_B by Eqn. (4.9). The magnetic field in z-direction and Stark shifts have been included in $\tilde{\nu}$.

For $\tilde{\delta}_r \approx \nu$, as shown before, decay dominates over heating:

$$A^- \gg A^+.$$

Then, the master equation has only decaying terms. Eqn. (4.11) describes a dissipative XXZ spin chain in a magnetic field with both x and z components. However, only B_x is fully tunable, while B_z is large (compared to $B_x, A^\pm$) and required to be so by the conditions for adiabatic elimination. In order to obtain an effective dissipative XXZ chain without any field in z-direction, we transform to a frame rotating with $\tilde{\nu}$. However, in the rotating frame, H_B becomes time dependent. To obtain a time independent field in x-direction, the detuned Raman pulses that lead to the effective magnetic field in x-direction have to be chosen time dependent, adapated to the rotating frame. This yields a time independent transversal magnetic field, and the master equation in the rotating frame is given by

$$\dot{\rho}_t = \quad \sum_k A^-(2\sigma_k^-\rho_t\sigma_k^+ - \{\sigma_k^+\sigma_k^-, \rho_t\}_+) - i\left[H_{\text{spin}} + H_B, \rho_t\right]. \tag{4.15}$$

It corresponds to the master equation given by Eqn. (4.1). In summary we have shown how to implement a one-dimensional spin chain with nearest-neighbor interaction described by the XXZ or the Ising model and a tunable effective magnetic field in x-direction under dissipation.

4.3 Conclusions

We have investigated one-dimensional spin chains in a transverse magnetic field under dissipation. A physical system that is well suited for the simulation of different spin models are cold atoms in optical lattices. We have shown, that in the Mott-insulator regime with one atom per lattice well, spin Hamiltonians, such as the XXZ model, the Ising model or the Heisenberg model, can be realized. Optical driving of internal atomic states allows the realization of engineered dissipation and a transversal magnetic field. This system is an ideal testbed for studying steady state dynamics of dissipative spin models. This will be discussed in the next chapter.

4.A Derivation of effective dissipative master equation

The internal levels of the atom that we consider are $|g\rangle$, $|r\rangle$, $|e\rangle$. Adiabatically eliminating the excited state $|e\rangle$ as discussed in Section 4.2.2, we get an effective two-level system $|g\rangle$ and $|r\rangle$ that is coupled with the effective Rabi frequency Ω_{eff} as depicted in Fig. 4.1.

In the following, we derive in detail the master equation given by Eqn. (4.4) in Section 4.2.2. The internal levels of the atom that we consider are $|g\rangle$, $|r\rangle$, $|e\rangle$, as depicted in the upper part of Fig. 4.1. The states $|g\rangle$-$|r\rangle$ are coupled by a detuned Raman transition via the excited state $|e\rangle$ by two standing wave laser fields. The coupling is described by the Hamiltonians

$$H_{l1} = \sum_k \Omega_1 \cos(k_1 x_k)(|e\rangle\langle g|_k + \text{h.c.}), \tag{4.16}$$

and

$$H_{l2} = \sum_k \Omega_2 \sin(k_2 x_k)(|r\rangle\langle g|_k + \text{h.c.}), \tag{4.17}$$

where Ω_1 and Ω_2 are the Rabi frequencies of the two lasers and k_1 and k_2 are the wave numbers of the lasers and k denotes the lattice site. x_k is the displacement from the equilibrium position of the atom at lattice site k. The phase of the lasers is for simplicity chosen such that $\cos(k_1(x_k + x_k^0)) = \cos(k_1 x_k)$ and $\cos(k_2(x_k + x_k^0)) = \sin(k_2 x_k)$ where x_k^0 the equilibrium position of the atom at lattice site k. Choosing

different phases of the lasers makes $A^{\pm}$ in Eqn. (4.5) dependent on the lattice site k. Adiabatic elimination of the excited state $|e\rangle$ leads to an effective coupling

$$H_1 = \sum_k \Omega_{\text{eff}} \eta_1 (\sigma_k^- + \sigma_k^+)(|r\rangle\langle g| + \text{h.c.}), \tag{4.18}$$

with $\Omega_{\text{eff}} = \Omega_1 \Omega_2 / \delta_{re}$ where δ_{re} is the detuning with respect to $|e\rangle$ and η_1 is the Lamb-Dicke parameter. Here, we have expressed the deviation from equilibrium position, x_k, in terms of harmonic oscillator operators truncated to the two lowest lying levels $\sin(k_1 x_k) \approx \eta_1(\sigma_k^- + \sigma_k^+)$ where $\sigma_k^+ = |1\rangle\langle 0|_k$ and $\sigma_k^- = |0\rangle\langle 1|_k$ and $\cos(k_2 x_k) \approx 1$. The effective coupling with Rabi frequency Ω_{eff} between states $|r\rangle$ and $|g\rangle$ is shown in Fig. 4.1.

Coupling the state $|r\rangle$ to the excited state $|e\rangle$ with a third standing wave laser field with Rabi frequency Ω_{er}, depicted with a red arrow in Fig. 4.1, we can derive an effective two-level system $|g\rangle$-$|r\rangle$ with designable decay rates as done in [157]. Here, we quickly review this result. Following [157], the upper level $|e\rangle$ can be adiabatically eliminated if the saturation parameter for the transition $|r\rangle$ and $|e\rangle$ is small

$$s_{r,e} = \frac{(\Omega_{re}/2)^2}{\delta_{re}^2 + (\Gamma_{er} + \Gamma_{eg})^2/4} \ll 1. \tag{4.19}$$

According to [157], the effective detuning and the effective decay rates are given by:

$$\delta_r = \delta_{gr} - \delta_{re} \frac{(\Omega_{re}/2)^2}{[(\Gamma_{eg} + \Gamma_{er})/2]^2 + \delta_{re}^2}, \tag{4.20}$$

$$\Gamma = \frac{(\Omega_{re}/2)^2}{[(\Gamma_{eg} + \Gamma_{er})/2]^2 + \delta_{re}^2} \Gamma_{eg}, \tag{4.21}$$

$$\gamma = \frac{(\Omega_{re}/2)^2}{[(\Gamma_{eg} + \Gamma_{er})/2]^2 + \delta_{re}^2} \frac{\Gamma_{eg} + \Gamma_{er}}{2}, \tag{4.22}$$

see also the lower part of Fig. 4.1. The effective two-level system $|g\rangle$-$|r\rangle$ with the effective decay rates Γ, γ and the effective detuning δ_r is the starting point of the following discussion. The full Hamiltonian describing the system is given by

$$H_{\text{full}} = H_1 + H_0, \tag{4.23}$$

where H_1 describes the atom-light interaction given by Eqn. (4.18) and H_0 defines the energies of the system

$$H_0 = \sum_k \delta_r \left|r\right\rangle\!\left\langle r\right|_k + \nu \left|1\right\rangle\!\left\langle 1\right|_k . \tag{4.24}$$

The effective dynamics of the system can be derived considering contributions to the Liouvillian up to second order in a perturbative approach. The full system is described by a Liouvillian given by:

$$\dot{\rho}(t) = (\mathcal{L}_0 + \mathcal{L}_1)\rho(t), \tag{4.25}$$

where $\mathcal{L}_0$ is the unperturbed part of the Liouvillian and $\mathcal{L}_1$ is the perturbative part. The unperturbed part of the Liouvillian is described by

$$\begin{aligned}\mathcal{L}_0\rho(t) = & \sum_k \Gamma \left(2 \left|g\right\rangle\!\left\langle r\right|_k \rho(t) \left|r\right\rangle\!\left\langle g\right|_k - \left\{\left|r\right\rangle\!\left\langle r\right|_k , \rho(t)\right\}_+\right) \\ & +\gamma \left(2 \left|r\right\rangle\!\left\langle r\right|_k \rho(t) \left|r\right\rangle\!\left\langle r\right|_k - \left\{\left|r\right\rangle\!\left\langle r\right|_k , \rho(t)\right\}_+\right) - i \left[H_0, \rho(t)\right] .\end{aligned} \tag{4.26}$$

The first part of the Liouvillian is the decay part with the effective decay rate Γ from state $|r\rangle$ to $|g\rangle$ and the dephasing rate γ. The perturbative part of the Liouvillian is given by

$$\mathcal{L}_1\rho(t) = -i \left[H_1, \rho(t)\right], \tag{4.27}$$

where H_1 is given by Eqn. (4.18) and describes the interaction of the two-level system with the effective laser field. Using a perturbative approach where $\mathcal{L}_1\rho(t)$ is treated as a perturbation, we derive an effective Liouvillian in the subspace of the ground internal state and the ground and first excited motional states, $|g\rangle\!\langle g| \otimes (|0\rangle\!\langle 0| + |1\rangle\!\langle 1|)$. The projection onto this subspace reads

$$\mathbb{P}\dot{\rho}(t) = \mathbb{P}\mathcal{L}\mathbb{P}\rho(t) + \mathbb{P}\mathcal{L}\mathbb{Q}\rho(t), \tag{4.28}$$

where $\mathbb{P}\rho = |g\rangle\!\langle g| \otimes (|0\rangle\!\langle 0| + |1\rangle\!\langle 1|)\rho\, |g\rangle\!\langle g| \otimes (|0\rangle\!\langle 0| + |1\rangle\!\langle 1|)$ and $\mathbb{Q} = 1 - \mathbb{P}$. Projecting onto the subspace we want to eliminate we get

$$\mathbb{Q}\dot{\rho}(t) = \mathbb{Q}\mathcal{L}\rho(t). \tag{4.29}$$

In the following, we integrate Eqn. (4.29) to get the time evolution of the density matrix in the fast space, $\mathbb{Q}\rho(t)$. We insert the result in Eqn. (4.28) to get an equation

of motion for the density matrix in the slow space. Therefore, we first go into the interaction picture where the density matrix is given by $\tilde{\rho}(t) = e^{-\mathcal{L}_0 t}\rho(t)$. The equation of motion in the fast space reads

$$\mathbb{Q}\dot{\tilde{\rho}}(t) = \mathbb{Q}W_I(t)\tilde{\rho}(t), \tag{4.30}$$

with $W_I(t) = e^{\mathcal{L}_0 t}\mathcal{L}_1 e^{\mathcal{L}_0 t}$. Solving this equation by iteration [158] we get

$$\mathbb{Q}\rho(t) = \mathbb{Q}e^{\mathcal{L}_0 t}\left[\int_0^t ds W_I(s)\mathbb{P}\tilde{\rho}(0) + \int_0^t ds_1 \int_0^{s_1} ds_2 W_I(s_1)W_I(s_2)\mathbb{P}\tilde{\rho}(0)\right]. \tag{4.31}$$

At time $t = 0$, $\tilde{\rho}(0)$=$\rho(0)$ and we assume that at $t = 0$, the population is in the ground state, i.e., $\tilde{\rho}(0) = \mathbb{P}\tilde{\rho}(0)$. Higher order integrals are neglected making the assumption that

$$\Gamma, \gamma, |\delta_r|, \nu \gg |\Omega_{\text{eff}}|\,. \tag{4.32}$$

We denote the first integrals in Eqn. (4.31) by $R_1(t)$ and the second integral by $R_2(t)$ such that

$$\mathbb{Q}\rho(t) = R_1(t) + R_2(t). \tag{4.33}$$

Inserting in Eqn. (4.28) leads to

$$\mathbb{P}\dot{\rho}(t) = \mathbb{P}\mathcal{L}\mathbb{P}\rho(t) + \mathbb{P}\mathcal{L}_0 R_1(t) + \mathbb{P}\mathcal{L}_1 R_1(t) + \mathbb{P}\mathcal{L}_0 R_2(t) + \mathbb{P}\mathcal{L}_1 R_2(t). \tag{4.34}$$

The term $\mathbb{P}\mathcal{L}_0 R_1(t) = 0$, and $\mathbb{P}\mathcal{L}_1 R_2(t)$ is a third order term and can be neglected. Neglecting terms rotating with $\exp(\pm i\nu t)$ we get the master equation given by Eqn. (4.4) where AC Stark shifts given by

$$H_S = s_- \sigma_k^+ \sigma_k^- + s_+ \sigma_k^- \sigma_k^+, \tag{4.35}$$

where

$$s_\pm = \Omega_{\text{eff}}^2 \eta_1^2 \frac{(\delta_r \pm \nu)}{(\Gamma + \gamma)^2 + (\delta_r \pm \nu)^2}.$$

4.B Derivation of the spin Hamiltonian

In the Mott-Insulator regime, bosonic atoms trapped by a lattice potential with two motional states are described by the two-band Bose-Hubbard model

$$H_{\text{BH}} = H_0 + H_t. \tag{4.36}$$

Here, the sum runs over the N sites k of the optical lattice. The unpertubed Hamiltonian H_0 is given by

$$H_0 = \sum_k \left(\tfrac{U_{01}}{2} \hat{n}_{k0}\hat{n}_{k1} + \sum_{x=0,1} \tfrac{U_{xx}}{2} \hat{n}_{kx}(\hat{n}_{kx} - 1) + \nu \left|1\right\rangle\!\left\langle 1\right|_k \right),$$

where $U_{xx'}$ is the on-site repulsion of two atoms on lattice site k, where one atom is in motional state $|x\rangle$ and the other one in $|x'\rangle$ with $x, x' = 0, 1$, respectively. The operator $\hat{n}_{kx} = |x\rangle\langle x|_k$ counts the number of atoms at lattice site k in the motional states $x = 0, 1$ and ν is the energy difference between ground and first excited motional states. We assume the system to be prepared in the ground state $|0\rangle$. Due to the anharmonicity of the potential, we do not leave the subspace of $n = 0$ and $n = 1$ excitations.

The perturbative part of the Hamiltonian describes the tunneling between neighboring lattice sites and is given by

$$H_t = \sum_k t_0 c^\dagger_{k,0} c_{k+1,0} + t_1 c^\dagger_{k,1} c_{k+1,1}. \tag{4.37}$$

Here, the operators c_{kx} with $x = 0, 1$ are bosonic destruction operators for atoms in the two motional states $|0\rangle$ and $|1\rangle$ at lattice site k. $t_0(t_1)$ are the tunneling amplitudes from state $|0\rangle$ ($|1\rangle$) at lattice site k to state $|0\rangle$ ($|1\rangle$) at $k + 1$.

As the on-site interaction $U_{xx'} \gg t_0, t_1$, tunneling between neighboring wells that leads to states with two atoms in one lattice well can be treated as a perturbation. For that, we consider two neighboring lattice sites k and $k + 1$ and write the effective Hamiltonian in the basis of eigenvectors of H_0, $|x_k, y_{k+1}\rangle$, where for example $|0_k, 1_{k+1}\rangle$ is the notation for the state with one particle in well k in state $|0\rangle$, and one particle in well $k + 1$ in state $|1\rangle$. In perturbation theory [156], the second-order effective Hamiltonian can be evaluated in the following way:

$$\left\langle x_k, y_{k+1}\right| H^{(3)}_{\text{eff}} \left|x'_k, y'_{k+1}\right\rangle = \tfrac{1}{2} \sum_\chi \left\langle x_k, y_{k+1}\right| H_t \left|\chi\right\rangle \tfrac{1}{E'} \left\langle \chi\right| H_t \left|x'_k, y'_{k+1}\right\rangle.$$

where

$$\frac{1}{E'} = \frac{1}{E_{xy} - E_\chi} + \frac{1}{E_{x'y'} - E_\chi},$$

and $|\chi\rangle$ are eigenstates of H_0 with two particles in one well (and no particle in the other one). E_{xy} and E_χ are the unperturbed energies $\langle x_k, y_{k+1}| H_0 |x_k, y_{k+1}\rangle$, $\langle\chi| H_0 |\chi\rangle$ etc.

Evaluating Eqn. (4.38) leads to the effective spin Hamiltonian $H_{\text{eff}}^{(3)}$ is given by:

$$H_{\text{eff}}^{(3)} = H_{\text{spin}} + B_z \sum_k |1\rangle\langle 1|_k \,. \tag{4.38}$$

with

$$H_{\text{spin}} = \sum_k \alpha_1(\sigma_k^x \sigma_{k+1}^x + \sigma_k^y \sigma_{k+1}^y) + \alpha_2 \sigma_k^z \sigma_{k+1}^z \tag{4.39}$$

Here

$$\alpha_1 = -2t_0 t_1 / U_{01},$$

$$\alpha_2 = (t_0^2 + t_1^2)/(2U_{01}) - t_0^2/U_0 - t_1^2/U_1,$$

the magnetic field in z-direction

$$B_z = t_1^2/U_1 - t_0^2/U_0,$$

and the Pauli spin matrices σ_k^x, σ_k^y. Thus, we have derived an effective XXZ-spin Hamiltonian with a magnetic field in z-direction.

Chapter 5

Steady state dynamics: Discontinuities and state preparation

We study the steady state properties of local one-dimensional spin Hamiltonians under different types of dissipation. For small spin chains and weak dissipation, steady state expectation values show pronounced peaks at certain critical system parameters. We find that in the limit of weak dissipation, these peaks indicate discontinuities in the steady state expectation values. We show how to use this effect to dissipatively probe the Hamiltonian's spectrum and derive a condition that elucidates the occurence of discontinuities in the steady state expectation values. We moreover study state preparation with dissipative spin systems and show, that for certain spin Hamiltonians under dissipation, fully entangled unique steady states of spin chains of N atoms can be prepared. Then, we show how collective dissipation can be realized with cold atoms in an optical cavity.

5.1 Introduction

Dissipation is a phenomenon naturally appearing in any realistic quantum system interacting with its surroundings. While it is usually considered as an obstacle, in recent years new approaches have been proposed harnessing dissipation for quantum state engineering [14, 15, 16, 20, 17] and quantum information processing [17, 18]. Moreover, the study of the steady state phase diagram of open quantum systems has turned into a fruitful direction itself [159, 160, 161, 162, 163, 164].

In the previous Chapter, we have shown that ultra-cold bosonic atoms in optical lattices are a good candidate for the realization of one-dimensional spin chains under engineerable dissipation. This system enables experimental studies of steady state properties of one-dimensional dissipative spin chains. Here, we study in more generality, independent of the physical realization, one-dimensional spin Hamiltonians under dissipation. We highlight a peculiar feature of the steady state phase diagram for small spin chains: in the limit of weak dissipation, abrupt changes of steady state expectation values for certain critical values of the system parameters are observed. Surprisingly, these critical values are related to degeneracy properties of the system's Hamiltonian and allow for dissipative probing of the spectrum of the Hamiltonian. Moreover, we study different classes of spin Hamiltonians under dissipation that enable engineering of interesting steady states. We show that for certain spin Hamiltonians, the system is dissipatively driven into (pure) fully entangled unique steady states. Here, we consider also collective dissipation of spins that are all coupled to one single mode, and show, that such a setup can be realized with a Bose-Einstein Condensates in an optical cavity. Finally, we derive the master equation for a laser-driven chain of atoms trapped with sub-wavelength distances, which might be realized with plasmonic structures or atoms encapsulated in a carbon nanotube. In the regime of sub-wavelength interatomic distances, long-range interactions like the electrical dipole-dipole and the magnetic dipole-dipole interaction (in case of a magnetic moment of the atomic levels) play a significant role. Moreover, such systems are potential candidates for studying strongly coupled spin systems as well as collective effects such as, e.g., Dicke superradiance [56].

5.1.1 Reader's guide

In Section 5.2 we discuss numerical studies of one-dimensional spin chains with few atoms. We find that the steady state expectation values show pronounced peaks that can be related to degeneracy properties of the system's Hamiltonian. In the limit of weak dissipation, the peaks indicate discontinuities in the steady state expectation values of the spin operators. In Section 5.2.2 we derive a general condition that elucidates the discontinuous behavior of the steady state expectation values at degeneracy points of the Hamiltonian. To get a better understanding of this condition, we study it in more detail for Ising Hamiltonians in Section 5.2.3. In Section 5.3 we investigate state engineering with dissipative spin chains. We study a general family of spin Hamiltonians under collective dissipation. We show that for certain spin Hamiltonians, the system is dissipatively driven into (pure) fully entangled unique steady states. In Section 5.4, we show how collective dissipation can be realized with cold atoms that are coupled to one single mode of an optical cavity. In Section 5.5 we derive a master equation for a laser-driven chain of atoms trapped with sub-wavelength distances which might be realized with plasmonic structures or atoms encapsulated in a carbon nanotube.

5.2 Discontinuities in the steady state dynamics of a general class of one-dimensional spin models under dissipation

We study the steady state behavior of short spin chains under dissipation in a magnetic field in x-direction with numerical simulations. In the previous Chapter, we discussed how to realize the XXZ model in a transversal magnetic field under engineerable dissipation with cold atoms in optical lattices. Studying the steady state properties of this system we find peculiar features. We consider the XXZ model with 4 spins as given by Eqn. (4.11) in the previous Chapter, where we chose $\alpha_1 = \frac{1}{4}\alpha_2$. We find that the steady state of this system shows a surprising behavior: Changing the external magnetic field in x-direction, peaks occur in the steady state expectation values of the collective spin operators $\langle J^x \rangle$ and $\langle J^z \rangle$ (where $J^{x/z} = \sum_k J_k^{x/z}$ are collective spin operators) for weak

dissipation, see Fig. 5.1. Here, we have considered dissipation as in Eqn. (4.15) with equal dissipation strength on each spin. We find that decreasing the strength of the dissipation the peaks become more narrow. The height of the peaks, however, does not change. For small γ we observe very narrow peaks. This indicates a discontinuity in the steady state expectation values of the spin operators. We find, that these narrow peaks appear exactly at degeneracy points of the spectrum of the Hamiltonian.

In the following, we study in more generality, independent of a physical implementation, local one dimensional spin Hamiltonians under dissipation of different kinds. We present a condition that elucidates the discontinuous behavior of the steady state at degeneracy points of the Hamiltonian. Then, we study this condition in more detail for Ising Hamiltonians.

5.2.1 Numerical studies of discontinuous behavior in the steady state

We numerically simulate short spin chains. First, we study the one dimensional Ising model, described by the Hamiltonian

$$H = H_{zz} + H_b \tag{5.1}$$

with

$$H_{zz} = \alpha_3 \sum_k J_k^z J_{k+1}^z, \tag{5.2}$$

and

$$H_b = B_x \sum_k J_k^x, \tag{5.3}$$

subject to local or collective dissipation. The master equation describing the full system with local dissipation is given by

$$\dot{\rho}_t = \sum_k \gamma_k \left(2J_k^- \rho_t J_k^+ - \{J_k^+ J_k^-, \rho_t\}_+\right) - i[H, \rho_t], \tag{5.4}$$

where J_k^+ and J_k^- are spin raising and lowering operators for the kth spin in a chain. The spin chain we consider here has open boundary conditions.

Changing the magnetic field B_x, we find that the steady state expectation values of the spin operators $\langle J^x \rangle$ and $\langle J^z \rangle$ change abruptly for weak dissipation, see Fig. 5.2.

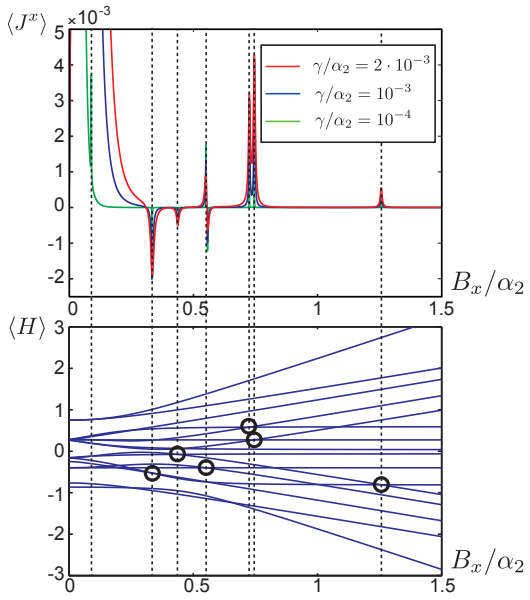

Figure 5.1: XXZ model with 4 spins, $\alpha_1 = \frac{1}{4}\alpha_2$ and open boundary conditions under local dissipation. Upper Figure: Steady state expectation value $\langle J^x \rangle$ plotted versus the magnetic field B_x/α_2. Lower Figure: Spectrum of the XXZ chain in the magnetic field B_x plotted versus B_x/α_2.

Here, we have considered dissipation as in Eqn. (5.4) with equal dissipation strength on each spin, $\gamma_k = \gamma$. Decreasing the strength of the dissipation, i.e., decreasing γ, the peaks narrow at constant height. For $\gamma \to 0$, we observe very narrow peaks, which indicate discontinuities in the steady state expectation values of the spin operators. We find, that these narrow peaks appear exactly at degeneracy points of the spectrum of the Hamiltonian. I.e., to every peak for $\gamma \to 0$ that is found for a given value of $x_0 = B_x$, at least one pair of degenerate eigenvalues λ_1, λ_2 of the local spin Hamiltonian H_{zz} can be found, i.e., $\lambda_1(x_0) = \lambda_2(x_0)$ at x_0. This effect can be observed for different kinds of spin Hamiltonians such as for example the XXZ model (see Fig. 5.1), both for periodic and open boundary conditions. Moreover, changing the type of dissipation, the observed behavior does not change. Collective dissipation[1] describes the dynamics

[1] In Chapter 5.4 we show how collective dissipation can be experimentally realized with cold atoms in an optical cavity.

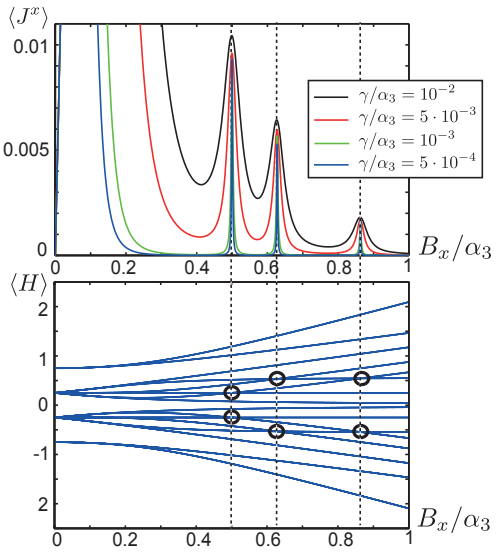

Figure 5.2: Ising model with 4 spins with open boundary conditions under local dissipation of form given by Eqn. (5.4). Upper figure: Steady state expectation value $\langle J^x \rangle$ plotted versus the magnetic field B_x/α_3. Peaks are observed that narrow for decreasing the dissipation strength. Lower Figure: Spectrum of the Ising Hamiltonian in a magnetic field B_x plotted versus B_x/α_3. Peaks in the steady state expectation value (upper figure) appear at crossing points of the Hamiltonian that are marked with black circles.

of spin all coupled to the same field mode and is decribed by the master equation

$$\dot{\rho}_t = \gamma(2J^- \rho_t J^+ - \{J^+ J^-, \rho_t\}_+) - i[H, \rho_t] \tag{5.5}$$

where $J^\pm = \sum_k J_k^\pm$ are collective spin operators. It also leads to discontinuous behavior in the steady state expectation values as shown in Fig. 5.3 for the Ising model. Choosing a "inhomogeneous" dissipation which is of the form of the dissipative part in Eqn. (5.4), where now the strengths of the dissipation γ_k are different for each spin, peaks can be observed for an even larger class of spin Hamiltonians: For $\gamma_k = \gamma$, and $H = H_H + H_b$, where H_H is the Heisenberg spin Hamiltonian, we do not observe any peaks. If we, however, choose different dissipation strengths γ_k for each spin, we find peaks at the degeneracy points of the Hamiltonian, as can be seen in Fig. 5.4.

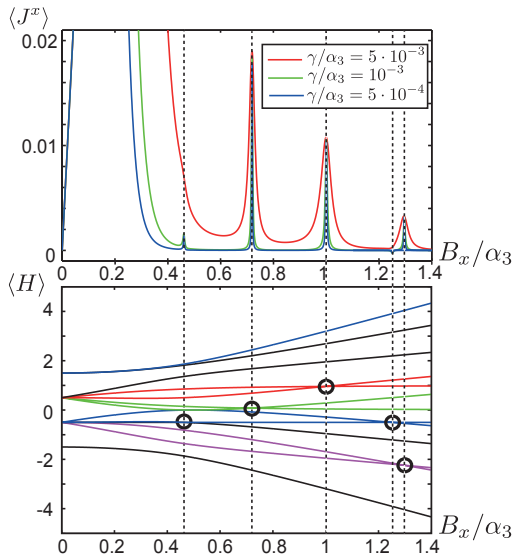

Figure 5.3: Ising model with 6 spins with periodic boundary conditions under collective dissipation of the form given by Eqn. (5.5) in the translation and reflexion symmetric subspace $T = R = 1$. Upper figure: Steady state expectation value $\langle J^x \rangle$ plotted versus the magnetic field B_x/α_3. Lower Figure: Spectrum of the Ising Hamiltonian in the magnetic field B_x plotted versus B_x/α_3.

5.2.2 General condition for discontinuities in the steady state

Since the Liouvillian depends smoothly on the system parameters, the observed discontinuities must be related to degeneracies in the spectrum of $\mathcal{L}$. As we shall see, in the weak dissipation limit they are directly related to degeneracy points of the Hamiltonian.

We consider a system described by the master equation

$$\dot{\rho}(t) = \mathcal{L}\rho \equiv [\mathcal{L}_0(x) + \gamma\mathcal{L}_1]\,\rho(t), \tag{5.6}$$

where

$$\mathcal{L}_0(x)(\rho) = -i[H(x), \rho]$$

with a Hamiltonian $H(x)$ depending (analytically) on a parameter x. For simplicity, we consider the case that $H_0(x)$ is non-degenerate for $x \neq x_0$. The term $\mathcal{L}_1$ contains dissipative terms and is independent of x. We are interested in the limit of weak dissipation $\gamma \to 0$ and in the change of the steady state at the degeneracy point $x = x_0$.

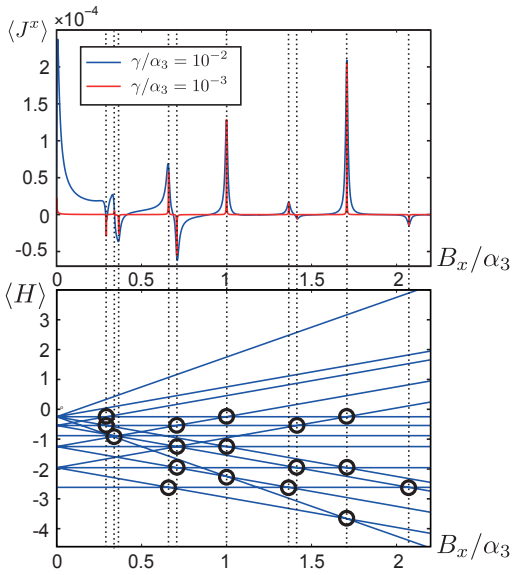

Figure 5.4: Heisenberg model with 4 spins with open boundary conditions under local dissipation as given by Eqn. (5.4) with different dissipation strengths γ_k. Upper Figure: Steady state expectation value $\langle J^x \rangle$ plotted versus B_x/α_3. Lower Figure: Spectrum of the Heisenberg Hamiltonian in a transverse magnetic field B_x, plotted versus B_x/α_3.

The steady state $\rho_{\rm ss}(x)$ is determined by $\mathcal{L}(x)\rho_{\rm ss}(x) = 0$ and can be determined perturbatively. The kernel of $\mathcal{L}_0(x)$ is highly degenerate, being spanned by all eigenprojectors $|\lambda_i(x)\rangle\langle\lambda_i(x)|$ of the (non-degenerate) $H_0(x)$. This degeneracy is lifted by $\mathcal{L}_1$ and the steady state for $\gamma \to 0$ is for $x \neq x_0$ given by

$$\mathrm{P}^D(x)\mathcal{L}_1\mathrm{P}^D(x)\rho_{ss}(x) = 0, \tag{5.7}$$

where

$$\mathrm{P}^D(x)\rho = \sum_i |\lambda_i(x)\rangle\langle\lambda_i(x)|\,\rho\,|\lambda_i(x)\rangle\langle\lambda_i(x)|\,. \tag{5.8}$$

The possibility of discontinuous behavior of $\rho_{\rm ss}(x)$ at $x = x_0$ arises from the enlargement of the kernel of $\mathcal{L}_0(x)$ at this point, since now also coherences between degenerate eigenvectors become stationary. We denote by P^Δ the projector on these additional elements in the kernel of $\mathcal{L}_0(x_0)$ [2]. As we show in Appendix 5.A, a discontinuity

[2]Here we use that if $H(x)$ is a holomorphic function of x (we are typically concerned with linear dependence on x only) the eigenvectors of $H(x)$ can be chosen as holomorphic (and thus continuous)

$\rho_{\rm ss}(x_0) \neq \lim_{x\to x_0} \rho_{\rm ss}(x)$ arises if

$$\mathrm{P}^{\Delta}\mathcal{L}_1 \lim_{x\to x_0} \rho_{ss}(x) \neq 0, \tag{5.9}$$

which means that $\mathcal{L}_1$ couples the steady state to the newly available subspace P^{Δ} in the kernel of $\mathcal{L}_0$. For simplicity, we made the assumption that the Hamiltonian is nondegenerate for $x \neq x_0$. If the Hamiltonian does have degeneracies outside x_0, the argumentation follows identical lines, as also in this case, $\mathcal{L}_1$ can couple the steady state to a newly available subspace P^{Δ}.

Note, that in Figs. 5.1 - 5.4, a large feature appears in the steady state expectation value $\langle J^x \rangle$ around $B_x = 0$. It narrows for decreasing γ, however, for the parameters used for γ it is not a sharp peak. For all spin models considered, the degeneracy of their respective Hamiltonian is very high at $B_x = 0$ and is lifted initially only very weakly by B_x. The above argumentation relies on γ being much smaller than all energy differences. Peaks can be only resolved if γ is small compared to the energy differences of eigenvalues around their degeneracy point x_0.

5.2.3 Steady state behavior for Ising Hamiltonians

To get a better insight into the condition given by Eqn. (5.9) we now specialize to the Ising model under collective dissipation given by Eqn. (5.5). Then we see that the steady state apart from the degeneracy points and the condition for discontinuity become very simple. For a detailed derivation of what follows, see Appendix 5.A.

The Hamiltonian in Eqn. (5.1) assuming periodic boundary conditions is in general degenerate due to translational and reflection symmetry. To obtain a non-degenerate H, we restrict our consideration to a specific subspace with eigenvalue 1 for the translation operator T and the reflection operator R [3]. Note that the Hamiltonian is also symmetric under the spin-flip operation $F = \sigma_x^{\otimes N}$, i.e., $FHF^{\dagger} = H$. Using the properties of $\mathcal{L}_1$ and F-invariance of H, we find that if the system has a unique steady state, it is, in

functions of $x \in \mathbb{R}$ [165]. Then $\lim_{x\to x_0} P^D(x_0)$ is well defined and we can define P^{Δ} as the difference of the projector on the kernel of $\mathcal{L}_0(x_0)$ and $\lim_{x\to x_0} P^D(x_0)$.

[3] Initializing a system in this subspace it will remain there since both $\mathcal{L}_0$ and $\mathcal{L}_1$ respect these symmetries.

the limit of weak dissipation, given by the maximally mixed state $\propto \mathbb{1}$: plugging $\mathbb{1}$ into Eqn. (5.7) we obtain $\mathrm{P}^D\mathcal{L}_1(\mathbb{1}) = \sum_i |\lambda_i(x)\rangle\langle\lambda_i(x)| J^z |\lambda_i(x)\rangle\langle\lambda_i(x)|$ and flip invariance of H implies $\langle\lambda_i(x)| J^z |\lambda_i(x)\rangle = 0$ for the eigenstates of a non-degenerate Hamiltonian H (see Appendix 5.A).

Thus if the steady state is unique, it is always maximally mixed outside degeneracy points and we see a discontinuity at $x = x_0$ if for the degenerate eigenstates $|\lambda_1(x_0)\rangle, |\lambda_2(x_0)\rangle$ we have

$$\langle\lambda_1| J^z |\lambda_2\rangle \neq 0. \tag{5.10}$$

This can be checked to hold for the points at which peaks are observed in Fig. 5.3.

For the Ising model in a transverse magnetic field, for larger N the peaks decrease in height, and disappear in the limit $N \longrightarrow \infty$. The spectrum for the Ising model in a transverse field is known analytically [166]. For large N, the spectrum gets very dense such that degeneracies in the Hamiltonian are so close together that γ can not be chosen smaller that the minimal energy difference between different eigenvalues.

5.3 State preparation with dissipative spin models

In the previous Sections, we studied discontinuous behavior in the steady state properties of spin Hamiltonians subject to individual or collective dissipation. In this Section we study general spin Hamiltonians under collective dissipation. We aim at finding systems which are dissipatively driven into (pure) steady states that show interesting behavior such as entanglement. Our main concept is to search for pure steady states that are eigenstates of the respective spin Hamiltonian and at the same time dark states of the dissipative part of the Liouvillian. Under this aspect, we first study spin Hamiltonians with nearest-neighbor interaction and show, that for short spin systems, interesting entangled states can be prepared. In Subsection 5.3.2 we include next-nearest neighbor interaction and study state preparation with the Majumdar-Gosh Hamiltonian subject to collective dissipation. We find, that in a steplike magnetic field, fully entangled unique steady states of N spins can be prepared.

5.3.1 Fully entangled steady states with short spin chains

We study a spin Hamiltonian with nearest-neighbor interaction given by

$$H = \sum_i \alpha_1 J_i^x J_{i+1}^x + \alpha_2 J_i^y J_{i+1}^y + \alpha_3 J_i^z J_{i+1}^z. \tag{5.11}$$

We assume that the spin system is subject to collective dissipation described by

$$\mathcal{L}\rho_t = \gamma(2J^-\rho_t J^+ - \{J^+J^-, \rho_t\}_+) - i[H, \rho_t]. \tag{5.12}$$

Note that it corresponds to Eqn. (5.5) in the previous Sections. As explained before, J^+ and J^- are collective spin raising and lowering operators.

We investigate whether for certain choices of the parameters in the spin Hamiltonian given by Eqn. (5.11), dissipation drives the spin system into interesting entangled states. Thus, we search for pure steady states $\rho_{\text{ss}} = |\psi_{ss}\rangle\langle\psi_{ss}|$ fulfilling $\mathcal{L}\rho_{\text{ss}} = 0$. Note that we did not extend our search to mixed steady states. We explore the parameter space of α_1, α_2 and α_3 in the Hamiltonian given by Eqn. (5.11). We calculate the intersection of the set of vectors in the Kernel of the dissipative part of the master equation

$$\mathcal{L}_{\text{diss}} = \gamma(2J^-\rho_t J^+ - \{J^+J^-, \rho_t\}_+) \tag{5.13}$$

and the set of states that are eigenstates of the Hamiltonian.

In the following, we will discuss for which families of Hamiltonians we find pure steady states that are entangled. We start with a system with two spins. We find that for $\alpha_1 = \cos(\theta)$, $\alpha_2 = \sin(\theta)$ and $\alpha_3 = -\cos(\theta) - \sin(\theta)$ in Eqn. (5.11) with $\theta \neq \frac{1}{4}\pi + n\pi$, the Singlet state $|\psi\rangle_{ss} = \frac{1}{\sqrt{2}}|S_{12}\rangle$ is a unique pure steady state. Here, $|S_{ij}\rangle$ is defined by

$$|S_{ij}\rangle = |\uparrow_i\downarrow_j\rangle - |\downarrow_i\uparrow_j\rangle. \tag{5.14}$$

For a spin chain of four spins, we find that the steady state is given by

$$|\psi\rangle_{ss} = \frac{1}{2\sqrt{3}}(2|S_{13}\rangle|S_{24}\rangle - |S_{14}\rangle|S_{23}\rangle) \tag{5.15}$$

and for six spins, it is given by

$$|\psi\rangle_{ss} = \frac{1}{2\sqrt{8}}(2|S_{16}\rangle|S_{23}\rangle|S_{45}\rangle + |S_{13}\rangle|S_{25}\rangle|S_{46}\rangle + |S_{14}\rangle|S_{25}\rangle|S_{36}\rangle. \tag{5.16}$$

For eight and more spins, however, we do not find any pure *unique* steady states within this family of Hamiltonians. We neither find any other family of Hamiltonians with α_1, α_2, α_3 in Eqn. (5.11) that leads to interesting *unique* pure entangled steady states.

We do find other families of Hamiltonians described by Eqn. (5.11) (for more than eight spins) with pure entangled states, however, they are not unique and the system is not so interesting for state preparation as it can always be driven into the (not so interesting) state where all spins are down $|\psi\rangle = |\downarrow\downarrow\downarrow .. \downarrow\rangle$.

5.3.2 Fully entangled steady states with N spins

Studying spin Hamiltonians with nearest-neighbor interaction under dissipation, we did find entangled unique pure steady states, however, only for spin chains with less than eight atoms. In the following, we show, that if we consider next-nearest neighbor interaction, fully entangled unique steady states of a spin chain of N spins can be generated.

We consider the Majumdar-Ghosh model [167], which is an extension of the one-dimensional Heisenberg spin model. An extra interaction is added that couples next-nearest neighbor spins at half strength as before.

The Majumdar-Ghosh Hamiltonian [167] with nearest-neighbor and next-nearest neighbor interaction is given by

$$H = \sum_{k=1}^{N} H_{nn}^k + H_{nnn}^k \tag{5.17}$$

with the Hamiltonian H_{nn} describing the nearest-neighbor interaction:

$$H_{nn}^k = \alpha_1 J_k^x J_{k+1}^x + \alpha_2 J_k^y J_{k+1}^y + \alpha_3 J_k^z J_{k+1}^z \tag{5.18}$$

and the next-nearest neighbor interaction

$$H_{nnn}^k = \alpha_1' J_k^x J_{k+2}^x + \alpha_2' J_k^y J_{k+2}^y + \alpha_3' J_k^z J_{k+2}^z \tag{5.19}$$

where $\alpha_1' = \frac{1}{2}\alpha_1$, $\alpha_2' = \frac{1}{2}\alpha_2$, $\alpha_3' = \frac{1}{2}\alpha_3$. To this model, we add a steplike magnetic field in x-direction

$$B_x = \sum_{k=1}^{N/2} (B + k\Delta B)(J_{2k-1}^x + J_{2k}^x), \tag{5.20}$$

such that two neighboring atoms see the same magnetic field strength. We numerically find that the Liouvillian given by Eqn. (5.12) with $H = H_{nn} + H_{nnn} + B_x$ describing a spin chain of N atoms in an external magnetic field has a fully entangled, *unique* steady state that fulfills $\mathcal{L}\rho_{\rm ss} = 0$ given by

$$|\psi_{\rm ss}\rangle = |S_{12}\rangle\,|S_{34}\rangle\,..\,|S_{N-1,N}\rangle\,, \tag{5.21}$$

for a spin chain of N atoms. $|\psi_{\rm ss}\rangle$ is in the kernel of the dissipative part of the master equation given by Eqn. (5.13), and an eigenstate of the Hamiltonian $H = H_{nn} + H_{nnn} + B_x$. This can be proven analytically: In Appendix 5.B we show that $|\psi_{\rm ss}\rangle$ is an eigenstate of the Hamiltonian H.

5.4 Collective dissipation: ultracold atoms coupled to a single cavity mode

In this Section we give an example for a system with collective dissipation as described by Eqn. (5.5). The system we consider are ultracold atoms in an optical cavity [54], such as a BEC coupled to one single mode of the cavity and pumped with a standig-wave laser field as in T. Esslingers experiments [55]. We assume the atom to have three internal states, $|g_1\rangle$, $|g_2\rangle$, $|e\rangle$ where the states $|g_1\rangle$-$|e\rangle$ are coupled by the cavity field and $|g_2\rangle$-$|e\rangle$ is coupled by the standing wave pump laser. Both optical couplings are far detuned from resonance. The Hamiltonian is given by

$$\begin{aligned} H = \;& \textstyle\sum_{k=1}^{N} \Omega_c(\vec{r}_k)(a^\dagger\,|g_1\rangle\langle e|_k + \text{h.c.}) + \Omega_l(\vec{r}_k)(e^{-i\omega_l t}\,|g_2\rangle\langle e|_k + \text{h.c.}) \\ & + \omega_{g_2}\,|g_2\rangle\langle g_2|_k + \omega_e\,|e\rangle\langle e|_k + \omega_c a^\dagger a. \end{aligned} \tag{5.22}$$

Here, the sum runs over N atoms and the frequencies of laser and cavity fields are denoted by ω_l and ω_c, respectively, and $\vec{r}_k$ is the position vector of the kth atom. $\Omega_l(\vec{r}_k) = \Omega_l \cos(\vec{k}_l \cdot \vec{r}_k)$ and $\Omega_c(\vec{r}_k) = \Omega_c \cos(\vec{k}_c \cdot \vec{r}_k)$ denote the position dependent Rabi frequencies of laser and cavity field, where $\vec{k}_l$, $\vec{k}_c$ are the wave vectors of the laser field and cavity field, respectively. ω_e and $\omega_{g_{1/2}}$ are the energies of the level (with $\hbar = 1$). In a frame rotating with the laser frequency $U = \exp\left[-i\omega_l t(a^\dagger a + |e\rangle\langle e|_k)\right]$ the

Hamiltonian is time-independent and given by

$$\begin{aligned} H = & \sum_{k=1}^{N} \Omega_c(\vec{r}_k) \left(a^\dagger \left|g_1\right\rangle\!\left\langle e\right|_k + \text{h.c.}\right) + \Omega_l(\vec{r}_k) \left(\left|g_2\right\rangle\!\left\langle e\right|_k + \text{h.c.}\right) \\ & + \Delta_e \left|e\right\rangle\!\left\langle e\right|_k + \omega_{g_2} \left|g_2\right\rangle\!\left\langle g_2\right|_k + \delta_c a^\dagger a, \end{aligned} \tag{5.23}$$

where $\delta_c = \omega_c - \omega_l$ and $\Delta_e = \omega_e - \omega_l$. After adiabatic elimination of the excited state $|e\rangle$, the effective Hamiltonian reads

$$\begin{aligned} H_{\text{eff}} = & \sum_{k=1}^{N} g(\vec{r}_k) \left(a\sigma_k^+ + a^\dagger \sigma_k^-\right) + \omega_{g_2} \left|g_2\right\rangle\!\left\langle g_2\right|_k \\ & + \delta_c a^\dagger a - \tfrac{\Omega_l(\vec{r}_k)^2}{\Delta_e} \left|g_2\right\rangle\!\left\langle g_2\right|_k - \tfrac{\Omega_c(\vec{r}_k)^2 a^\dagger a}{\Delta_e} \left|g_1\right\rangle\!\left\langle g_1\right|_k, \end{aligned} \tag{5.24}$$

where the coupling $g(\vec{r}_k)$ is given by $g(\vec{r}_k) = -\frac{\Omega_l(\vec{r}_k)\Omega_c(\vec{r}_k)}{\Delta_e}$ and $\sigma_k^+ = \left|g_2\right\rangle\!\left\langle g_1\right|_k$. For $k_l = k_c$ and $\vec{k_c} \cdot \vec{r}_k = 2\pi$, the coupling $g(\vec{r}_k)$ is constant.

The full system including the decay of the cavity is described by the master equation

$$\dot{\rho}(t) = -i[H_{\text{eff}}, \rho(t)] + \kappa(2a\rho(t)a^\dagger - a^\dagger a\rho(t) - \rho(t)a^\dagger a) \tag{5.25}$$

where H_{eff} is the Hamiltonian given by Eqn. (5.24) and κ is the cavity decay constant.

We assume that we are in the bad cavity limit with $\kappa \gg g$ such that the cavity mode can be adiabatically eliminated. This can be done as follows: Projecting Eqn. (5.25) onto the subspace of 0 and 1 photons, we get four coupled differential equations $\langle 0|\,\dot{\rho}(t)\,|0\rangle$, $\langle 0|\,\dot{\rho}(t)\,|1\rangle$, $\langle 1|\,\dot{\rho}(t)\,|0\rangle$ and $\langle 1|\,\dot{\rho}(t)\,|1\rangle$. Setting $\langle 0|\,\dot{\rho(t)}\,|1\rangle = 0$, $\langle 1|\,\dot{\rho(t)}\,|0\rangle = 0$ and $\langle 1|\,\dot{\rho(t)}\,|1\rangle = 0$ as they are fast decaying and neglecting all terms of $\mathcal{O}\left(\frac{g^2}{\kappa^2}\right)$ and higher, we get

$$\langle 0|\,\rho(t)\,|1\rangle \approx \sum_i^N \frac{-ig\,\langle 0|\,\rho(t)\,|0\rangle\,\sigma_i^+}{\kappa - i\delta_c}, \tag{5.26}$$

$$\langle 1|\,\rho(t)\,|1\rangle \approx \sum_i^N \frac{ig\left(\langle 0|\,\rho(t)\,|1\rangle\,\sigma_i^- - \langle 0|\,\rho(t)\,|1\rangle\,\sigma_i^+\right)}{2\kappa} \tag{5.27}$$

and $\langle 1|\,\rho(t)\,|0\rangle = \langle 0|\,\rho(t)\,|1\rangle^*$. Inserting these equations in $\langle 0|\,\dot{\rho}(t)\,|0\rangle$ we get

$$\begin{aligned} \dot{\rho}(t)_{00} = & \sum_{k=1}^{N} \Gamma_{\text{eff}} \left(2\sigma_k^- \rho_{00} \sigma_k^+ - \{\sigma_k^+ \sigma_k^-, \rho_{00}\}_+\right)\right) \\ & -i\left[\left(\omega_{g_2} - \tfrac{\Omega_l^2}{\Delta_e}\right) \left|g_2\right\rangle\!\left\langle g_2\right|_k, \rho_{00}\right] \end{aligned} \tag{5.28}$$

where $\rho_{00} = \langle 0| \rho(t) |0\rangle$ and

$$\Gamma_{\text{eff}} = \frac{g^2\kappa}{\kappa^2 + \delta_c^2}$$

is the strength of the collective dissipation described by the first two terms in Eqn. (5.28). Eqn. (5.28) can be written in terms of collective operators

$$\dot{\rho}(t)_{00} = \Gamma_{\text{eff}} \left(2J^- \rho_{00} J^+ - \{J^+ J^-, \rho_{00}\}_+\right) - i \left[\left(\omega_{g_2} - \frac{\Omega_l^2}{\Delta_e}\right) |g_2\rangle\langle g_2|_k \,, \rho_{00}\right], \quad (5.29)$$

where $J^- = \sum_{k=1}^{N} \sigma_k^-$. Therefore, we have shown, that atoms that are all coupled to one single rapidly decaying mode of the light field, e.g. in a cavity, undergo collective dissipation. Thus, we have given an example for the physical realization of collective dissipation described by Eqns. (5.5) and (5.12) in the previous Sections.

5.5 Derivation of the master equation for sub-wavelength atomic chains

Here we derive a master equation for a chain of atoms that are trapped in a sub-wavelength region. The internal levels of the atom are driven by an (optical) field and are subject to spontaneous emission. We assume the size of the atomic chain to be smaller than the wavelength of the driving (optical) field. As derived in the following, in this regime, long-range interactions like the electrical dipole-dipole and the magnetic dipole-dipole interaction (in case of a magnetic moment of the atomic levels) play a significant role. Moreover, such systems are potential candidates for studying collective effects such as, e.g., Dicke superradiance [56], where the atoms interact with each other through the radiation field. Trapping particles on distances that are much smaller than an optical wavelength, i.e., on the order of ångströms, is difficult. Optical lattices for example are not suited for this approach as the distances between neighboring atoms trapped in the lattice potential are on the order of an optical wavelength. Possible systems for trapping particles in the sub-wavelength regime might be plasmonic structures. Proposals exist to optically trap an atom via the strong near-field generated by a sharp metallic nanotip [168] and sub-wavelength patterning of the optical near-field has been reported [169].

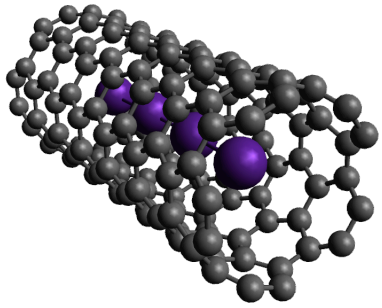

Figure 5.5: Atoms encapsulated in a carbon nanotube. For a TEM picture see [170].

Another potential system for the purpose of sub-wavelength trapping might be single atoms encapsulated in single walled carbon nanotubes (see Fig. 5.5). Encapsulation of single atoms in carbon nanotubes has been realised in various groups with atoms such as Cs, Li, K, P, O, Fe, Ag, for a TEM image of Cs encapsulated in a carbon nanotube see [170]. Trapping atoms in carbon nanotubes is highly interesting as the distance between the trapped atoms is on the order of ångströms. We are interested in sub-wavelength trapped atoms that are optically addressable with laser light. The optical properties of atoms trapped in CNTs have not been studied in detail, in particular it is not clear how the atomic levels and the spectral properties are affected by the carbon nanotube.

Therefore, the system we investigate in the following should be studied under a more general point of view. In the following, we assume that atoms can be trapped with interatomic distances on the order of a few ångströms. We show, that optical couplings of internal levels of the atoms and spontaneous emission leads to a master equation that describes electrical dipole-dipole interactions and decay. Due to the small distances between the atoms, magnetic dipole-dipole interaction also have to be included in the description if the participating levels have magnetic moments.

5.5.1 Atom-light interaction

First, we derive the interaction of the atoms with the laser light. We assume the atoms to have two ground states $|g\rangle$ and $|s\rangle$ that have a magnetic moment, e.g., hyperfine states, and an excited state $|e\rangle$ that is dipole coupled to the ground states. The transi-

tion $|s\rangle$-$|e\rangle$ is driven by a laser with detuning Δ with respect to the atomic transition energy, see Fig. 5.6. The atoms are assumed to decay only from state $|e\rangle$ to state $|g\rangle$, and not to state $|s\rangle$, see [171] for more details. We will follow the derivation as done by D. Porras et al. [171]. Note that D. Porras et al. work in the regime where the wavelength of the light is comparable to the interatomic distance.

The Hamiltonian for the coupling between the states $|e\rangle$ and $|s\rangle$ is given by

$$H_L = \sum_j \frac{\hbar\Omega_L}{2}\left(\sigma_{es}^+ e^{i\vec{k}_L\cdot\vec{r}_j - i\omega_L t} + \text{h.c.}\right), \tag{5.30}$$

where Ω_L is the Rabi frequency of the laser, $\sigma_{es,j}^+ = |e\rangle\langle s|$ the operator that excites the jth atom from state $|s\rangle$ to $|e\rangle$, ω_L the laser frequency, $\vec{k}_L$ the wave vector of the laser and $\vec{r}_j$ the position of the atoms of the jth atom. The decay from state $|e\rangle$ to state $|g\rangle$ is described by

$$H_{dec} = \sum_{j,\vec{k},\lambda} \sqrt{\frac{\hbar\omega_k}{2\epsilon_0 V}}\vec{\epsilon}_{k,\lambda}\cdot\vec{d}_{ge}\sigma_{eg,j}^+ e^{i\vec{k}\cdot\vec{r}_j} a_{\vec{k},\lambda} + \text{h.c.}, \tag{5.31}$$

where $\sigma_{eg,j}^+ = |e\rangle\langle g|_j$ is the operator that excites the jth atom from state $|g\rangle$ to $|e\rangle$, d_{ge} is the dipole matrix element of the $g-e$ transition and $a_{\vec{k}}$ is the bosonic operator for the annihilation of a photon. After adiabatic elimination of the excited state $|e\rangle$, the atom-light interaction is described by

$$H_I(t) = \sum_{j,\vec{k},\lambda} g_{\vec{k},\lambda}^{eg}\left(\sigma_j^+ a_{\vec{k},\lambda} e^{i(\vec{k}-\vec{k}_L)\cdot r_j + i\omega_L t} + \sigma_j^+ a_{\vec{k},\lambda}^\dagger e^{-i(\vec{k}-\vec{k}_L)\cdot r_j + i\omega_L t} + \text{h.c.}\right) \tag{5.32}$$

where $\sigma_j^+ = |s\rangle\langle g|_j$ and the coupling is given by

$$g_{k,\lambda}^{eg} = \frac{\Omega_L}{2\Delta}\sqrt{\frac{\hbar\omega_k}{2\epsilon_0 V}}\left(\vec{\epsilon}_{\vec{k},\lambda}\cdot\vec{d}_{ge}\right).$$

In the interaction picture the density matrix evolves like:

$$\partial_t\rho_T = \frac{1}{i\hbar}[H_I(t), \rho_T(t)]. \tag{5.33}$$

Following [156] we find

$$\rho_T(t+\Delta t) - \rho_T(t) = -\frac{1}{\hbar^2}\int_0^{\Delta t} d\tau \int_t^{t+\Delta t} dt'[H_I(t'), [H_I(t'-\tau), \rho_T(t')]]. \tag{5.34}$$

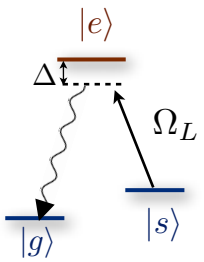

Figure 5.6: Λ system

In the limit where $1/\Gamma, 1/\nu \gg \Delta t \gg \tau_c$, where τ_c is the correlation time of the electromagnetic field, we can do the Born-Markov approximation: $\int_0^{\Delta t} d\tau \to \int_0^{\infty} d\tau$. Tracing over the bath we get the master equation

$$\partial\rho_T/\partial t = \sum_{ij}(J_{ij}\sigma_i^-\rho\sigma_j^+ - J_{ij}\sigma_i^+\sigma_j^-\rho + \text{h.c.}), \tag{5.35}$$

where

$$J_{ij} = \int_0^{\infty} d\tau \sum_{\vec{k},\lambda}\left(\frac{\Omega_L}{2\Delta}\right)^2 \frac{\omega_k}{2\hbar\epsilon_0 V}\left(\vec{\epsilon}_{\vec{k},\lambda}\cdot\vec{d}_{eg}\right)^2 \left[e^{(i(\omega_k-\omega_L)\tau+i(\vec{k}-\vec{k}_L)\cdot\vec{r}_{ij})} + e^{(i(\omega_k+\omega_L)\tau+i(\vec{k}-\vec{k}_L)\cdot\vec{r}_{ij})}\right]. \tag{5.36}$$

Here, $\vec{r}_{ij} = \vec{r}_i - \vec{r}_j$ is the vector connecting the atoms at positions i and j. Using the equality

$$\sum_{\lambda}(\vec{\epsilon}_{\vec{k},\lambda}\cdot\vec{n}_{eg})^2 = 1 - \left(\frac{\vec{k}\cdot\vec{n}_{eg}}{|k|}\right)^2, \tag{5.37}$$

where we have defined $\vec{d}_{eg} = d_{eg}\vec{n}_{eg}$ where $\vec{n}_{eg}$ is the unit vector, and using the identity

$$\int d\tau e^{i\omega\tau} = \pi\delta(\omega) + iP(1/\omega), \tag{5.38}$$

we can evaluate the expression in Eqn. (5.36) (see also [172]) and find

$$J_{ij} = \frac{1}{2}\bar{\Gamma}e^{-i\vec{k}_L\cdot\vec{r}_{ij}}\left[\frac{\left[1-3(\vec{d}_{eg}\cdot\hat{\vec{r}}_{ij})^2\right]\cos(k_L r_{ij})}{(k_L r_{ij})^2} + \frac{\left[1-(\vec{d}_{eg}\cdot\hat{\vec{r}}_{ij})^2\right]\sin(k_L r_{ij})}{k_L r_{ij}} - \frac{\left[1-3\left(\vec{d}_{eg}\cdot\hat{\vec{r}}_{ij}\right)^2\right]\sin(\vec{k}_L\cdot\vec{r}_{ij})}{(k_L r_{ij})^3} - i\left(\left[1-3(\vec{d}_{eg}\cdot\hat{\vec{r}}_{ij})^2\right]\left(\frac{\cos(k_L r_{ij})}{(k_L r_{ij})^3} + \frac{\sin(k_L r_{ij})}{(k_L r_{ij})^2}\right) - \left[1-(\vec{d}_{eg}\cdot\hat{\vec{r}}_{ij})^2\right]\frac{\cos(k_L r_{ij})}{k_L r_{ij}}\right)\right],$$

where $k_L = |\vec{k}_L|$, $r_{ij} = |\vec{r}_{ij}|$ and $\hat{\vec{r}}_{ij} = \vec{r}_{ij}/|\vec{r}_{ij}|$. We assume $\vec{r}_{ij}$ to be aligned along the z-axis and $\bar{\Gamma}$ is given by

$$\bar{\Gamma} = \frac{1}{3\pi}\left(\frac{\Omega_L}{2\Delta}\right)^2 \frac{\omega_L^3}{\epsilon_0 c^3} d_{eg}^2.$$

In the limit $k_L r_{ij} \ll 1$ the real part of J_{ij} can be approximated as

$$\mathrm{Re}(J_{ij}) \approx \frac{1}{3}\bar{\Gamma} \tag{5.39}$$

and the dissipative part of the master equation then reads

$$\mathcal{L}_{\mathrm{diss}}\rho_T = \frac{1}{3}\bar{\Gamma}\sum_{ij}(\hat{\sigma}_i^- \rho \hat{\sigma}_j^+ - \hat{\sigma}_i^+ \hat{\sigma}_j^- \rho + \mathrm{h.c.}), \tag{5.40}$$

where we have defined phase factor into the operators and defined $\hat{\sigma}_i^+$ as $\hat{\sigma}_i^+ = e^{+i\vec{k}_L\cdot\vec{r}_{ij}}\sigma_i^+$. The imaginary part of J_{ij} leads to the Hamiltonian part of the master equation and describes the electric dipole-dipole interaction

$$\mathcal{L}_H \rho_T = -i[H_{\mathrm{el}}, \rho_T(t)] \tag{5.41}$$

with

$$H_{\mathrm{el}} = \sum_{ij}\mathrm{Im}(J_{ij})(\hat{\sigma}_i^+ \hat{\sigma}_j^- + \mathrm{h.c.}). \tag{5.42}$$

As $k_L r_{ij} \ll 1$, the imaginary part of J_{ij}, $\mathrm{Im}(J_{ij})$, can be approximated by

$$\begin{aligned}\mathrm{Im}(J_{ij}) \approx \; & -\tfrac{1}{2}\bar{\Gamma}\left[\left(1-3(\vec{d}_{eg}\cdot\hat{\vec{r}}_{ij})^2\right)\left(\tfrac{1}{(k_L r_{ij})^3}\right)\right. \\ & \left. + \left(1+(\vec{d}_{eg}\cdot\hat{\vec{r}}_{ij})^2\right)\tfrac{1}{k_L r_{ij}}\right].\end{aligned} \tag{5.43}$$

5.5.2 Magnetic dipole-dipole interaction

As the interatomic distances are assumed to be on the order of ångströms, magnetic dipole-dipole interactions between the atoms (if present) may be sizeable. The Hamiltonian of the magnetic dipole-dipole interaction between two atoms at sites i and j is given by [173]

$$H_{\mathrm{mag}} = \frac{\mu_0}{4\pi}\gamma_i\gamma_j\frac{1}{r_{ij}^3}\left[\vec{\sigma}_i\cdot\vec{\sigma}_j - 3(\vec{\sigma}_i\cdot\vec{r}_{ij})(\vec{\sigma}_j\cdot\vec{r}_{ij})\right]. \tag{5.44}$$

As stated before, we assume that $\vec{r}_{ij}$ is aligned along the z-axis, $\vec{r}_{ij} = (0,0,1)$. Then, the magnetic dipolar interaction reads:

$$H_{\mathrm{mag}} = \sum_{\langle ij\rangle}\frac{\mu_0}{4\pi}\gamma_i\gamma_j\frac{1}{r_{ij}^3}\left[\sigma_i^x\sigma_j^x + \sigma_i^y\sigma_j^y + 2\sigma_i^z\sigma_j^z\right] \tag{5.45}$$

5.5.3 Description of the full system

The master equation of the full system is given by

$$\dot{\rho}_T = \mathcal{L}_{\text{diss}}\rho_T - i\left[H_{\text{el}} + H_{\text{mag}}\right] = \quad \tfrac{1}{3}\bar{\Gamma}\sum_{ij}(\hat{\sigma}_i^- \rho_T \hat{\sigma}_j^+ - \hat{\sigma}_i^+\hat{\sigma}_j^- \rho_T + \text{h.c.}) \\ -i\left[\text{Im}(J_{ij})(\hat{\sigma}_i^+\hat{\sigma}_j^- + \text{h.c.}) + H_{\text{mag}}, \rho_T\right]. \quad (5.46)$$

where H_{mag} is given by Eqn. (5.45). This master equation describes a laser driven chain of atoms with subwavelength interatomic distances. As discussed before, such a system might be realized with atoms encapsulated in carbon nanotubes or sub-wavelength plasmonic structures.

5.6 Conclusions

We have discovered a peculiar feature of the steady state diagram for small spin chains: in the limit of weak dissipation, the expectation values of the collective spin operators exhibit abrupt changes that hint at discontinuities in the steady state. These discontinuities occur at degeneracy points of the Hamiltonian. We have studied this phenomenon for different spin models with open and periodic boundary conditions subject to individual and collective dissipation. We have presented conditions that elucidate the discontinuous behavior of the steady state at degeneracy points of the Hamiltonian. Therefore, measurements of the steady state dynamics of cold atoms in optical lattices would allow to draw conclusions on the spectrum of the respective spin model. Moreover, we have studied different classes of spin Hamiltonians under dissipation. We showed, that for certain spin Hamiltonians, fully entangled unique steady states can be prepared as steady states of a dissipative dynamics induced by optical driving and decay. We have shown that collective dissipation can be realized with cold atoms that are coupled to one single mode of an optical cavity. Finally, we have derived a master equation for a chain of atoms with sub-wavelength interatomic distances and discuss possible realizations of such system.

5.A Condition for discontinuous behavior

Here, we first derive a general condition for the discontinuous behavior in the steady state at a degeneracy point of a large class of spin Hamiltonians. Then, we focus on more specific Hamiltonians. We study the steady state of flip-invariant Hamiltonians outside the degeneracy point and, starting with the general condition for finding discontinuities in the steady state, we derive a more precise condition for flip-invariant Hamiltonians.

5.A.1 General condition for discontinuities in steady state

First, we derive a general condition for discontinuous behavior in the steady state at the degeneracy point $x = x_0$ of a general Hamiltonian H, where $H = H(x)$ is an analytic function of x. We consider a system described by the master equation

$$\dot{\rho}(t) = (\mathcal{L}_0 + \mathcal{L}_1)\rho(t), \tag{5.47}$$

where the Hamiltonian part of the Liouvillian is given by $\mathcal{L}_0 = -i[H, \rho]$ and the local decay Liouvillian

$$\mathcal{L}_1\rho(t) = \sum_k \gamma_k \left[2J_k^- \rho(t) J_k^+ - \left(J_k^+ J_k^- \rho(t) + \rho(t) J_k^+ J_k^-\right)\right]. \tag{5.48}$$

First, we want to describe the system outside the degeneracy point, i.e., for $x \neq x_0$. We assume that in the vicinity of x_0, the Hamiltonian is nondegenerate (for $x \neq x_0$) and that the dissipation is weak. The steady state ρ_{ss} that fulfills $(\mathcal{L}_0 + \mathcal{L}_1)\rho_{ss} = 0$ is, in the limit $\gamma \to 0$ given by

$$\mathrm{P}^D(x)\mathcal{L}_1\mathrm{P}^D(x)\rho_{ss} = 0, \tag{5.49}$$

where $\mathrm{P}^D(x)$ is the projector onto the kernel($\mathcal{L}_0$). As the kernel of $\mathcal{L}_0$ is spanned by the eigenprojectors $|\lambda_k(x)\rangle\langle\lambda_k(x)|$ of H we have for arbitrary A:

$$\mathrm{P}^D A = \sum_k |\lambda_k(x)\rangle\langle\lambda_k(x)|\, A\, |\lambda_k(x)\rangle\langle\lambda_k(x)|, \tag{5.50}$$

where $|\lambda_k(x)\rangle$ are eigenstates of the Hamiltonian H_0 which is assumed to be nondegenerate.

Now, let us consider the case that at $x = x_0$, the Hamiltonian has a degeneracy point at which two or more eigenvalues cross. At this degeneracy point, we expect an discontinuous behavior of the steady state that leads to the peaks we observe in our numerical simulation (see Figs. 5.1-5.4). At $x = x_0$ the projector onto the kernel of $\mathcal{L}_0$ has to be extended. It now also projects onto coherences between eigenstates of H: $|\lambda_1\rangle$,$|\lambda_2\rangle$ which are eigenvectors to the degenerate eigenvalues $\lambda_1 = \lambda_2$. Therefore the projector on the coherences reads:

$$\mathrm{P}^{\Delta} A = |\lambda_1\rangle\langle\lambda_1| \, A \, |\lambda_2\rangle\langle\lambda_2| + \text{h.c.} \tag{5.51}$$

It is convenient to define a continuous extension of the projector P^D at $x = x_0$ which reads

$$\mathrm{P}^D(x = x_0) = \lim_{x \to x_0} \mathrm{P}^D(x). \tag{5.52}$$

Thus, at $x = x_0$, the full projector onto the kernel of $\mathcal{L}_0$ reads $\mathrm{P}^D(x_0) + \delta_{x_0}(x_0) P^{\Delta}$. Now the condition for the steady state $\rho_{ss}(x = x_0)$ at the degeneracy point is given by

$$\left[\mathrm{P}^D(x_0) + \mathrm{P}^{\Delta}\right] \mathcal{L}_1 \left[\mathrm{P}^D(x_0) + \mathrm{P}^{\Delta}\right] \rho_{ss}(x_0) = 0. \tag{5.53}$$

We want to find a condition for the steady state to show discontinuous behavior. This means that

$$\rho_{ss}(x_0) - \lim_{x \to x_0} \rho_{ss}(x) \neq 0, \tag{5.54}$$

where $\lim_{x \to x_0} \rho_{ss}(x)$ is the continuous extension of $\rho_{ss}(x) \forall x \neq x_0$. From Eqn. (5.54) follows that the continuous extension of the steady state has to fulfill

$$\left[\mathrm{P}^D(x_0) + \mathrm{P}^{\Delta}\right] \mathcal{L}_1 \left[\mathrm{P}^D(x_0) + \mathrm{P}^{\Delta}\right] \lim_{x \to x_0} \rho_{ss}(x) \neq 0, \tag{5.55}$$

as $\rho_{ss}(x_0)$ fulfills the condition given by Eqn. (5.53). The last part of Eqn. (5.55) can be simplified using

$$\left[\mathrm{P}^D(x_0) + \mathrm{P}^{\Delta}\right] \lim_{x \to x_0} \rho_{ss}(x) = \lim_{x \to x_0} \rho_{ss}(x),$$

which holds since $\lim_{x \to x_0} \rho_{ss}(x)$ is per definition in the space onto which $\mathrm{P}^D(x_0)$ projects, therefore

$$\mathrm{P}^D(x_0) \lim_{x \to x_0} \rho_{ss}(x) = \lim_{x \to x_0} \rho_{ss}(x),$$

[see Eqn. (5.49)]. Also per definition,

$$\mathrm{P}^D(x_0)\mathcal{L}_1\mathrm{P}^D(x_0)\lim_{x\to x_0}\rho_{ss}(x)=0.$$

As P^Δ is orthogonal to P^D, $\mathrm{P}^\Delta\lim_{x\to x_0}\rho_{ss}(x)=0$. Thus Eqn. (5.55) reduces to the condition

$$\mathrm{P}^\Delta\mathcal{L}_1\lim_{x\to x_0}\rho_{ss}(x)\neq 0. \tag{5.56}$$

If this condition is fulfilled, then $\rho_{ss}(x_0)-\lim_{x\to x_0}\rho_{ss}(x)\neq 0$ which means that the steady state shows discontinuous behavior at the degeneracy point $x=x_0$.

5.A.2 Condition for discontinuous behavior for Ising Hamiltonians

Here, we want to get a better insight how the condition given by Eqn. (5.56) relates to the peaks observed in our numerical simulation. In the following, we will apply it to the Ising model in a transverse magnetic field. In the numerical simulation (see Fig. 5.3) for the Ising Hamiltonian with periodic boundary conditions under collective dissipation described by Eqn. (5.5), we restrict our consideration to a specific subspace with eigenvalue 1 for translation operator T and reflexion operator R: $T=R=1$.

First, we want to prove that if the steady-state is unique, it is the fully mixed state outside the degeneracy points as indicated by our numerical simulation. Then we show that starting from the condition given by Eqn. (5.56), specialization to the Ising model allows to derive a more precise condition for finding a discontinuity in the steady-state at the degeneracy points.

First, we show that $\mathbb{1}$ satisfies $(\mathcal{L}_0+\mathcal{L}_1)\mathbb{1}=0$ outside the degeneracy point $x=x_0$. Therefore, for systems with unique steady-state, it is given by the fully mixed state for $x\neq x_0$ in the limit $\gamma\to 0$. The Hamiltonian given by Eqn. (5.1) is assumed to be non-degenerate for $x\neq x_0$ and invariant under the spin flip operator $F=\sigma_x^{\otimes N}$, i.e., $FHF^\dagger=H$. Thus, we want to show that for $x\neq x_0$:

$$\mathrm{P}^D\mathcal{L}_1\mathbb{1}=0, \tag{5.57}$$

where P^D is given by Eqn. (5.50). Then,

$$\mathrm{P}^D\mathcal{L}_1(\mathbb{1})=2\gamma(J^-J^+-J^+J^-)\propto\gamma J^z. \tag{5.58}$$

Therefore, Eqn. (5.57) reads

$$\mathrm{P}^D\mathcal{L}_1(\mathbb{1}) = \mathrm{P}^D J^z = \sum_k |\lambda_k\rangle\langle\lambda_k| J^z |\lambda_k\rangle\langle\lambda_k| = 0. \tag{5.59}$$

If we can show that each term of the sum on the right hand side of Eqn. (5.59),

$$\langle\lambda_k| J^z |\lambda_k\rangle = 0, \tag{5.60}$$

then we have shown that the fully mixed state is a steady state of our system outside the degeneracy points of the Hamiltonian. As the Hamiltonian is nondegenerate and invariant under the flip operator F, the eigenvectors of H are eigenvectors of F: $F|\alpha\rangle = \alpha|\alpha\rangle$. As $|\alpha\rangle$ can be written $|\alpha\rangle = \alpha^2|\alpha\rangle = \alpha F|\alpha\rangle$ (the eigenvalues of the flip operator can only be ± 1), we can write Eqn. (5.60) as

$$\begin{aligned}\langle\alpha| J^z |\alpha\rangle &= \alpha \langle\alpha| J^z F |\alpha\rangle \\ &= -\alpha \langle\alpha| F J^z |\alpha\rangle = -\alpha^2 \langle\alpha| J^z |\alpha\rangle\end{aligned} \tag{5.61}$$

where we have used that J^z and F anticommute, $\{F, J^z\}^+ = 0$. As $-\alpha^2 \neq \alpha$, it follows from Eqn. (5.61) that

$$\langle\alpha| J^z |\alpha\rangle = 0. \tag{5.62}$$

Then, $\mathrm{P}^D\mathcal{L}_1(\mathbb{1}) = 0$ and we have shown that in the limit of weak dissipation, the steady state, if it is unique, is the fully mixed state. We know from our numerics that for the Ising model with up to 8 spins and collective dissipation, the steady state is unique.

To see that the steady state shows discontinuous behavior at the degeneracy point $x = x_0$, we need to show that in this case, the fully mixed state is not the steady state of the system. Thus, we need to show that

$$\mathrm{P}^\Delta\mathcal{L}_1(\mathbb{1}) = \mathrm{P}^\Delta J^z = \sum_{k,l,k\neq l} |\lambda_k\rangle\langle\lambda_k| J^z |\lambda_l\rangle\langle\lambda_l| \neq 0 \tag{5.63}$$

where P^Δ is given by Eqn. (5.51). This is true if $\exists k \neq l$ such that

$$\langle\lambda_k| J^z |\lambda_l\rangle \neq 0. \tag{5.64}$$

Therefore, Eqn. (5.64) gives a condition for finding discontinuous behavior of the steady state of the Ising model in a transverse field under collective dissipation. Note that

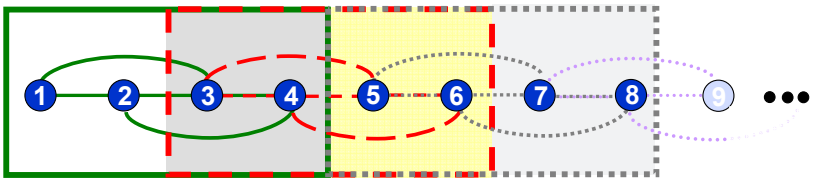

Figure 5.7: Spin chain with nearest-neighbor and next-nearest neighbor interaction. Groups of 4 neighboring spins are denoted by green, red and grey overlapping rectangles respectively. Next-neighbor and next-nearest neighbor interaction are marked with the color of the respective rectangle.

this derivation can be easily extended to all non-degenerate Hamiltonians that are flip-invariant. Here, we specialize to the Ising model as we know, that the system has a unique steady state for small spin chains and for collective dissipation in $T = R = 1$.

5.B Proof: Fully entangled state with N spins

We write the Hamiltonian as a sum of Majumdar-Gosh Hamiltonians of four neighboring spins and subtract the next-nearest neighbor Hamiltonian $H^{k,k+1}$ of the two spins that are double counted (see Fig. 5.7):

$$H = \sum_{k=1}^{4} H^k + \sum_{k=3}^{6} H^k + ... \sum_{k=N-4}^{N} H^k - H_{nn}^{3,4} - H_{nn}^{5,6} .. - H_{nn}^{N-1,N}. \tag{5.65}$$

One can easily show that $|\psi_{\text{ss}}\rangle$ given by Eqn. (5.21) is an eigenstate of the first term in H:

$$\sum_{k=1}^{4} H^k |\psi_{\text{ss}}\rangle = \lambda_1 |\psi_{\text{ss}}\rangle . \tag{5.66}$$

This Hamiltonian is symbolized by the green rectangle in Fig. 5.7. If $|\psi_{\text{ss}}\rangle$ is an eigenstate of $\sum_{k=1}^{4} H^k$, it is, due to symmetry, also an eigenstate of all the other four-spin Hamiltonians in the sum in Eqn. (5.65). Moreover, it is easy to verify that $|\psi_{\text{ss}}\rangle$ is an eigenstate of $H_{nn}^{3,4}$:

$$H_{nn}^{3,4} |\psi_{\text{ss}}\rangle = \lambda_2 |\psi_{\text{ss}}\rangle \tag{5.67}$$

Therefore, it is also an eigenstate of $H_{nn}^{5,6}$, and we have shown that $|\psi_{\mathrm{ss}}\rangle$ is an eigenstate of the Hamiltonian given by Eqn. (5.65), which corresponds to the Hamiltonian given by Eqn. (5.17). It can be easily seen that $|\psi_{\mathrm{ss}}\rangle$ is an eigenstate of the steplike magnetic field given in Eqn. (5.45). As $|\psi_{\mathrm{ss}}\rangle$ is in the kernel of the dissipative part of the master equation given by Eqn. (5.13), it is a pure fully entangled steady state.

Bibliography

[1] A. Einstein, B. Podolsky, and N.Rosen. *Can Quantum-mechanical description of physical reality be considered complete?* Phys. Review **47**, 777 (1935).

[2] J. Bardeen and W. H. Brattain. *The Transistor, A Semi-Conductor Triode.* Phys. Rev. **74**, 230231 (1948).

[3] J. S. Bell. *On the Einstein-Podolsky-Rosen-Paradox.* Physics **1**, 195 (1964).

[4] M. A. Nielsen and I. L. Chuang. *Quantum Computation and Quantum Information.* Cambridge University Press, Cambridge (2000).

[5] J. Preskill. *Course Notes for Physics 219: Quantum Computation.* http://www.theory.caltech.edu/ preskill/ph219. .

[6] N. Gisin, G. Ribordy, W. Tittel, and H. Zbinden. *Quantum cryptography.* Rev. Mod. Phys. **74**, 145 (2002).

[7] R. Ursin, *et al. Entanglement based quantum communication over 144 km.* Nature Physics **3**, 481 (2007).

[8] V. Giovannetti, S. Lloyd, and L. Maccone. *Quantum Metrology.* Phys. Rev. Lett. **96**, 010401 (2006).

[9] T. D. Ladd, F. Jelezko, R. Laflamme, Y. Nakamura, C. Monroe, and J. L. OBrien. *Quantum computers.* Nature **464**, 45 (2010).

[10] J. I. Cirac and P. Zoller. *Quantum Computations with Cold Trapped Ions.* Phys. Rev. Lett. **74**, 4091 (1995).

[11] R. Blatt and D. J. Wineland. *Entangled states of trapped atomic ions.* Nature **453**, 1008 (2008).

[12] T. Monz, P. Schindler, J. T. Barreiro, M. Chwalla, D. Nigg, W. A. Coish, M. Harlander, W. Hnsel, M. Hennrich1, and R. Blatt. *14-Qubit Entanglement: Creation and Coherence.* Phys. Rev. Lett. **106**, 130506 (2011).

[13] M. Anderlini, P. J. Lee, B. L. Brown, J. Sebby-Strabley, W. D. Phillips, and J. V. Porto. *Controlled exchange interaction between pairs of neutral atoms in an optical lattice.* Nature **448**, 452 (2007).

[14] A. Beige, S. Bose, D. Braun, S. F. Huelga, P. L. Knight, M. B. Plenio, and V. Vedral. *Entangling Atoms and Ions in Dissipative Environments.* J. Mod. Opt. **47**, 2583 (2000).

[15] F. Benatti, R. Floreanini, and M. Piani. *Environment Induced Entanglement in Markovian Dissipative Dynamics.* Phys. Rev. Lett. **91**(7), 070402 (2003).

[16] B. Kraus, H. P. Büchler, S. Diehl, A. Kantian, A. Micheli, and P. Zoller. *Preparation of entangled states by quantum Markov processes.* Phys. Rev. A **78**, 042307 (2008).

[17] F. Verstraete, M. M. Wolf, and J. Ignacio Cirac. *Quantum computation and quantum-state engineering driven by dissipation.* Nature Physics **5**, 633 (2009).

[18] K. G. H. Vollbrecht, C. A. Muschik, and J. I. Cirac. *Entanglement Distillation by Dissipation and Continuous Quantum Repeaters.* Phys. Rev. Lett. **107**, 120502 (2011).

[19] H. Krauter, C. A. Muschik, K. Jensen, W. Wasilewski, J. M. Petersen, J. I. Cirac, and E. S. Polzik. *Entanglement generated by dissipation and steady state entanglement of two macroscopic objects.* Phys. Rev. Lett. **107**, 080503 (2011).

[20] C. A. Muschik, E. S. Polzik, and J. I. Cirac. *Dissipatively driven entanglement of two macroscopic atomic ensembles.* Phys. Rev. A **83**, 052312 (2011).

[21] P. Michler (ed.). *Single Quantum Dots*. Springer Verlag, Berlin (2003).

[22] F. Rossi. *Semiconductor Macroatoms: Basic Physics And Quantum-device Applications*. Imperial College Press (2005).

[23] D. Loss and D. P. DiVincenzo. *Quantum Computation with Quantum Dots*. Phys. Rev. A **57**, 120 (1998).

[24] J. M. Elzerman, R. Hanson, L. H. W. van Beveren, B. Witkamp, L. M. K. Vandersypen, and L. P. Kouwenhoven. *Single-shot read-out of an individual electron spin in a quantum dot*. Nature **430**, 431 (2004).

[25] J. R. Petta, A. C. Johnson, J. M. Taylor, E. A. Laird, A. Yacoby, M. D. Lukin, C. M. Marcus, M. P. Hanson, and A. C. Gossard. *Coherent manipulation of coupled electron spins in semiconductor quantum dots*. Science **309**, 2180 (2005).

[26] F. H. L. Koppens, C. Buizert, K. J. Tielrooij, I. T. Vink, K. C. Nowack, T. Meunier, L. P. Kouwenhoven, and L. M. K. Vandersypen. *Driven coherent oscillations of a single electron spin in a quantum dot*. Nature **442**, 766 (2006).

[27] D. Englund, D. Fattal, E. Waks, G. Solomon, B. Zhang, T. Nakaoka, Y. Arakawa, Y. Yamamoto, and J. Vuckovic. *Controlling the Spontaneous Emission Rate of Single Quantum Dots in a Two-Dimensional Photonic Crystal*. Phys. Rev. Lett. **95**, 013904 (2005).

[28] A. Badolato, K. Hennessy, M. Atatüre, J. Dreiser, E. Hu, P. M. Petroff, and A. Imamoğlu. *Deterministic Coupling of Single Quantum Dots to Single Nanocavity Modes*. Science **308**, 1158 (2005).

[29] A. Kress, F. Hofbauer, N. Reinelt, M. Kaniber, H. Krenner, R. Meyer, G. Bohm, and J. Finley. *Manipulation of the Spontaneous Emission Dynamics of Quantum Dots in Two-Dimensional Photonic Crystals*. Phys. Rev. B **71**, 241304 (2005).

[30] A. Imamoğlu, D. D. Awschalom, G. Burkard, D. P. DiVincenzo, D. Loss, M. Sherwin, and A. Small. *Quantum information processing using quantum dot spins and cavity-QED*. Phys. Rev. Lett. **83**, 4204 (1999).

[31] B. D. Gerardot, D. Brunner, P. A. Dalgarno, P. Öhberg, S. Seidl, M. Kroner, K. Karrai, N. G. Stoltz, P. M. Petroff, and R. J. Warburton. *Optical pumping of a single hole spin in a quantum dot.* Nature **451**, 441 (2008).

[32] M. Atatüre, J. Dreiser, A. Badolato, A. Högele, K. Karrai, and A. Imamoğlu. *Quantum-Dot Spin-State Preparation with Near-Unity Fidelity.* Science **312**, 551 (2006).

[33] D. Press, T. D. Ladd, B. Zhang, and Y. Yamamoto. *Complete quantum control of a single quantum dot spin using ultrafast optical pulses.* Nature **456**, 218 (2008).

[34] I. Fushman, D. Englund, A. Faraon, N. Stoltz, P. Petroff, and J. Vuckovic. *Controlled Phase Shifts with a Single Quantum Dot.* Science **320**, 769 (2008).

[35] A. Laucht, J. M. Villas-Boas, S. Stobbe, N. Hauke, F. Hofbauer, G. Böhm, P. Lodahl, M.-C. Amann, M. Kaniber, and J. J. Finley. *Mutual coupling of two semiconductor quantum dots via an optical nanocavity.* Phys. Rev. B **82**, 075305 (2010).

[36] B. Urbaszek, X. Marie, T. Amand, O. Krebs, P. Voisin, P. Maletinsky, A. Högele, and A. Imamoglu. *Nuclear spin physics in quantum dots: an optical investigation.* arXiv: **1202.4637** (2012).

[37] F. Klotz, V. Jovanov, J. Kierig, E. Clark, M. Bichler, G. Abstreiter, M. Brandt, J. Finley, H. Schwager, and G. Giedke. *A comprehensive experimental and theoretical study of asymmetric optical nuclear spin pumping in single neutral InGaAs quantum dots.* in preparation (2012).

[38] P. Maletinsky, M. Kroner, and A. Imamoğlu. *Demagnetization of Quantum Dot Nuclear Spins: Breakdown of the Nuclear Spin Temperature Approach.* Nature Physics **5**, 407 (2009).

[39] J. M. Taylor, C. M. Marcus, and M. D. Lukin. *Long-Lived Memory for Mesoscopic Quantum Bits.* Phys. Rev. Lett. **90**, 206803 (2003).

[40] J. M. Taylor, A. Imamoğlu, and M. D. Lukin. *Controlling a mesoscopic spin environment by quantum bit manipulation.* Phys. Rev. Lett. **91**, 246802 (2003).

[41] J. M. Taylor, G. Giedke, H. Christ, B. Paredes, J. I. Cirac, P. Zoller, M. D. Lukin, and A. Imamoğlu. *Quantum information processing using localized ensembles of nuclear spins.* arXiv:cond-mat **0407640v2** (2004).

[42] S. L. Braunstein and H. J. Kimble. *Teleportation of Continuous Quantum Variables.* Phys. Rev. Lett. **80**, 869 (1998).

[43] F. Klotz, V. Jovanov, J. Kierig, E. C. Clark, M. Bichler, G. Abstreiter, M. S. Brandt, J. J. Finley, H. Schwager, and G. Giedke. *Asymmetric optical nuclear spin pumping in a single uncharged quantum dot.* Phys. Rev. B **82**, 121307 (2010).

[44] M. Greiner, O. Mandel, T. Esslinger, T. W. Hänsch, and I. Bloch. *Quantum phase transition from a superfluid to a Mott insulator in a gas of ultracold atoms.* Nature **415**, 39 (2002).

[45] D. Jaksch, C. Bruder, J. I. Cirac, C. W. Gardiner, and P. Zoller. *Cold Bosonic Atoms in Optical Lattices.* Phys. Rev. Lett. **81**, 3108 (1998).

[46] B. Paredes, A. Widera, V. Murg, O. Mandel, S. Fölling, I. Cirac, G. V. Shlyapnikov, T. W. Hänsch, and I. Bloch. *Tonks-Girardeau gas of ultracold atoms in an optical lattice.* Nature **429**, 277 (2004).

[47] T. Kinoshita, T. Wenger, and D. Weiss. *Observation of a one-dimensional Tonks-Girardeau gas.* Science **305**, 11251128 (2004).

[48] M. W. Zwierlein, C. A. Stan, C. H. Schunck, S. M. F. Raupach, A. J. Kerman, and W. Ketterle. *Condensation of Pairs of Fermionic Atoms near a Feshbach Resonance.* Phys. Rev. Lett. **92**, 120403 (2004).

[49] M. Bartenstein, A. Altmeyer, S. Riedl, S. Jochim, C. Chin, J. Denschlag, and R. Grimm. *Collective Excitations of a Degenerate Gas at the BEC-BCS Crossover.* Phys. Rev. Lett. **92**, 203201 (2004).

[50] C. A. Regal, M. Greiner, and D. Jin. *Observation of Resonance Condensation of Fermionic Atom Pairs.* Phys. Rev. Lett. 92 **92**, 0404034 (2004).

[51] U. Schneider, L. Hackermueller, S. Will, T. Best, I. Bloch, T. A. Costi, R. W. Helmes, D. Rasch, and A. Rosch. *Metallic and Insulating Phases of Repulsively Interacting Fermions in a 3D Optical Lattice.* Science **322**, 15201525 (2008).

[52] R. Jördens, N. Strohmaier, K. Günter, H. Moritz, and T. Esslinger. *A Mott insulator of fermionic atoms in an optical lattice.* Nature **455**, 204207 (2008).

[53] J. F. Sherson, C. Weitenberg, M. Endres, M. Cheneau, I. Bloch, and S. Kuhr. *Single-atom-resolved fluorescence imaging of an atomic Mott insulator.* Nature **467**, 68 (2010).

[54] F. Brennecke, T. Donner, S. Ritter, T. Bourdel, M. Köhl, and T. Esslinger. *Cavity QED with a BoseEinstein condensate.* Nature **450**, 268 (2007).

[55] K. Baumann, C. Guerlin, F. Brennecke, and T. Esslinger. *Dicke quantum phase transition with a superfluid gas in an optical cavity.* Nature **464**, 1301 (2010).

[56] R. H. Dicke. *Coherence in Spontaneous Radiation Processes.* Phys. Rev. **93**, 99110 (1954).

[57] K. Hepp and E. Lieb. *On the superradiant phase transition for molecules in a quantized radiation field: the Dicke maser model.* Annals of Physics **76(2)**, 360404 (1973).

[58] Y. K. Wang and F. T. Hioe. *Phase Transition in the Dicke Model of Superradiance.* Phys. Rev. A **7(3)**, 831 (1973).

[59] S. Trotzky, P. Cheinet, S. Fölling, M. Feld, U. Schnorrberger, A. M. Rey, A. Polkovnikov, E. A. Demler, M. D. Lukin, and I. Bloch. *Time-resolved observation and control of superexchange interactions with ultracold atoms in optical lattices.* Science **319**, 295299 (2008).

[60] J. Simon, W. S. Bakr, R. Ma, M. E. Tai, P. M. Preiss, and M. Greiner. *Quantum simulation of antiferromagnetic spin chains in an optical lattice.* Nature **472**, 307312 (2011).

[61] D. P. DiVincenzo. *The Physical Implementation of Quantum Computation.* Fort. Phys. **48**, 771 (2000).

[62] P. Zoller, *et al. Quantum information processing and communication.* Eur. Phys. J. D **36**, 203 (2005).

[63] J. I. Cirac, P. Zoller, H. J. Kimble, and H. Mabuchi. *Quantum state transfer and entanglement distribution among distant nodes in a quantum network.* Phys. Rev. Lett. **78**, 3221 (1997).

[64] A. E. Kozekhin, K. Mølmer, and E. S. Polzik. *Quantum Memory for Light.* Phys. Rev. A **62**, 033809 (2000).

[65] M. Fleischhauer and M. D. Lukin. *Quantum memory for photons: Dark state polaritons.* Phys. Rev. A **65**, 022314 (2002).

[66] X. Maître, E. Hagley, G. Nogues, C. Wunderlich, P. Goy, M. Brune, J. M. Raimond, and S. Haroche. *Quantum Memory with a Single Photon in a Cavity.* Phys. Rev. Lett. **79**, 769 (1997).

[67] B. Julsgaard, J. Sherson, I. Cirac, J. Fiurášek, and E. S. Polzik. *Experimental demonstration of quantum memory for light.* Nature **432**, 482 (2004).

[68] T. Wilk, S. C. Webster, A. Kuhn, and G. Rempe. *Single-Atom Single-Photon Quantum Interface.* Science **317**(5837), 488 (2007).

[69] W. Rosenfeld, S. Berner, J. Volz, M. Weber, and H. Weinfurter. *Remote Preparation of an Atomic Quantum Memory.* Phys. Rev. Lett. **98**, 050504 (2007).

[70] K. S. Choi, H. Deng, J. Laurat, and H. J. Kimble. *Mapping photonic entanglement into and out of a quantum memory.* Nature **452**, 67 (2008).

[71] B. B. Blinov, D. L. Moehring, L.-M. Duan, and C. Monroe. *Observation of entanglement between a single trapped atom and a single photon.* Nature **428**, 153 (2004).

[72] R. Hanson and D. D. Awschalom. *Coherent manipulation of single spins in semiconductors.* Nature **453**, 1043 (2008).

[73] W. Yao, R.-B. Liu, and L. J. Sham. *Theory of Control of the Spin-Photon Interface for Quantum Networks.* Phys. Rev. Lett. **95**, 030504 (2005).

[74] J. P. Reithmaier, G. Sek, A. Loffler, C. Hofmann, S. Kuhn, S. Reitzenstein, L. V. Keldysh, V. D. Kulakovskii, T. L. Reinecke, and A. Forchel. *Strong coupling in a single quantum dot-semiconductor microcavity system.* Nature **432**, 197 (2004).

[75] T. Yoshie, A. Scherer, J. Hendrickson, G. Khitrova, H. M. Gibbs, G. Rupper, C. Ell, O. B. Shchekin, and D. G. Deppe. *Vacuum Rabi splitting with a single quantum dot in a photonic crystal nanocavity.* Nature **432**, 200 (2004).

[76] K. Hennessy, A. Badolato, M. Winger, D. Gerace, M. Atature, S. Gulde, S. Fält, E. L. Hu, and A. Imamoğlu. *Quantum nature of a strongly coupled single quantum dot-cavity system.* Nature **445**, 896 (2007).

[77] J. P. Reithmaier. *Strong exciton–photon coupling in semiconductor quantum dot systems.* Semiconductor Science and Technology **23**, 123001 (2008).

[78] H. Schwager, J. I. Cirac, and G. Giedke. *A quantum interface between light and nuclear spins in quantum dots.* Phys. Rev. B **81**, 045309 (2010).

[79] H. Schwager. *A quantum memory for light in nuclear spins of a quantum dot.* Master's thesis, Max-Planck-Institut für Quantenoptik & Universität Tübingen (2008).

[80] J. Schliemann, A. Khaetskii, and D. Loss. *Electron spin dynamics in quantum dots and related nanostructures due to hyperfine interaction with nuclei.* J. Phys: Cond. Mat. **15**, R1809 (2003).

[81] P. Maletinsky. Ph.D. thesis, ETH Zürich, http://e-collection.ethbib.ethz.ch/view/eth:30788 (2008).

[82] T. Holstein and H. Primakoff. *Field dependence of the intrinsic domain magnetization of ferromagnet.* Phys. Rev. **58**, 1098 (1940).

[83] H. Christ, J. I. Cirac, and G. Giedke. *Nuclear Spin Polarization in Quantum Dots-The Homogeneous Limit.* Solid State Sciences **11, Issue 5**, 965969 (2009).

[84] H. Christ. *Quantum Computation with Nuclear Spins in Quantum Dots.* Ph.D. thesis, TU München (2008).

[85] E. Brion, L. Pedersen, and K. Mølmer. *Adiabatic Elimination in a Lambda System.* Phys. A: Math. Theor. **40**, 10331043 (2007).

[86] X. Xu, Y. Wu, B. Sun, Q. Huang, J. Cheng, D. G. Steel, A. S. Bracker, D. Gammon, C. Emary, and L. J. Sham. *Fast Spin State Initialization in a Singly Charged InAs-GaAs Quantum Dot by Optical Cooling.* Phys. Rev. Lett. **99**, 097401 (2007).

[87] H. Schwager, J. I. Cirac, and G. Giedke. *Interfacing nuclear spins in quantum dots to cavity or traveling-wave fields.* New J. Phys. **12**, 043026 (2010).

[88] M. G. Paris. *Displacement operator by beam splitter.* Phys. Lett. A **217**, 78 (1996).

[89] C. W. Gardiner and P. Zoller. *Quantum Noise.* Springer Verlag, Berlin, 2nd edn. (2000).

[90] J. Williamson. American Journal of Mathematics **58**, 141 (1936).

[91] M. M. Wolf, G. Giedke, O. Krüger, R. F. Werner, and J. I. Cirac. *Gaussian entanglement of formation.* Phys. Rev. A **69**, 052320 (2003).

[92] G. Vidal and R. F. Werner. *A computable measure of entanglement.* Phys. Rev. A **65**, 032314 (2002).

[93] C. H. Bennett, H. J. Bernstein, S. Popescu, and B. Schumacher. *Concentrating partial entanglement by local operations.* Phys. Rev. A **53**, 2046 (1996).

[94] L. Vaidman. *Teleportation of quantum states.* Phys. Rev. A **49**, 1473 (1994).

[95] K. Hammerer, M. Wolf, E. Polzik, and J. Cirac. *Quantum benchmark for storage and transmission of coherent states.* Phys. Rev. Lett. **94**, 150503 (2005).

[96] J. Fiurášek. *Improving the fidelity of continuous-variable teleportation via local operations.* Phys. Rev. A **66**, 012304 (2002).

[97] C. M. Caves. *Quantum limits on noise in linear amplifiers.* Phys. Rev. D **26**, 1817 (1982).

[98] H. Scutaru. *Transition Probabilities for Quasifree States.* J. Math. Phys. **39**, 6403 (1998).

[99] G. Giedke and J. I. Cirac. *The characterization of Gaussian operations and distillation of Gaussian states.* Phys. Rev. A **66**, 032316 (2002).

[100] B. Kraus, K. Hammerer, G. Giedke, and J. I. Cirac. *Entanglement generation and Hamiltonian simulation in Continuous-Variable Systems.* Phys. Rev. A **67**, 042314 (2002).

[101] Z. Kurucz, M. W. Sørensen, J. M. Taylor, M. D. Lukin, and M. Fleischhauer. *Qubit protection in nuclear-spin quantum dot memories.* Phys. Rev. Lett. **103**, 010502 (2009).

[102] C. P. Slichter. *Principles of Magnetic Resonance.* Springer Verlag, Berlin (1990).

[103] W. Yao, R.-B. Liu, and L. J. Sham. *Theory of electron spin decoherence by interacting nuclear spins in a quantum dot.* Phys. Rev. B **74**, 195301 (2006).

[104] Z. Kurucz and M. Fleischhauer. *Continuous-variable versus electromagnetically-induced-transparency-based quantum memories.* Phys. Rev. A **78**, 023805 (2008).

[105] A. Imamoğlu, E. Knill, L. Tian, and P. Zoller. *Optical Pumping of Quantum-Dot Nuclear Spins.* Phys. Rev. Lett. **91**, 017402 (2003).

[106] F. T. Arecchi, E. Courtens, R. Gilmore, and H. Thomas. *Atomic Coherent States in Quantum Optics.* Phys. Rev. A **6**, 2211 (1972).

[107] S. L. Braunstein and P. van Loock. *Quantum information with continuous variables.* Rev. Mod. Phys. **77**, 513 (2005).

[108] J. Manuceau and A. Verbeure. *Quasi-Free States of the C.C.R.–Algebra and Bogoliubov Transformations.* Comm. Math. Phys. **9**, 293 (1968).

[109] L.-M. Duan, G. Giedke, J. Cirac, and P. Zoller. *Physical implementation for entanglement purification of Gaussian continuous-variable quantum states.* Phys. Rev. A **62**, 032304 (2000).

[110] R. Simon. *Peres-Horodecki separability criterion for continuous variable systems.* Phys. Rev. Lett. **84**, 2726 (2000).

[111] A. Peres. *Separability Criterion for Density Matrices.* Phys. Rev. Lett. **77**, 1413 (1996).

[112] R. F. Werner and M. M. Wolf. *Bound entangled Gaussian States.* Phys. Rev. Lett. **86**, 3658 (2001).

[113] G. Giedke, B. Kraus, M. Lewenstein, and J. I. Cirac. *Separability Properties of Three-mode Gaussian States.* Phys. Rev. A **64**, 052303 (2001).

[114] P. Hyllus and J. Eisert. *Optimal entanglement witnesses for continuous-variable systems.* N. J. Phys. **8**, 51 (2006).

[115] G. Giedke, J. Eisert, J. I. Cirac, and M. B. Plenio. *Entanglement transformations of pure Gaussian states.* J. Quant. Inf. Comp. **3(3)**, 211 (2003).

[116] G. Giedke, M. M. Wolf, O. Krüger, R. F. Werner, and J. I. Cirac. *Entanglement of formation for Gaussian states.* Phys. Rev. Lett. **91**, 107901 (2003).

[117] M. M. Wolf, G. Giedke, and J. I. Cirac. *Extremality of Gaussian quantum states.* Phys. Rev. Lett. **96**, 080502 (2006).

[118] S. L. Braunstein. *Squeezing as an irreducible resource.* Phys. Rev. A **71**(5), 055801 (pages 4) (2005).

[119] W. Coish and J. Baugh. *Nuclear spins in nanostructures.* Phys. Status Solidi B **246**, 2203 (2009).

[120] A. V. Khaetskii, D. Loss, and L. Glazman. *Electron spin decoherence in quantum dots due to interaction with nuclei.* Phys. Rev. Lett. **88**, 186802 (2002).

[121] R. Oulton, *et al. Subsecond Spin Relaxation Times in Quantum Dots at Zero Applied Magnetic Field Due to a Strong Electron-Nuclear Interaction.* Phys. Rev. Lett. **98**, 107401 (2007).

[122] X. Xu, W. Yao, B. Sun, D. G. Steel, A. S. Bracker, D. Gammon, and L. J. Sham. *Optically controlled locking of the nuclear field via coherent dark-state spectroscopy.* Nature **459**, 1105 (2009).

[123] P. Maletinsky, A. Badolato, and A. Imamoğlu. *Dynamics of Quantum Dot Nuclear Spin Polarization Controlled by a Single Electron.* Phys. Rev. Lett. **99**, 056804 (2007).

[124] B. Eble, O. Krebs, A. Lemaitre, K. Kowalik, A. Kudelski, P. Voisin, B. Urbaszek, X. Marie, and T. Amand. *Dynamic nuclear polarization of a single charge-tunable InAs/GaAs quantum dot.* Phys. Rev. B **74**, 081306(R) (2006).

[125] A. S. Bracker, *et al. Optical pumping of electronic and nuclear spin in single charge-tunable quantum dots.* Phys. Rev. Lett. **94**, 047402 (2005).

[126] D. Gammon, A. L. Efros, T. A. Kennedy, M. Rosen, D. S. Katzer, D. Park, S. W. Brown, V. L. Korenev, and I. A. Merkulov. *Electron and Nuclear Spin Interactions in the Optical Spectra of Single GaAs Quantum Dots.* Phys. Rev. Lett. **86**, 5176 (2001).

[127] A. I. Tartakovskii, *et al. Nuclear Spin Switch in Semiconductor Quantum Dots.* Phys. Rev. Lett. **98**, 026806 (2007).

[128] T. Yokoi, S. Adachi, H. Sasakura, S. Muto, H. Z. Song, T. Usuki, and S. Hirose. *Polarization-dependent shift in excitonic Zeeman splitting of self-assembled $In_{0.75}Al_{0.25}As/Al_{0.3}Ga_{0.7}As$ quantum dots.* Phys. Rev. B **71**(4), 041307 (2005).

[129] E. S. Moskalenko, L. A. Larsson, and P. O. Holtz. *Spin polarization of the neutral exciton in a single InAs quantum dot at zero magnetic field.* Phys. Rev. B **80**, 193413 (2009).

[130] M. N. Makhonin, A. I. Tartakovskii, A. Ebbens, M. S. Skolnick, A. Russell, V. I. Falko, and M. Hopkinson. *Nuclear spin pumping under resonant optical excitation in a quantum dot.* Appl. Phys. Lett. **93**, 073113 (2008).

[131] T. Brandes. *Coherent and collective quantum optical effects in mesoscopic systems.* Phys. Rep. **408**, 315 (2005).

[132] A. I. Tartakovskii. *Nuclear Spin Switch in Semiconductor Quantum Dots.* Phys. Rev. Lett. **98**, 026806 (2007).

[133] P. Fry, *et al. Inverted electron-hole alignment in InAs-GaAs self-assembled quantum dots.* Phys. Rev. Lett. **84**, 733 (2000).

[134] M. Bayer, G. Ortner, O. Stern, A. Kuther, A. A. Gorbunov, S. F. A. Forchel P. Hawrylak, and K. Hinzer. *Fine structure of neutral and charged excitons in self-assembled In(Ga)As/(Al)GaAs quantum dots.* Phys. Rev. B **65**, 195315 (2002).

[135] T. Andlauer. Ph.D. thesis, TU München (2009).

[136] M. Kroner, *et al. Optical detection of single electron spin resonance in a quantum dot.* Phys. Rev. Lett. **100**, 156803 (2008).

[137] M. Bayer, A. Kuther, A. Forchel, A. Gorbunov, V. B. Timofeev, F. Schaefer, J. P. Reithmaier, T. L. Reinecke, and S. N. Walck. Phys. Rev. Lett. **82**, 1748 (1999).

[138] V. Korenev. *The Nuclear Spin Nanomagnet.* Phys. Rev. Lett. **99**, 256405 (2007).

[139] R. I. Dzhioev and V. L. Korenev. *Stabilization of the Electron-Nuclear Spin Orientation in Quantum Dots by the Nuclear Quadrupole Interaction.* Phys. Rev. Lett. **99**, 037401 (2007).

[140] W. Yang and L. J. Sham. *Hole-induced Dynamic Nuclear Polarization in Quantum Dots*. arXiv: **1012.0060v1** (2010).

[141] A. Högele, M. Kroner, C. Latta, M. Claassen, I. Carusotto, C. Bulutay, and A. Imamoglu. *Dynamic nuclear spin polarization in resonant laser spectroscopy of a quantum dot*. arXiv: **1110.5524v1** (2011).

[142] J. J. Sakurai and S. F. Tuan. *Modern Quantum Mechanics*. Addison-Wesley, 2nd edn. (1994).

[143] A. V. Andreev, V. I. Emelyanov, and Y. A. Ilinski. *Cooperative effects in optics: Superradiance and phase transitions*. IOP Publishing (1993). Superradiance and phase transitions.

[144] H. Christ, J. I. Cirac, and G. Giedke. *Quantum Description of Nuclear Spin Cooling in a Quantum Dot*. Phys. Rev. B **75**, 155324 (2007).

[145] E. M. Kessler, S. Yelin, M. D. Lukin, J. I. Cirac, and G. Giedke. *Optical Superradiance from Nuclear Spin Environment of Single Photon Emitters*. Phys. Rev. Lett. **104**, 143601 (2010).

[146] C. Latta, *et al. Confluence of resonant laser excitation and bi-directional quantum dot nuclear spin polarization*. Nature Physics **5**, 758 (2009).

[147] S. Sachdev. *Quantum Phase Transitions*. Cambridge University Press (1999).

[148] I. Bloch. *Ultracold quantum gases in optical lattices*. Nature Physics **1**, 23 (2005).

[149] W. H. Zurek. *Decoherence, einselection, and the quantum origins of the classical*. Rev. Mod. Phys. **75**, 715 (2003).

[150] B. Baumgartner and H. Narnhofer. *The structures of state space concerning Quantum Dynamical Semigroups*. Reviews in Mathematical Physics, **24, 02**, 1250001 (2011).

[151] M. Lewenstein, A. Sanpera, and V. Ahufinger. *Ultracold Atoms in Optical Lattices*. Oxford University Press (2012).

[152] J. J. García-Ripoll and J. I. Cirac. *Spin dynamics for bosons in an optical lattice.* New Journal of Physics **5**(1), 76 (2003).

[153] D. Jaksch and P. Zoller. *The cold atom Hubbard toolbox.* Annals of Physics **315**, 52 (2005).

[154] C. Navarrete-Benlloch, I. de Vega, D. Porras, and J. I. Cirac. *Simulating quantum-optical phenomena with cold atoms in optical lattices.* New Journal of Physics **13**, 023024 (2011).

[155] E. Charron, E. Tiesinga, F. Mies, and C. Williams. *Quantum Gates Using Motional States in an Optical Lattice.* Quantum Communication, Computing, and Measurement 3 **III**, 227 (2002).

[156] C. Cohen-Tannoudji, J. Dupont-Roc, and G. Grynberg. *Atom-Photon Interactions.* Wiley-Interscience (1992).

[157] I. Marzoli, J. I. Cirac, R. Blatt, and P. Zoller. *Laser cooling of trapped three-level ions: Designing two-level systems for sideband cooling.* Phys. Rev. A **49**, 2771 (1994).

[158] A. Messiah. *Quantenmechanik Band 2.* de Gruyter (1985).

[159] H. J. Carmichael. *Analytical and numerical results for the steady state in cooperative resonance fluorescence.* J. Phys. B **13**, 3551 (1980).

[160] F. Dimer, B. Estienne, A. S. Parkins, and H. J. Carmichael. *Proposed realization of the Dicke-model quantum phase transition in an optical cavity QED system.* Phys. Rev. A **75**, 013804 (2007).

[161] S. Morrison and A. S. Parkins. *Collective spin systems in dispersive optical cavity QED: Quantum phase transitions and entanglement.* Phys. Rev. A **77**(4), 043810 (2008).

[162] S. Diehl, A. Micheli, A. Kantian, B. Kraus, H. P. Buchler, and P. Zoller. *Quantum states and phases in driven open quantum systems with cold atoms.* Nature Physics **4**, 878 (2008).

[163] J. Eisert and T. Prosen. *Noise-driven quantum criticality* (2011).

[164] M. Müller, S. Diehl, G. Pupillo, and P. Zoller. *Engineered Open Systems and Quantum Simulations with Atoms and Ions*. arXiv.org:1203.6595v1 (2012).

[165] T. Kato. *Perturbation Theory for Linear Operators*. Springer Berlin Heidelberg (1995).

[166] P. Pfeuty. *The one-dimensional Ising model with a transverse field*. Annals of Physics **57**, 7990 (1970).

[167] C. K. Majumdar and D. K. Ghosh. *On Next-Nearest-Neighbor Interaction in Linear Chain. I.* J. Math. Phys. **10**, 1388 (1969).

[168] D. E. Chang, J. D. Thompson, H. Park, V. Vuletic, A. S. Zibrov, P. Zoller, and M. D. Lukin. *Trapping and Manipulation of Isolated Atoms Using Nanoscale Plasmonic Structures*. Phys. Rev. Lett. **103**, 123004 (2009).

[169] R. Quidant, G. al Badenes, S. Cheylan, R. Alcubilla, J.-C. Weeber, and C. Girard. *Sub-wavelength patterning of the optical near-field*. Optics Express **12**, 282 (2004).

[170] G. H. Jeong, A. A. Farajian, T. Hirata, R. Hatakeyama, K. Tohji, T. M. Briere, H. Mizuseki, and Y. Kawazoe. *Encapsulation of Cesium inside Single-Walled Carbon Nanotubes by Plasma-Ion Irradiation Method*. Thin Solid Films **435**, 307 (2003).

[171] D. Porras and J. I. Cirac. *Collective generation of quantum states of light by entangled atoms*. Phys. Rev. A **78**, 053816 (2008).

[172] M. Gross and S. Haroche. *Superradiance: An essay on the theory of collective spontaneous emission*. Physics Reports **93**, 301 (1982).

[173] F. L. Cohen-Tannoudji, Bernhard Diu. *Quantum Mechanics*. Wiley-Interscience (1977).

Acknowledgements

I am deeply grateful to my thesis supervisor J. Ignacio Cirac for his invaluable support. His deep understanding of physics and his ingenious ideas fascinate me, and I am very grateful for all the interesting discussions about physics, for the great ideas he provided me with and for always taking his time for me despite his busy schedule. His enthusiasm and friendliness create an amazing atmosphere, it was a pleasure and a honor to be part of his group. And of course, I want to thank him for all the great times we had together with other people from our group on many unforgettable workshops and conferences.

Also, my work would not have been possible without the invaluable guidance of my advisor and coworker Géza Giedke. He has an unbelievable wide knowledge and understanding of physics and great ideas, I learned a lot from him. I am very grateful to him for *always* having a lot of time and patience for me. He is the most helpful person I ever met and a really good soul, and he enriches me and the whole group and the institute with his constant support in any respect and with the organisation of many important issues. I want to thank him for the uncountable discussions about physics (and also about other topics) and for invaluable support he gave me throughout the course of my thesis. I am very grateful for thorough proofreading of my thesis (in a very tight timeframe). I am very deeply indebted and grateful.

It was a great pleasure to work with Florian Klotz and Jonathan Finley from the Walter-Schottky Institute. I am very grateful for the fantastic collaboration on nuclear spin polarization and all the interesting discussions about physics we had. I learned a lot about quantum dots from them, and it was a lot of fun discussing new experimental results on the phone with Flo. I also want to thank the group of Jonathan Finley for organising barbecues and other great leisure activities.

I thank Jonathan Finley and Rudolf Gross very much for being on my Ph.D. examination committee.

I want to thank all my colleagues and friends that made the years at the MPQ a great time of my life! I want to thank Anika Pflanzer, Fernando Pastawski, Eric Kessler, Tassilo Keilmann, Maria Eckholt and Leonardo Mazza for their friendship and for all the fun that we had together, in the institute, on workshops and going out together in Munich. Fernando was the best office mate I can imagine and I will never forget the

nice atmosphere we had in our office. I want to thank Anika for being such a good friend, for the great time we had when we were sharing the room on workshops and our really nice leisure activities in and outside Munich.

I thank Lucas Clemente for being a great office neighbor and for the many long and nice discussions we had. I am very grateful for the many, many times he helped me out with computer problems.

I thank Verena Maier and Veronika Lechner for the great support they gave and give to me and to our group and for the good atmosphere they both created. I thank Mari-Carmen Bañuls, Martin Schütz, Dominic Kohler, Gemma De las Cuevas, Oriol Romero-Isart, Maarten van den Nest, Matteo Rizzi, Roman Schmied, Philipp Hauke, Christina Kraus, Diego Porras, Mikel Sanz, Sébastien Perseguers, Johannes Kofler, Ines de Vega, Tommaso Roscilde, Norbert Schuch, Carlos Navarrete-Benlloch and the rest of the group for making life at the MPQ so highly enjoyable, I will never forget how much fun we had together, especially in Hintertux and Galtür!

I thank Hagen Langhuth, Florian Klotz, Norman Hauke, Arne Laucht and Kai Müller from the WSI for the amazing time we had at the NTT School in Japan and in Tokyo and Kyoto and Simon Frédérick for organizing so many nice dinners for all of us.

I also want to thank my friends outside work, especially Annika Schad and Enrica Puggioni, Hagen Langhuth, Kristine Teske, Sigrid Gehann, Michael Weihing, Mareike Göritz and Pau Montes, Nils Agster, Victoria Beck and Arne Bohner for the great times we had together in the last years, that made me forget about work completely.

I want to thank Christian Kasztelan for his love and support and for enduring the writing of this thesis in the last weeks.

I am deeply grateful to my parents Doris and Jürgen Schwager and my sister Andrea Schwager for their love and support in all possible ways and everything else.

I gratefully acknowledge financial support from the DFG within SFB631 and the Max-Planck Society.